SCUOLA INTERNAZIONALE SUPERIORE DI STUDI AVANZATI
INTERNATIONAL SCHOOL FOR ADVANCED STUDIES

Adiabatic dynamics of many-body systems close to a quantum critical point

Thesis submitted for the degree of
Doctor Philosophiæ

CANDIDATE:
Tommaso Caneva

SUPERVISORS:
Prof. Giuseppe E. Santoro
Prof. Rosario Fazio

October, 30$^{\text{th}}$ 2009

Contents

List of Figures

Introduction

The loss of adiabaticity and the production of defects in a system driven across a quantum phase transition have attracted a lot of attention in the last years. This problem was initially considered in cosmology in trying to understand signatures of the phase transition that took place in the early universe[1]. More recently with the Quantum Annealing[2, 3, 4, 5] and the Adiabatic Quantum Computation[6, 7] a renewed research activity has been devoted to the subject also in the field of condensed matter and quantum information science.

The idea behind the annealing technique is to transform a given optimization problem onto the determination of the ground state of a corresponding model Hamiltonian. A typical example is offered by the research of the minimum energy configuration of a spin glass[4, 8, 9]: Quantum Annealing tries to solve the issue by continuously changing (i.e. by annealing) an initial Hamiltonian with a perfectly known ground state into the Hamiltonian to solve; if adiabaticity holds, the starting ground state is brought by the evolution into the required unknown ground state, providing the desired answer to the problem. The main difficulty encountered in this kind of problem is that the energy landscape of a spin glass is characterized by many local minima separated by barriers from the global one; standard optimization techniques[1] are then easily trapped into the wrong solutions. Quantum Annealing instead exploits the quantum tunneling to pass through such barriers and reveal the true minimum. In many situations QA is able to outperform also its precursor, the Classical Annealing[8], in which the temperature drives the transformation and thermal fluctuations are used to explore all the configurations space[4].

Almost contemporary to Quantum Annealing, Adiabatic Quantum Computation (AQC) was proposed as an alternative to the circuit-theory approach to implement quantum algorithms. It is commonly reckoned that quantum computers can

[1] Like steepest descent methods.

efficiently solve problems otherwise intractable with classical computers. There are indeed problems whose solution through classical algorithms requires a running time increasing exponentially with the input length, i.e. the number of digits. In some cases, as for the integer factorization problem through the Shor's algorithm[10], quantum mechanics is able to convert such an exponential dependence into a manageable power law, definitely cutting the running time. Ten years ago, in Ref[6], an approach to quantum computation based on quantum adiabatic evolution was presented, marking the birth of Quantum Adiabatic Computation. In analogy with QA, this protocol worked out the answer to a satisfiability search problem (K-SAT) following the evolution of the ground state of an initial easily solvable Hamiltonian when the latter is slowly transformed into the final Hamiltonian whose ground state encodes the satisfying assignments. Subsequently in Refs[11, 12] the issue has been cast in a more wider perspective, with the demonstration that an arbitrary quantum algorithm can be efficiently simulated with AQC. Obviously this is only one possible way to build quantum algorithms and leaves open the matter about how slow must be the evolution in order to be adiabatic.

The key point to reach the target in QA-AQC is the adiabaticity of the evolution. The adiabatic theorem ensures such a condition when the time scale over which the Hamiltonian is changed is large with respect to the typical inverse spectral gap; so adiabaticity is guaranteed if the ground state energy is well separated from all the other excited states for the whole transformation process. Unfortunately it is not rare the condition in which the controlled initial state and the unknown target sit on opposite sides of a quantum phase transition, so that a critical closed gap has to be crossed[13]. In this situation, no matter how slow the annealing is, the adiabaticity is lost nearby the critical point and the evolved state may differ from desired final ground state. For instance employing QA in the case of a disordered magnet[4, 9], typically the initial state is built by strongly polarizing the spins with a transverse field (paramagnetic phase) and the final ground state (ferromagnetic phase) is reached by annealing the field intensity, crossing a quantum critical point. In AQC this corresponds to run into steps of the computation at which the von Neumann entropy diverges with the size of the system (quantum register), so that the algorithm cannot be effectively simulated by classical computers[14].

Understanding what computational problems can be solved efficiently through

QA-AQC, or which advantage can be taken from QA with respect to other optimization techniques (for instance, its classical counterpart, simulated annealing[8]) is in general a formidable task and there is no unique prescription. In this perspective, tractable, exactly solvable systems can be of great help in exploring the issue. In those test models, the production of defects in the evolved state with respect to the desired instantaneous ground state, quantifying the loss of adiabaticity, becomes a measure of the power of the method in providing the correct result. Recently a large amount of work has been devoted to the characterization of the defect production density[15, 16, 17, 18, 19, 20, 21, 22, 23, 24, 25, 26] and two scenarios have been proposed to derive its behavior as function of the total evolution time: the Kibble-Zurek mechanism[15] (KZM) and the perturbative analysis based on the Fermi Golden rule[16, 23, 27] (FGR). The KZM was originally introduced in the context of classical transitions driven by thermal fluctuations[1] and only few years ago adapted to quantum, zero temperature critical points for particular quench regimes[15, 28]. The idea at the basis of KZM is that the evolution of a system driven through a quantum phase transition becomes diabatic when the time scale at which the Hamiltonian is varied is of the order of the relaxation time, determined by the inverse of the instantaneous gap. The adiabaticity is recovered only when, crossed the critical point, the relaxation time comes back to be smaller than the transition rate and the defect density can be estimated via the correlation length ξ at the instant of the loss of adiabaticity[2]. KZM has been tested in various models through both analytical and numerical studies[17, 18, 21, 22, 29] and is also supported by experiments[30]. The Fermi Golden Rule (FGR) approach[16], appeared almost contemporary to the quantum rielaboration of KZM, moves instead from a different perspective: the excitation probability during the dynamics is estimated by considering only transitions involving the instantaneous ground state and neglecting the contribution of direct population exchange between excited states. Then general scaling arguments can be invoked in order to extract the dependence of the defect density on the transition rate. It should be mentioned that recent studies have highlighted particular transitions apparently not describable with these approaches[22, 24, 25, 26, 31, 32, 33, 34].

This thesis aims at probing the effectiveness and the limits of QA-AQC techniques by using as test different exactly solvable quantum many-body systems. In particular the attention has been focused on the effect of disorder that as known can

[2] In average for every domain of size ξ a defect is produced.

produce extremely small energy excitations[9, 35] particularly dangerous for the adiabaticity condition. On the contrary, an high coordination number, i.e. an high dimensionality, intuitively reinforces the system against dynamical perturbation, making QA-AQC more effective, so that the extreme limit of an infinitely coordinated system has been also investigated. Another possibility to improve the adiabaticity is to engineer an optimal time dependence for the parameter driving the evolution. It can be done via many techniques and one of the most promising is the optimal control through the Krotov algorithm[36]; the latter has been then selected to improve the adiabaticity in the Landau-Zener system and in the Ordered Ising model.

The structure of the present Thesis is the following. The first part is devoted to the analysis of the performance of standard (i.e. transformations linear in time) Quantum Annealing in different quantum critical models. After reviewing the status of art in Chapter 1, the random Ising chain is considered in Chapter 2; it will be shown that the presence of disorder dramatically reduces the power of the method also in simple $1D$ systems without frustration. This is one of the first examples in which a logarithmic decay of the residual energy and defect density as a function of the total evolution time is clearly revealed; a mechanism based on the Landau-Zener tunneling theory and on a Fisher's type renormalization group analysis is proposed to justify the observed numerical results.
In Chapter 3 the Lipkin-Meshkov-Glick (LMG) model, a system with infinite range interactions, is analyzed. The work represents the first study of QA in a prototype of high-dimensional system; due to the fact that a finite dimension is not defined for the model, standard approaches like the Kibble-Zurek mechanism cannot be applied to explain the residual energy behavior. However, as it will be argued, a Landau-Zener argument can be still invoked to recover the correct scaling.
Chapter 4 and Chapter 5 are devoted to the problem of optimization of time dependent transformations: the condition of linear annealing is relaxed and the optimal shape of the time-dependent transformation is investigated. Among the various techniques at disposal to implement this new ingredient, the quantum control through Krotov's algorithm is considered. This numerical method, in contrast to other analytical approaches, offers the advantage of being flexible and easily implementable also for complex systems. In Chapter 4 the Krotov algorithm is employed to work out the optimal time evolution in two paradigmatic cases: the Landau-Zener model and the ordered Ising model. The performance of the

method is analyzed as a function of the total evolution time; the results show that the optimal control technique is able to reach the maximum speed allowed by quantum mechanics, the so called Quantum Speed Limit (QSL). Finally in Chapter 5 the QSL theory is directly connected to the loss of adiabaticity in a general non linear annealing process across a second order quantum phase transition: the QSL perspective for deriving the production of defect is then discussed.

Chapter 1

Adiabatic Dynamics close to a Quantum Phase Transition

1.1 Second order Quantum Phase Transition

A phase transition is a drastic change in the structure of a system: daily life examples are the change of state substances from the gaseous to the liquid state or viceversa, etc. Classical transitions are driven by thermal fluctuations and and occurs at a finite temperature, the critical temperature. Quantum phase transitions, instead, occur at T=0 and are entirely driven by quantum fluctuations. Both classical and quantum are characterized by the existence of an order parameter which becomes non-zero in the ordered phase. The order parameter can be continuous or manifests a jump at the transition point depending if transition is of the second or the first order. In this thesis the attention will be focused exclusively on systems which cross a second-order quantum phase transition[13].
Consider a parameter dependent-Hamiltonian $H(g)$, where g is dimensionless. By following the evolution of the ground state energy induced by the variation of the parameter, it can happen that, at a specific value $g = g_c$, the ground state energy becomes very close to the energy of the first excited states and in the thermodynamic limit the gap vanishes. Under such circumstances the system undergoes a quantum phase transition. For second order quantum phase transitions, the gap Δ between the ground state and the first excited state vanishes as

$$\Delta \sim J|g - g_c|^{z\nu} \tag{1.1}$$

where J is the typical scale of the microscopic coupling and z, ν are the critical exponents, which depend only on the universality class of the underlying Hamiltonian.
The time scale on which a system is able to respond to a perturbation of its state, is measured by the inverse of the minimum instantaneous gap. The adiabatic theorem establishes that a system can be adiabatically driven without introducing excitations only if the transformation rate is much larger than the minimum gap encountered during the whole dynamics[37]. The critical closure of the gap then sets up an insurmountable obstacle for the adiabaticity condition: no matter how slow the system is driven through the transition, its evolution becomes diabatic compromising the effectiveness of QA-AQC techniques. From this perspective a lot of attention should be paid to the choice of the path connecting the initial and the target state and the study of quenches crossing critical regions acquires a specific relevance because it can reveal the ultimate limit of the methods. Together with the vanishing of the energy gap the system acquires a macroscopic correlation characterized by a length, the correlation length, which diverges at the critical point as

$$\xi^{-1} \propto |g - g_c|^{\nu}, \tag{1.2}$$

and which is a further manifestation of the collective nature of the phenomenon.

1.2 Dynamics through a Quantum Phase Transition

Usually a QPT takes place when the governing Hamiltonian is characterized by two (or more) competing parts: in Bose Hubbard-like models the kinetic term copes with the onsite repulsion; in ferromagnetic Ising-like models the coupling between spins along a particular direction has to struggle with a transverse field. Typically when the relative weight of one term respect to the other is very large, the system belongs to a specific phase; the transition happens when the competing forces have an intensity of the same order. The dynamics through a QPT can be then performed by introducing a time modulation of the relative strength or, borrowing the terminology from QA, by annealing one component in time.
QA and AQC aim to reach the ground state $|\psi_{\rm gs}(t_{\rm fin})\rangle$ of an Hamiltonian $H(t_{\rm fin})$,

by adiabatically following its evolution from an instant $t_{\rm in}$ at which it is assumed exactly known. The evolution of a system is determined by the Scrhödinger equation

$$i\hbar\frac{d}{dt}|\psi(t)\rangle = H(t)|\psi(t)\rangle \tag{1.3}$$

and in the QA-AQC framework it is assumed

$$H(t) = H_{\rm p} + \Gamma(t)H_{\rm t}, \tag{1.4}$$

where $H_{\rm p}$ is the Hamiltonian whose ground state is looked for, $H_{\rm t}$ is solvable and $\Gamma(t)$ is the time dependent intensity driving the transformation. In the annealing process, the value of $\Gamma(t)$ is reduced from some large initial value to zero in a time $\tau = t_{\rm fin} - t_{\rm in}$, for instance in linear way

$$\Gamma(t) = \Gamma_0\left(1 - \frac{t - t_{\rm in}}{\tau}\right), \quad \text{with} \quad \Gamma_0 \gg 1. \tag{1.5}$$

By starting the evolution in the initial ground state,

$$|\psi(t_{\rm in})\rangle = |\psi_{\rm gs}(t_{\rm in})\rangle, \tag{1.6}$$

if adiabaticity holds, $|\psi(t)\rangle$ corresponds to the instantaneous ground state during all the dynamics and also at the final time

$$|\psi(t_{\rm fin})\rangle = |\psi_{\rm gs}(t_{\rm fin})\rangle = |\psi_{\rm gs}^{H_{\rm P}}\rangle, \tag{1.7}$$

furnishing the desired solution.

1.3 Measures of the loss of adiabaticity

As outlined in the Introduction, the most interesting problems tackled with QA-AQC methods involve the crossing of a quantum critical point, the initial known state and final unknown target usually belonging to different quantum phases[38]. But as noticed in Sec. 1.1, a system driven across a second order quantum phase

transition loses the adiabaticity due to the critical closure of the gap[1]. This implies that during the annealing the system is unavoidably excited respect to the instantaneous ground state; therefore the state reached at the end of the evolution may differ from the real target, or, referring to the possible presence of an order parameter, it may present defects. The main scope of the thesis is to quantify the amount of the loss of adiabaticity and analyze its behavior in different contexts to test the response and the flexibility of the QA-AQC respect to general effects like the presence of disorder (Chapter 2), long range interactions (Chapter 3) or to which extent is possible to improve the performance of the method with an optimized time dependence of the driving term (Chapter 4). Solvable models are an ideal ground to this purpose due to the fact that the result of the annealing can be compared at each instant of the evolution with the exact solution. In this Section various measures of the loss of adiabaticity are presented, everyone more suitable depending on the specific problem at hand; these quantities will be repeatedly used in the thesis.

The first natural measure of the loss of adiabaticity is the residual energy defined as

$$E_{\rm res} = E_{\rm fin} - E_{\rm gs} \ , \tag{1.8}$$

where $E_{\rm gs}$ is the ground state energy of $H(t_{\rm fin})$, and $E_{\rm fin} = \langle\psi(t_{\rm fin})|H(t_{\rm fin})|\psi(t_{\rm fin})\rangle$ is the average energy of the final time-evolved state $|\psi(t_{\rm fin})\rangle$. Obviously $E_{\rm fin}$, and hence $E_{\rm res}$, depends on the annealing time τ; the slower the evolution the closer the final energy to $E_{\rm gs}$, hence the smaller the residual energy.

An alternative general way of quantifying the degree of adiabaticity of the evolution is in term of the infidelity that measures the total excitation probability of the evolved state respect to the target ground state

$$\mathcal{I} = 1 - |\langle\psi(t_{\rm fin})|\psi_{\rm gs}(t_{\rm fin})\rangle|^2 \tag{1.9}$$

where $|\psi_{\rm gs}(t_{\rm fin})\rangle$ represents the ground state of $H(t_{\rm fin})$.

Finally another estimation widely used in literature is the density of defects ρ. Its definition is strongly dependent on the model in analysis and on what is considered as a defect. In the thesis this concept will be applied to ferromagnetic spin systems

[1]However, as shown in Ref.[23], in integrable systems the presence of a quantum phase transition is not a necessary condition to induce a non-adiabatic process.

so that a defect corresponds to a spin reversed respect to its interacting neighbors. In particular for Ising chains, the defect density is identified with the kink density and can be defined as

$$\rho = \frac{1}{N}\sum_{i}^{N-1}\langle\psi(t_{\text{fin}})|\frac{1}{2}\left(1-\sigma_i^z\sigma_{i+1}^z\right)|\psi(t_{\text{fin}})\rangle \tag{1.10}$$

where N is the size of the chain and σ_i^α are the Pauli operators.

In the following different approaches to obtain a prediction about the loss of adiabaticity will be described.

1.3.1 Kibble-Zurek Mechanism

Assumed that the not adiabatic behavior manifests only nearby the critical point, it is natural to wonder whether the loss of adiabaticity can be described in terms of the static features of the transition, for instance through its critical exponents. The Kibble-Zurek mechanism[1] addresses exactly this issue, providing an elegant connection between statics and non-equilibrium properties. According to KZM the time scale at which the system is able to react to an external change diverges at the transition point as manifestation of the critical slowing down, observed also in the classical case[15]. This effect allows to distinguish two regimes for the evolution: the *adiabatic regime*, in which the system is able to adjust to the variation of the time dependent Hamiltonian, so that there is no population transfer between the instantaneous energy eigenstates, and the *impulse regime*, embracing the critical point, in which the relaxation times are so long that there is no change in the wave function except for an overall phase factor. The instant of the evolution which signals the boundary between the two regimes, is called the freeze-out time, $\hat{t}$ see Fig.(1.1).
According the KZM, the adiabaticity is lost when the time remaining to the transition is equal to the relaxation time, given by the inverse of the instantaneous gap Δ. Being $\epsilon = g - g_c$ the dimensionless parameter measuring the distance from the transition, near the critical point ($\epsilon = 0$) its time dependence can be linearized:

$$\epsilon = t/\tau, \tag{1.11}$$

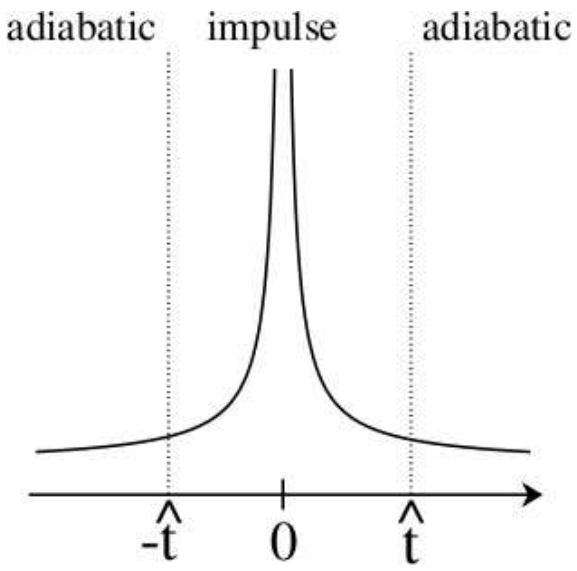

FIGURE 1.1: Relaxation time scale from KZ theory; $\hat{t}$ represents the freeze-out time (picture from Ref[39]).

where τ represents the quench time. In formula:

$$\hat{t} \sim \Delta^{-1}(\hat{t}) = |\epsilon(\hat{t})|^{-z\nu}, \tag{1.12}$$

or

$$\hat{t} \sim \tau^{-z\nu/(1+z\nu)}, \tag{1.13}$$

$z\nu$ being the critical exponents entering in Eq(1.1). The correlation length at the freezing time, giving an estimate of the size of the typical ordered domain, can be employed to evaluate the defect density ρ, assuming that on average one defect per domain is produced. The Kibble-Zurek prediction is then

$$\rho \sim \xi^{-d}(\hat{t}), \tag{1.14}$$

where d is the space dimension and by using $\xi(\hat{t}) \sim |\epsilon(\hat{t})|^{-\nu}$ it finally leads to

$$\rho \sim \tau^{-d\nu/(1+z\nu)}. \tag{1.15}$$

This formula has been tested in various models through both analytical and numerical studies[15, 16, 17, 18, 21, 22, 29] and is also supported by experiments[30]. Recently Eq(1.15) has been generalized to the case of inhomogeneous quantum

phase transitions[2], a more realistic condition for the experimental setup[40]. For the ordered quantum Ising chain[15], in which $z = \nu = 1$, Eq(1.15) gives the well known result[17] $\rho \sim \tau^{-1/2}$.

1.3.2 Fermi Golden Rule approach

Almost contemporary to the application of KZM to QPT, in Ref[16] it has been proposed a description of the loss of adiabaticity on the basis of the perturbation theory and Fermi Golden Rule (FGR). Following Ref[16] let's consider a time-parameter dependent Hamiltonian $H[\epsilon(t)]$ in which $\epsilon \gtrless 0$ describes different phases. A general state can be decomposed as

$$\psi(t) = \sum_p a_p(t)\phi_p(t) \tag{1.16}$$

where $\phi_p(t)$'s are the instantaneous eigenvectors of $H[\epsilon(t)]$ with eigenvalues $\omega_p(t)$'s. Let's insert this decomposition into the Schrödinger equation

$$i[\sum_p \dot{a}_p(t)\phi_p(t) + \sum_p a_p(t)\dot{\phi}_p(t)] = \sum_p \omega_p(t)a_p(t)\phi_p(t) \tag{1.17}$$

and exploit the orthogonality of the states:

$$i\dot{a}_p(t) + i\sum_q a_q(t)\langle p,t|\partial_t|q,t\rangle = \omega_p(t)a_p(t). \tag{1.18}$$

Then performing the gauge transformation

$$a_p(t) = \tilde{a}_p(t)e^{-i\int^t \omega_p(t')dt'} \tag{1.19}$$

the following exact equation is obtained

$$\dot{\tilde{a}}_p e^{-i\int^t \omega_p(t')dt'} + \sum_q \tilde{a}_q(t)e^{-i\int^t \omega_q(t')dt'}\langle p,t|\partial_t|q,t\rangle = 0. \tag{1.20}$$

[2]That is transitions in which the annealing is not exactly homogeneous throughout the system, i.e. $\epsilon(t) \to \epsilon(j,t)$ where j is the site index.

The problem can be solved through perturbation theory. Indeed by making a perturbative expansion into the quench time τ, from Eq(1.18) we have

$$i\dot{a}_p^{(n+1)}(t) = -i\frac{d\epsilon}{dt}\sum_q a_q^{(n)}(t)\langle p,\epsilon|\partial_\epsilon|q,\epsilon\rangle + \omega_p(t)a_p^{(n)}(t) \quad \text{with} \quad \frac{d\epsilon}{dt} \propto \frac{1}{\tau} \tag{1.21}$$

so that assuming to start the quench into the ground state $p = 0$ we obtain

$$\tilde{a}_p = \delta_{p,0} + \tilde{a}_p^{(1)} + ... + \tilde{a}_p^{(n)}... \tag{1.22}$$

where $\tilde{a}_p^{(n)} \sim (1/\tau)^n$. In the limit of slow quench, $\tau \gg 1$, we can keep only the first term in the expansion, i.e. with the Fermi Golden Rule:

$$\dot{\tilde{a}}_p = -e^{i\int^t[\omega_p(t')-\omega_0(t')]dt'}\langle p,t|\partial_t|0,t\rangle. \tag{1.23}$$

Then the density of excited states is simply given by integrating and summing[27] over all $p \neq 0$:

$$P_{\text{ex}} = \rho \sim \sum_{p\neq 0}\left|\int_{-\infty}^{\infty} dt\langle p,t|\partial_t|0,t\rangle e^{i\int^t dt'[\omega_p(t')-\omega_0(t')]}\right|^2 \tag{1.24}$$

where $|p,t\rangle$ is the p-th instantaneous eigenstate of the Hamiltonian describing the system [3].

By assuming of dealing with a uniform d-dimensional system, previous equation can be rewritten in momentum space leading to

$$\rho \sim \int \frac{d^dk}{(2\pi)^d}\left|\int_{-\infty}^{\infty} d\epsilon\langle k,\epsilon|\partial_\epsilon|0,\epsilon\rangle e^{i\tau\int^\epsilon d\epsilon'[\omega_k(\epsilon')-\omega_0(\epsilon')]}\right|^2 \tag{1.25}$$

where the time dependence of ϵ has been also exploited. From general scaling argument, by remembering that from Eq(1.1) $\Delta \propto |\epsilon|^{z\nu}$, it can be written

$$\omega_k - \omega_0 = k^z F(\epsilon^{z\nu}/k^z) \tag{1.26}$$

with

$$F(x) \sim \begin{cases} 1 & \text{for} \quad x \ll 1 \\ x & \text{for} \quad x \gg 1, \end{cases} \tag{1.27}$$

[3] Notice that the definition used in Refs.[16, 41] holds only in the case of linear quench $\lambda = t/\tau$.

the latter condition implying $\omega_k - \omega_0 \sim \Delta$ for $k \to 0$. Then by introducing the variable $y = \epsilon^{z\nu}/k^z$ it turns out

$$d\epsilon = \frac{k^{1/\nu}}{z\nu y^{1+1/(z\nu)}} dy. \tag{1.28}$$

So the integral of the phase transforms into

$$\begin{aligned} i\tau \int^{\epsilon} d\epsilon' [\omega_k(\epsilon') - \omega_0(\epsilon')] &= i\tau \int^{\epsilon} d\epsilon' k^z F(\epsilon'^{z\nu}/k^z) \\ &= i\tau \int^{y} k^z F(y') k^{1/\nu} \frac{1}{z\nu} y'^{-(1+1/(z\nu))} dy' \\ &= \tau k^{z+1/\nu} f(y), \end{aligned} \tag{1.29}$$

instead the matrix element, assuming[16] $\langle k, \epsilon | \partial_\Delta | 0, \epsilon \rangle = k^{-z} V\left(\Delta/k^z\right)$, brings to

$$\langle k, \epsilon | \partial_\epsilon | 0, \epsilon \rangle d\epsilon = k^{-z} V \left(\frac{\Delta}{k^z}\right) \frac{d\Delta}{d\epsilon} d\epsilon = V(y) dy. \tag{1.30}$$

Previous equations suggest a second change of variable, $q = k\tau^{\nu/(1+z\nu)}$ so that $dk = \tau^{-\nu/(1+z\nu)} dq$ and finally for the defect density it is obtained

$$\rho \sim C\tau^{-d\nu/(1+z\nu)}, \tag{1.31}$$

where C is a constant to be determined and the scaling of Eq(1.15) is gained again. The perturbative approach has been also generalized to non linear quench of polynomial form[41], $\epsilon \propto \text{sign}(t)|t/\tau|^r$, and has been also exploited to construct the optimal power dependence of such a polynomial shape[27] for the ordered Ising model.

1.3.3 Landau-Zener approximation

In Ref[15] an alternative approach based on the quantum tunneling effect has been also proposed. For finite-size systems with a small but non-vanishing gap, the thermodynamical critical closure of the gap is rounded off in an avoided crossing that can be locally approximated with a Landau-Zener model[42]. Under the assumption that only the first gap accessible during the dynamics is responsible for the loss of adiabaticity, the Landau-Zener formula can be used to give a lower

bound to the true, global excitation probability of the system:

$$P_{\text{ex}} = e^{-\pi(\Delta/2)^2\tau} \tag{1.32}$$

where Δ represents the amplitude of the gap at the finite size critical point and τ is the rate of the linear quench., Notice that for particular models, like the ordered Ising chain[17], or the $1d$ Kitaev model[41], the first instantaneous gap can be exactly mapped onto a LZ-like Hamiltonian.
Then once the scaling of the critical gap with the size is known, $\Delta = f(N)$, Eq(1.32) can be exploited to determine the behavior of the maximum defect-free size after a quench, N_{free}, as function of τ. Once an arbitrary small but fixed probability $\tilde{P}$ is chosen, it turns out that

$$\tilde{P}_{\text{ex}} = e^{-\pi(f(N_{\text{free}})/2)^2\tau} \Longrightarrow N_{\text{free}} \sim f^{-1}\left(\sqrt{\frac{\kappa}{\tau}}\right). \tag{1.33}$$

with $\kappa = -4(\ln \tilde{P})/\pi$. Finally, once the relation connecting N_{free} and the selected measure of the loss of adiabaticity (residual energy, defect density, infidelity etc.) is established, the desired behavior is obtained. For instance, for the ordered Ising chain it is known[43] that $\Delta \sim N^{-1}$ and $\rho \sim N_{\text{free}}^{-1}$; so Eq(1.33) leads to the correct result $\rho \sim \tau^{-1/2}$.
For systems exhibiting a dominant isolated critical point[34], this alternative approach provides the same result as KZM; however the LZ estimate of Eq(1.33) works also in some cases in which KZM fails[22, 24, 25], see next section. This is the reason why the LZ perspective has been preferentially adopted in this thesis.

1.3.4 Quenches eluding KZM and FGR descriptions

As mentioned in the Introduction, a possible way to improve the adiabaticity in QA-AQC techniques is to relax the linear dependence on time of the annealing as well as to look for a convenient path in the parameter space spanned by the Hamiltonian under consideration. For instance in XY spin-1/2 models[18] a quench can be performed not only by modulating the transverse field along the Z direction but also the anisotropy in the XY-plane. The idea behind the procedure is to investigate the possibility of finding a gentle way to cross the transition in order to reduce the impact of the loss of adiabaticity. For the ordered Ising model the issue has been recently analyzed[22], enlightening the existence of peculiar paths, specifically

through a multicritical point, for which the observed anomalous τ^{-6} decay of the defect density with the quench time cannot be described via usual KZM or FGR arguments -as shown in previous sections predicting $1/\sqrt{\tau}$ behavior. And this is not an isolated case. Other pathological situations, unmanageable with standard tools has been revealed, such as while crossing a multicritical point[22, 31] or a $(d-m)$ dimensional critical surface[4][32], quenching along a gapless line[33, 34]or going through a BKT quantum phase transition [25, 26]; moreover KZ, FGR formula cannot be used for infinitely coordinated systems, i.e. without a definite space dimensionality d[24], see Chapter 3.

The problem with these situations is that the critical exponents and also the effective model dimension characterizing the quantum phase transition turns out to be dependent on the path followed during the quench in the Hamiltonian parameter space[34]. This issue unluckily cannot be easily cured within KZM or FGR derivation of Eq(1.15); the only possibility is to introduce *ad hoc* substitutions. It turns out that crossing a multicritical point the exponent z has to be changed by a new dynamical exponent z_2[31]; instead going through a $(d-m)$ dimensional critical surface not all the phase space is at disposal and this influences the scaling of the variables in such a way that d must be corrected with m[32]. In many situations, for finite size systems, the issue can be cured by exploiting Landau-Zener (LZ) effective models (see Sec. 1.3.3) locally approximating the dynamical critical gap[15, 20, 24, 25, 44][5]. This approach although based on the assumption that the contribution to the non adiabatic behavior is due to the first minimum gap only, is quite more general, bypassing the knowledge of critical exponents and dimension, and focusing the attention only on the spectral properties of the system: the path dependence of the critical exponents is directly taken in account by the spectrum shape close to the anticrossing point.

[4]Here m denotes the number of directions orthogonal to the critical surface.

[5]It should be stressed that in presence of a BKT transition, in which it is not possible to identify a dominant gap[25, 26], an effective theory is still lacking.

Chapter 2

Adiabatic quantum dynamics of a random Ising chain

2.1 Introduction

In this Chapter the adiabatic dynamics in a one-dimensional quantum disordered Ising model in a transverse field is analyzed. The reasons for considering this problem are various. First of all it is an important test for the effectiveness of QA-AQC method in presence of disorder. The randomness of the coupling can produce extremely low excitations over the instantaneous ground state not only nearby the critical point, as pointed out in the Introduction, but also in extended regions as in presence of Griffith's phases[13, 35]. It is well established that the effects of disorder strongly weaken the performances of QA-AQC for single instances of NP-complete problems[7] or single realizations of bidimensional quantum spin-glasses[9]; but the definitive evidence of the ineffectivity of the technique in presence of randomness is still argument of debate. For this purpose the random Ising chain constitutes an ideal ground: it is solvable, so totally under control, and it is easily simulatable. The latter condition allows for the analysis of large systems, reducing the influence of finite size effects, and for the statistical study of its properties averaged over a large number of disorder configurations. In addition, although in a very simplified manner, it may help in understanding more interesting problems that can be formulated in terms of interacting Ising spins, the Traveling Salesman problem[45] and Satisfiability[46] problem being only two well-known examples. The simplicity of our test problem lies in the particularly

simple geometry of the interactions, which forbids frustration. The only ingredient that our problem shares with more challenging computational tasks is the fact that the interactions are chosen to be random. This feature, the presence of disorder, makes the problem interesting and non-trivial for a physically inspired computational approach based on QA-AQC. Lastly it can be used as further test of the prediction of the KZM-perturbative scaling of Eq(1.15) and Eq(1.31).

In this Chapter the anomalously slow dynamics characterized by an average density of kinks, which vanishes only logarithmically with the annealing rate, is presented[19, 20]. Moreover a detailed analysis of the statistics of both the residual energy and kink density is presented. In a disordered chain, the formation of kinks is no longer translational invariant and therefore it affects in a non-trivial way, as it will be shown below, the scaling of the residual energy.

The rest of the Chapter is organized as follows: In Sec. 2.2 the problem and the technique to solve the its adiabatic dynamics are defined. Next, in Sec. 2.3, are introduced the quantities — residual energy and density of defects — that are calculated to quantify the departure from the adiabatic ground state. In Sec. 2.4 numerical results for both these quantities are presented, together with an analysis of the large-annealing-time behavior of the density of defects, based on the Landau-Zener theory, explicitly showing the slow dynamics which the disorder entails.

2.2 The model

The one-dimensional random Ising model is defined by the Hamiltonian

$$H(t) = -\sum_i J_i \sigma_i^z \sigma_{i+1}^z - \Gamma(t) \sum_i h_i \sigma_i^x \ . \tag{2.1}$$

where σ_i^α ($\alpha = x, z$) are Pauli matrices for the i-th spin of the chain, J_i are random couplings between neighboring spins, and h_i are random transverse fields. The time-dependent function $\Gamma(t)$ rescaling the transverse field term allows to drive the system from a region of infinitely high transverse fields ($\Gamma = \infty$, where the ground state has all spins aligned along x, see below), to the case of a classical Ising model ($\Gamma = 0$). Specifically, in the following $\Gamma(t)$ will be taken to be a linear

function of time characterized by an annealing rate τ^{-1}

$$\Gamma(t) = -\frac{t}{\tau} \qquad \text{for } t \in (-\infty, 0] \ .$$

In one-dimension, and for nearest-neighbor couplings, there is no frustration associated to the random nature of the couplings J_i: by appropriately performing spin rotations of π along the x-spin axis, it is always possible to change the desired σ_i^z into $-\sigma_i^z$ and invert accordingly the signs of the couplings in such a way that all J_i's turn out to be non-negative. Therefore it is assumed that the J_i are randomly distributed in the interval $[0, 1]$, specifically with a flat distribution $\pi[J] = \theta(J)\theta(1 - J)$, where θ is the Heaviside function. The same distribution is used for the random field $\pi[h] = \theta(h)\theta(1 - h)$. This is different from the model considered in Ref.[19], where the disorder was introduced in the exchange coupling only. The present choice is found quite convenient since, by duality arguments [35], the critical point separating the large-Γ quantum paramagnetic phase from the low-Γ ferromagnetic region is exactly known to be located at $\Gamma_c = 1$.

At the initial time $t_{\rm in} = -\infty$ the ground state of $H(t_{\rm in})$, completely dominated by the transverse field term, is simply the state with all spins aligned along the $+\hat{x}$ spin direction: $|\Psi_{\rm in}\rangle = \prod_i |\hat{x}\rangle_i = \prod_i [|\uparrow\rangle_i + |\downarrow\rangle_i]/\sqrt{2}$. On the other side of the transition point Γ_c, the final Hamiltonian $H(t_{\rm fin}) = H_{cl}$ describes a *random ferromagnet* whose ground states, which are the targets to be reached by adiabatically switching off $\Gamma(t)$, are obviously the two trivial states $|\Psi_\uparrow\rangle = \prod_i |\uparrow\rangle_i$ and $|\Psi_\downarrow\rangle = \prod_i |\downarrow\rangle_i$: as an optimization problem, $H_{\rm fin}$ represents, therefore, a trivial problem.

Even if the ground states in the two limiting cases, $\Gamma = \infty$ and $\Gamma = 0$, are very easy to find, when it comes to dynamics, the evolution dictated by $H(t)$ is no longer a trivial problem. The instantaneous spectrum of the Hamiltonian $H(t)$ is gapless in the thermodynamic limit [35]. This implies that, during the adiabatic evolution, defects in the form of domain walls between differently aligned ferromagnetic ground states, of the type

$$|\ldots\uparrow\downarrow\downarrow\downarrow\downarrow\uparrow\uparrow\uparrow\uparrow\uparrow\uparrow\uparrow\uparrow\downarrow\downarrow\downarrow\downarrow\ldots\rangle$$

are formed, and reflected in a whole structure of closing gaps will appear in the instantaneous spectrum.

2.2.1 Fermion representation and Bogoliubov-de Gennes equations

By means of the Jordan-Wigner transformation, the one-dimensional Ising model is reduced to a free fermion model. One first writes the spin operators in terms of hard-core bosons a_i and $a_i^\dagger$ in a representation that maps the state $|\sigma_i^z = +1\rangle \rightarrow |1\rangle_i = a_i^\dagger|0\rangle_i$ and $|\sigma_i^z = -1\rangle \rightarrow |0\rangle_i$, with the hard-core constraint $(a_i^\dagger)^2|0\rangle_i = 0$: $\sigma_i^z = 2a_i^\dagger a_i - 1$, $\sigma_i^x = a_i + a_i^\dagger$, and $\sigma_i^y = -i(a_i^\dagger - a_i)$. The hard-core boson operators a_i are then re-expressed in terms of spinless fermions operators c_i: $a_i = e^{i\pi\sum_{j<i} c_j^\dagger c_j} c_i$. After a $\pi/2$ rotation around the y-axis, which maps $\sigma^x \rightarrow \sigma^z$ and $\sigma^z \rightarrow -\sigma^x$, the Hamiltonian in Eq(2.1) can be rewritten in terms of fermion operators as

$$H = -\sum_i^{L-1} J_i\{c_i^\dagger c_{i+1}^\dagger + c_i^\dagger c_{i+1} + \text{H.c.}\} - 2\Gamma\sum_i^L h_i c_i^\dagger c_i \ , \tag{2.2}$$

where open boundary conditions (OBC) for the spin-chain have been assumed. For the case of periodic boundary conditions (PBC) on the spins, $\sigma_{L+1} = \sigma_1$, extra boundary terms appear in the fermionic Hamiltonian, of the form $\Delta H_{\text{PBC}} = J_L(-1)^{N_F}\{c_L^\dagger c_1^\dagger + c_L^\dagger c_1 + \text{H.c.}\}$, where $N_F = \sum_i c_i^\dagger c_i$ is the total number of fermions. Notice that although N_F is not conserved by the Hamiltonian (2.2), the parity of N_F is conserved because fermions are created (destroyed) in pairs, like in a BCS model: $(-1)^{N_F}$ is a constant of motion with value 1 or -1.

The model in Eq(2.2) can be diagonalized through a Bogoliubov rotation [47, 48], by introducing the new fermionic operators γ_μ and $\gamma_\mu^\dagger$

$$\begin{aligned} \gamma_\mu &= \sum_{j=1}^L (u_{j\mu}^* c_j + v_{j\mu}^* c_j^\dagger) \\ c_i &= \sum_{\mu=1}^L (u_{i\mu}\gamma_\mu + v_{i\mu}^*\gamma_\mu^\dagger) \ , \end{aligned} \tag{2.3}$$

where the L-dimensional vectors $\mathbf{u}_\mu$ and $\mathbf{v}_\mu$, for $\mu = 1, \cdots, L$, satisfy the Bogoliubov-de Gennes equations:

$$\begin{aligned} A\cdot\mathbf{u}_\mu + B\cdot\mathbf{v}_\mu &= \epsilon_\mu \mathbf{u}_\mu \\ -B\cdot\mathbf{u}_\mu - A\cdot\mathbf{v}_\mu &= \epsilon_\mu \mathbf{v}_\mu \ . \end{aligned} \tag{2.4}$$

Here A and B are real $L \times L$ matrices whose non-zero elements are given by $A_{i,i} = -\Gamma h_i$, $A_{i,i+1} = A_{i+1,i} = -J_i/2$, $B_{i,i+1} = -B_{i+1,i} = -J_i/2$. (For the PBC spin-chain case, we have the additional matrix elements $A_{L,1} = A_{1,L} = (J_L/2)(-1)^{N_F}$, and $B_{L,1} = -B_{1,L} = (J_L/2)(-1)^{N_F}$). While in the ordered case the solution of Eqs(2.4) can be reduced, by switching to momentum-space, to independent 2×2 problems, in the general disordered case one has to diagonalize the $2L \times 2L$ problem numerically in Eq(2.4) [49, 50].

The spectrum of Eqs(2.4) turns out to be given by $\pm\epsilon_\mu$, with $\epsilon_\mu \geq 0$, and in terms of the new fermion operators, H becomes:

$$H = \sum_{\mu=1}^{L} (\epsilon_\mu \gamma_\mu^\dagger \gamma_\mu - \epsilon_\mu \gamma_\mu \gamma_\mu^\dagger) = \sum_{\mu=1}^{L} 2\epsilon_\mu (\gamma_\mu^\dagger \gamma_\mu - \frac{1}{2}) \; . \tag{2.5}$$

The ground state of H is the Bogoliubov vacuum state $|\Psi_0\rangle$ annihilated by all γ_μ for $\mu = 1 \cdots L$, $\gamma_\mu |\Psi_0\rangle = 0$, with an energy $E_0 = -\sum_{\mu=1}^{L} \epsilon_\mu$.

2.2.1.1 Dynamics

The Schrödinger dynamics associated to a time-dependent $H(t)$ can be solved by a time-dependent Bogoliubov theory [51]. The basic fact that makes the solution possible even in the time-dependent case is that the Heisenberg's equations of motion for the operators $c_{i,H}(t)$ are *linear*, because the Hamiltonian is quadratic:

$$i\hbar \frac{d}{dt} c_{i,H}(t) = 2 \sum_{j=1}^{L} \Big[A_{i,j}(t) c_{j,H}(t) + B_{i,j}(t) c_{j,H}^\dagger(t) \Big] \; . \tag{2.6}$$

Here the matrices A and B have the same form given previously, except that now the time-dependence of $\Gamma(t)$ is explicitly accounted for. If $\gamma_{\mu,\mathrm{in}}$ denote the Bogoliubov operators that diagonalize $H(t_{\mathrm{in}})$ at the initial time, and $\mathbf{u}_\mu^{\mathrm{in}}$, $\mathbf{v}_\mu^{\mathrm{in}}$ the corresponding initial eigenvectors, it is simple to verify that the *Ansatz*

$$c_{i,H}(t) = \sum_{\mu=1}^{L} \Big(u_{i\mu}(t) \gamma_{\mu,\mathrm{in}} + v_{i\mu}^*(t) \gamma_{\mu,\mathrm{in}}^\dagger \Big) \; , \tag{2.7}$$

does indeed solve the Heisenberg equations (2.6), provided the time-dependent coefficients $u_{i\mu}(t)$ and $v_{i\mu}(t)$, satisfy the following system of first-order differential

equations

$$
\begin{aligned}
i\frac{d}{dt}u_{i\mu}(t) &= \frac{2}{\hbar}\sum_{j=1}^{L}\left[A_{i,j}(t)u_{j\mu}(t)+B_{i,j}(t)v_{j\mu}(t)\right] \\
i\frac{d}{dt}v_{i\mu}(t) &= -\frac{2}{\hbar}\sum_{j=1}^{L}\left[A_{i,j}(t)v_{j\mu}(t)+B_{i,j}(t)u_{j\mu}(t)\right] \ ,
\end{aligned}
\tag{2.8}
$$

with initial condition $u_{i\mu}(t_{\rm in}) = u^{\rm in}_{i\mu}$, $v_{i\mu}(t_{\rm in}) = v^{\rm in}_{i\mu}$. Eqs(2.8) are the natural time-dependent generalizations of the static Bogoliubov-de Gennes Eqs(2.4), and, once again, they have to be solved numerically in the general disordered case.

2.3 Residual energy and kink density

How effectively the Schrödinger dynamics drives the system from the initial disordered quantum ground state $|\Psi_{\rm in}\rangle$ towards the classical ground state $|\Psi_{\uparrow}\rangle = \prod_i |\uparrow\rangle_i$ (or the fully reversed one $|\Psi_{\downarrow}\rangle = \prod_i |\downarrow\rangle_i$)?
The two most natural way of quantifying the degree of adiabaticity in the random Ising chain are the residual energy of Eq(1.8) and kinks density of Eq(1.10).
When no disorder is present the two quantities coincide, apart from trivial constants. In the disordered case, however, this is not the case. A defect will form with higher probability at a link where the corresponding exchange coupling J_i is small. Therefore the residual energy is not simply given by the kink density times the exchange coupling.

The calculation of quantities like $E_{\rm fin}$ or ρ_k is straightforward. Quite generally, given an operator $\hat{O}(c_i, c_i^\dagger)$ expressed in terms of the c_i's and $c_i^\dagger$'s, its expectation value over the final state $|\Psi(t_{\rm fin}=0)\rangle$ can be expressed, switching from the Schrödinger to the Heisenberg picture, as

$$
\langle\Psi(0)|\hat{O}(c_i,c_i^\dagger)|\Psi(0)\rangle = \langle\Psi(t_{\rm in})|\hat{O}(c_{i,H}(0),c_{i,H}^\dagger(0))|\Psi(t_{\rm in})\rangle. \tag{2.9}
$$

Next, one uses the expressions (2.7) for the $c_{i,H}(0)$'s and $c^\dagger_{i,H}(0)$ in terms of $\gamma_{\mu,in}$, $\gamma^\dagger_{\mu,in}$, $u_{i,\mu}(0)$, and $v_{i,\mu}(0)$, and uses the fact that the $\gamma_{\mu,in}$ annihilates by construction the initial state $|\Psi(t_{\rm in})\rangle$. By applying this procedure to the calculation of $E_{\rm fin}$ it

turns out:

$$E_{\rm fin} = \sum_{i,j} \Big(A_{ij}(0) \left[v(0)v^\dagger(0) - u(0)u^\dagger(0) \right]_{ij} + B_{ij}(0) \left[v(0)u^\dagger(0) - u(0)v^\dagger(0) \right]_{ij} \Big) \ , \tag{2.10}$$

where $u(0)$ and $v(0)$ are $L \times L$ matrices with elements $u_{i,\mu}(0)$ and $v_{i,\mu}(0)$. Similarly, the density of defects ρ_k can be expressed as:

$$\rho_k = \frac{1}{2L} \sum_{i}^{L-1} \left\{ 1 - \left(\left[v(0) - u(0) \right] \left[u^\dagger(0) + v^\dagger(0) \right] \right)_{i,i+1} \right\} \ . \tag{2.11}$$

2.4 Results

The results for the dynamics are obtained by integrating numerically the time-dependent Bogoliubov-de Gennes equations (2.8). As initial point of the evolution it is enough to consider $t_{\rm in} = -5\tau$, taking $\mathbf{u}_\mu^{\rm in}$ and $\mathbf{v}_\mu^{\rm in}$ from the diagonalization of $H(t_{\rm in})$ according to Eq(2.4): it has been checked that the results do not depend on the precise value of $t_{\rm in}$, as long as it is not too small. Systems up to $L = 512$ and annealing times up to $\tau = 1000$ have been considered. Ensemble averages are calculated over a suitably large number of disorder realizations (of the order of 1000). The analysis of the instantaneous spectrum and its statistics has been obtained by solving the static Bogoliubov-de Gennes eigenvalue equations (2.4) for systems up to $L = 512$ (with a huge number of disorder realizations, of order 10^6).

In order to get an initial understanding on the mechanism that leads to breaking of adiabaticity in the present system, it is instructive to consider in more detail the time-evolution of a single realization of the disorder. To be specific, Fig.(2.1) shows the time-evolution of the residual energy for a single $L = 64$ sample and for values of τ up to 5000. The instantaneous spectral gaps of the problem are also plotted (thick solid lines), obtained by diagonalizing the Hamiltonian for any given value of the parameter Γ. As mentioned previously, the dynamics conserves the fermion parity, so that only excitations in the same fermion parity sector are accessible. If the single-particle eigenvalues are ordered as $\epsilon_1 \leq \epsilon_2 \leq \cdots \leq \epsilon_L$, then the lowest excited state accessible to the dynamics (i.e., conserving the fermionic parity) is associated with an excitation energy $\Delta_1 = 2(\epsilon_1 + \epsilon_2)$, rather than $\Delta = 2\epsilon_1$. The

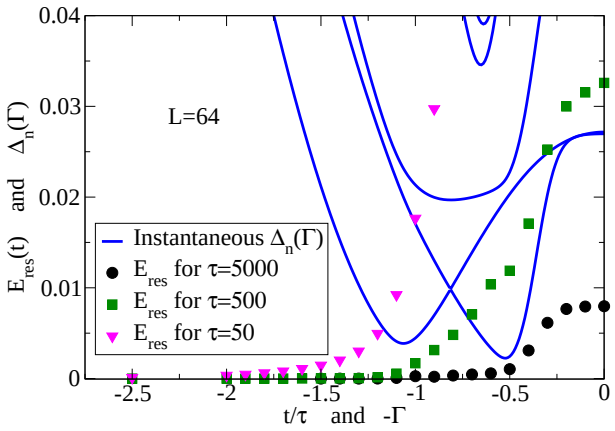

FIGURE 2.1: (Color online) Residual energy $E_{\rm res}(t)$ versus t for a given instance with $L = 64$ of the random Ising model with transverse field, at different values of τ. The solid lines are the lowest-lying instantaneous spectral gaps Δ_n as a function of Γ.

next excited state is $\Delta_2 = 2(\epsilon_1 + \epsilon_3)$, and so on. These are the instantaneous gaps shown in Fig.(2.1).

An important feature which emerges from this example is that one cannot in general locate a single specific value of Γ where the minimum and most important gap is present. Certainly, typically the first occurrence of a small gap during the annealing trajectory is close to the critical point, $\Gamma_c = 1$. Usually, this critical-point gap is also the smallest one that the systems encounters during its evolution. However, it can happen, as Fig.(2.1) shows, that the system safely goes through the critical-point small gap (see $\tau = 5000$ results) but then looses adiabaticity due to a comparable gap encountered later on (here at $\Gamma \sim 0.5$). Once adiabaticity is lost, the system will generally miss to follow the first excited state either, getting more and more excited as time goes by.

The energy landscape sketched in Fig.(2.1) is strongly dependent on the particular configuration of couplings and fields adopted in the simulation. In order to give a general description of the issue, as the treatment of the statical properties done in Ref[35, 49] has shown, the analysis of the adiabatic dynamics of a disordered Ising chain requires a knowledge of the statistics of these low-lying gaps in the spectrum (in the pertinent parity sector). The attention has been concentrated on the region close to the critical point, where the smallest gaps are found, for large L. The first question is how these smallest gaps are distributed, for different realizations of the disorder. Let denote by $P(\Delta_1, L)$ the distribution of gaps $\Delta_1 = 2(\epsilon_1 + \epsilon_2)$ (the lowest one relevant for the dynamics) for a chain of length L, assumed to be normalized: $\int_0^\infty d\Delta_1 \; P(\Delta_1, L) = 1$. For the smallest gap $\Delta = 2\epsilon_1$, Young

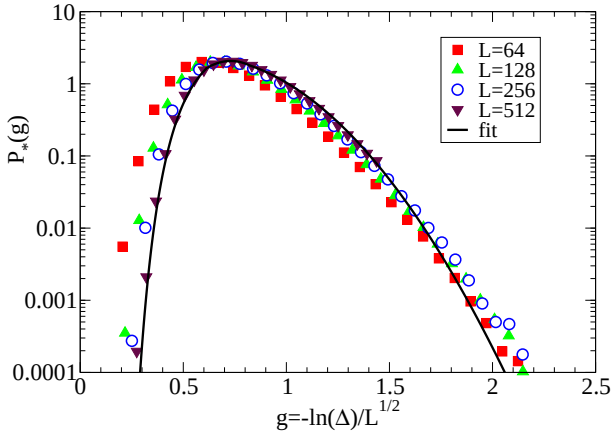

FIGURE 2.2: (Color online) Distribution of $\Delta_1 = 2(\epsilon_1 + \epsilon_2)$, the smallest gap relevant for the dynamics, at the critical point $\Gamma_c = 1$ for different systems sizes, showing the collapse of the distributions $P(\Delta_1, L)$ when the scaling variable $g = -\log(\Delta_1)/\sqrt{L}$ is used. The resulting distribution is the $P_*(g)$ discussed in the text.

and Rieger [49] have shown that the correct scaling variable which makes the critical point distribution universal, for different L, is $-\log(\Delta)/\sqrt{L}$. By using a scaling variable of the same form, $g = -\log(\Delta_1)/\sqrt{L}$, it can be seen that the gaps Δ_1 are also distributed in the same universal way, see Fig.(2.2). This implies that at the critical point, $P_*(g) = \sqrt{L}e^{-g\sqrt{L}}P(e^{-g\sqrt{L}}; L)$ is, for large L, universal and normalized. As a consequence, gaps at the critical point have an extremely wide distribution, for large L, with typical gaps which are exponentially small [35, 49, 50] in the system size: $[\Delta_1]_{\rm typ} \propto e^{-C\sqrt{L}}$.

2.4.1 Density of kinks

Given the wide distribution of the instantaneous gaps, it is important to understand how this reflects itself in the distribution of various observables. First the behavior of the density of defects ρ_k defined in Eq(1.10) has been considered. The results for the probability distribution function of ρ_k, $P(\rho_k)$, are presented in Fig.(2.3) for $\tau = 10$ and $\tau = 1000$. The distribution $P(\rho_k)$, for given τ, is found to be approximately log-normal:

$$P(\rho_k) = \frac{1}{\sqrt{2\pi}\sigma_L}\,\frac{1}{\rho_k}\,e^{-\left(\ln\rho_k - \overline{\ln\rho_k}\right)^2/2\sigma_L^2}\,,$$

with a standard deviation σ_L decreasing as $1/\sqrt{L}$. The data collapse of the results for different L, in terms of the variable $(\ln\rho_k - \overline{\ln\rho_k})/\sigma_L$, shown in the inset,

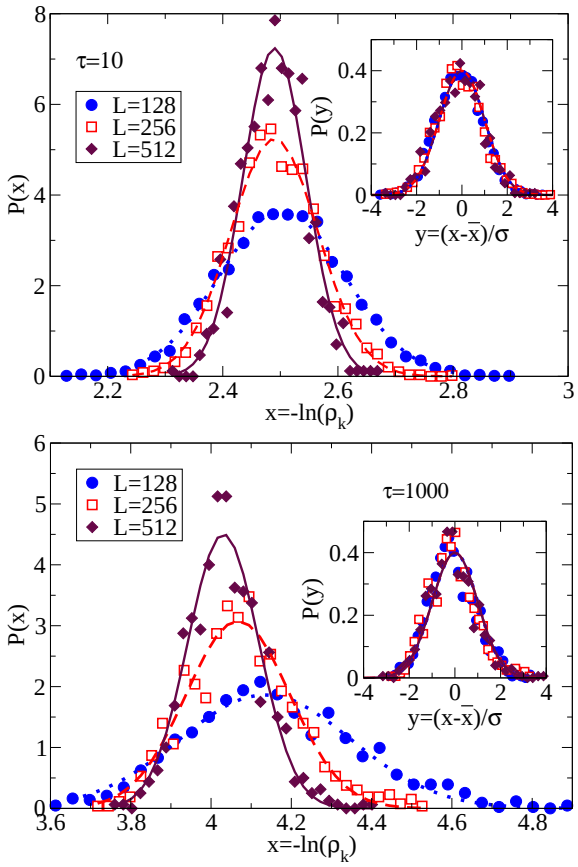

FIGURE 2.3: (Color online) Probability distribution for the logarithm of the density of defects $x = -\ln \rho_k$, for two different annealing rates τ. The distribution function is universal and log-normal with a variance σ_L which scales as $1/\sqrt{L}$. In the insets we show the data collapse of all the curves when plotted as a function of the reduced variable $(x - \bar{x})/\sigma_L$, where $x = -\ln \rho_k$.

qualifies the accuracy of this statement. This $\sqrt{L}$-reduction of the width of the log-normal distribution $P(\rho_k)$ with increasing L is at variance with the result obtained for the distribution of the gaps at the critical point, whose width *increases* as $\sqrt{L}$: here, on the contrary, the correct scaling variable appears to be $(\ln \rho_k - \overline{\ln \rho_k})\sqrt{L}$, rather than $(\ln \rho_k - \overline{\ln \rho_k})/\sqrt{L}$. This width reduction, for increasing L, implies that the *average* density of defects $[\rho_k]_{\rm av}$ approaches the *typical* value $[\rho_k]_{\rm typ} = e^{[\ln \rho_k]_{\rm av}}$ for large enough L, since $[\rho_k]_{\rm av} = e^{\overline{\ln \rho_k} + \sigma_L^2/2}$ implies that:

$$\frac{[\rho_k]_{\rm av} - [\rho_k]_{\rm typ}}{[\rho_k]_{\rm typ}} = e^{\sigma_L^2/2} - 1 \sim \frac{1}{L} \, . \tag{2.12}$$

This fact is shown explicitly in Fig.(2.4) (top), where it can be seen that large deviations between $[\rho_k]_{\rm typ} = e^{[\ln \rho_k]_{\rm av}}$ and $[\rho_k]_{\rm av}$ are seen only for $L \leq 64$. For large systems, $L \geq 128$, the two quantities are essentially coincident, for all values

of τ. Despite the universal behavior of the distribution $P(\rho_k)$ at all annealing rates, the behavior of $[\rho_k]_{\rm av}(\tau)$ changes drastically between short and long τ's [19]. Fig.(2.4)(bottom) focuses on the average kink density $[\rho_k]_{\rm av}$ for various L, as a function of τ. The initial small-τ behavior of $[\rho_k]_{\rm av}(\tau)$, indicated by the dashed line in Fig.(2.4), seems a power-law, $[\rho_k]_{\rm av}(\tau) \sim \tau^{-0.5}$, i.e., exactly what one finds for the ordered Ising chain [15], where the result is interpreted in terms of the Kibble-Zurek mechanism. A possible explanation resides in the fact that the model presents a Griffiths phase extending for all $\Gamma > \Gamma_c$ [52]. This phase is characterized by a gap $\Delta \sim L^{-z}$, where the dynamical exponent $z(\Gamma)$ is a continuous function of the parameter Γ, diverging, $z \to \infty$, for $\Gamma \to \Gamma_c$, while saturating to a constant for large Γ. The second gap, which is relevant for our dynamical problem, shows a similar behavior,[52] $\Delta_1 \sim L^{-z'}$, with a dynamical exponent $z'(\Gamma) = z(\Gamma)/2$. For fast annealing rates, the system loses adiabaticity before reaching the critical point, well inside the $\Gamma > \Gamma_c$ Griffiths phase. As in the ordered case, the gaps exhibited by such a phase would induce a defect density decreasing as a power-law of the annealing time τ, with the crucial difference that the power-law exponent is not constant here, due to the Γ-dependence of z'. One should expect, presumably, a gradual crossover with a power-law exponent which becomes smaller and smaller, connecting in a gentle way with the large τ behavior of $[\rho_k]_{av}$, which shows marked deviations from a power-law behavior. Dziarmaga, based on scaling arguments [19], showed that at large τ the density of kinks should decrease as the inverse square of the logarithm of τ. Our data for the largest systems agree very well with this prediction (solid line in Fig.(2.4)).

A bound to $[\rho_k]_{\rm av}(\tau)$ can also be constructed by a Landau-Zener argument — complemented by a knowledge of the distribution of the first gap $P(\Delta_1, L)$ —, in a similar fashion to that presented by Zurek *et al.* [15] for the ordered Ising case. The derivation starts by considering the probability $P_{\rm ex}(\tau, L)$ of loosing adiabaticity for a system of size L, when turning off Γ with an annealing rate τ^{-1}. Evidently, $P_{\rm ex}(\tau, L) \geq P_{\rm ex}^{\rm cr.point}(\tau, L)$, where by $P_{\rm ex}^{\rm cr.point}(\tau, L)$ has been denoted the probability of getting excited by Landau-Zener events *at the critical point* (indeed, it has been shown that there is a chance of getting excited also by gaps well below the critical point). $P_{\rm ex}^{\rm cr.point}(\tau, L)$, in turn, can be constructed by knowing the distribution of the gaps Δ_1 at the critical point, and the simple two-level Landau-Zener formula $P_{\rm ex}^{\rm LZ} = e^{-\pi\Delta_1^2\tau/(4\hbar\alpha)}$ (α being the slope of the two approaching eigenvalues). Lumping all constants together, $\gamma = \pi/(4\hbar\alpha)$, it can be written $P_{\rm ex}^{\rm LZ} = e^{-\gamma\tau\Delta_1^2}$ and it can be assumed that the distribution of $\gamma \propto \alpha^{-1}$ is not important in the estimate,

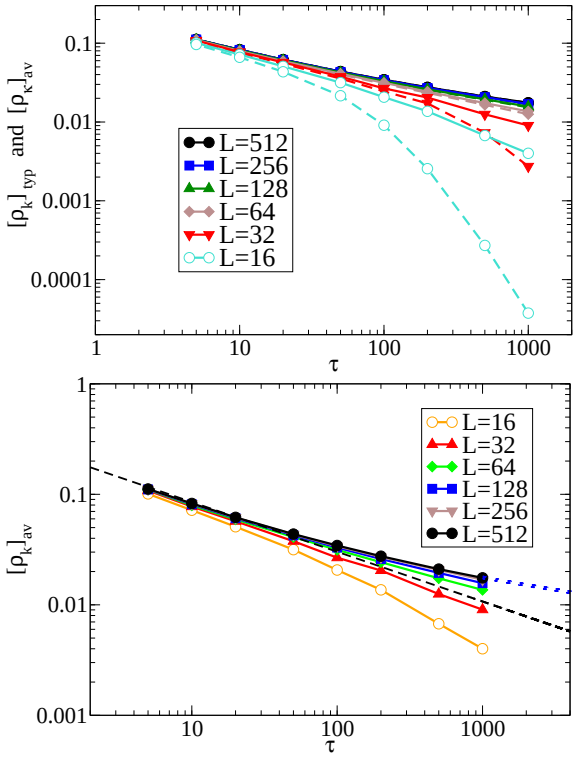

FIGURE 2.4: (Color online) Top: Comparison between average $[\rho_k]_{\rm av}$ and typical $[\rho_k]_{\rm typ} = e^{[\ln \rho_k]_{\rm av}}$ kink density for different system sizes on varying the annealing rate τ. The same symbol is used for both cases. The typical value (dashed line) lies always below the average value (continuous line), but the difference between the two is negligible for $L \geq 128$. Bottom: Average kink density $[\rho_k]_{\rm av}$ as a function of the annealing rate τ for chains of different lengths $L = 16, 32, 64, 128, 256, 512$. The data for $[\rho_k]_{\rm av}$ are the same appearing in the top part of the figure. The dashed line is a power-law describing the small-τ behavior, $[\rho_k]_{\rm av}(\tau) \sim \tau^{-0.5}$. The solid thick line through the $[\rho_k]_{\rm av}$ data is a fit with a function $A/\log^2(\gamma\tau)$, described in the text. The averages are calculated over 1000 different realizations of disorder.

while that of Δ_1 is, so that:

$$\begin{aligned} P_{\rm ex}^{\rm cr.point}(\tau, L) &= \int_0^\infty d\Delta_1 \; P(\Delta_1, L)\, e^{-\gamma\tau\Delta_1^2} \\ &= \int_{-\infty}^\infty dg \; P_*(g)\, e^{-\gamma\tau e^{-2\sqrt{L}g}} \,, \end{aligned} \tag{2.13}$$

where the second equality follows from switching to the scaling variable $g = -\log(\Delta_1)/\sqrt{L}$. Obviously, for $\tau = 0$ it is correctly obtained $P_{\rm ex}^{\rm cr.point}(\tau = 0, L) = \int_{-\infty}^{\infty} dg \;\; P_*(g) \;=\; 1$, from the normalization condition. When τ is finite, the LZ factor $e^{-\gamma\tau e^{-2\sqrt{L}g}}$ provides a lower cut-off in the integral at a characteristic $g_c = \log(\gamma\tau)/(2\sqrt{L})$, and this cut-off is sharper and sharper as L increases: one can verify that, for large L, $e^{-\gamma\tau e^{-2\sqrt{L}g}} \approx \theta(g - g_c)$. As a consequence, for large

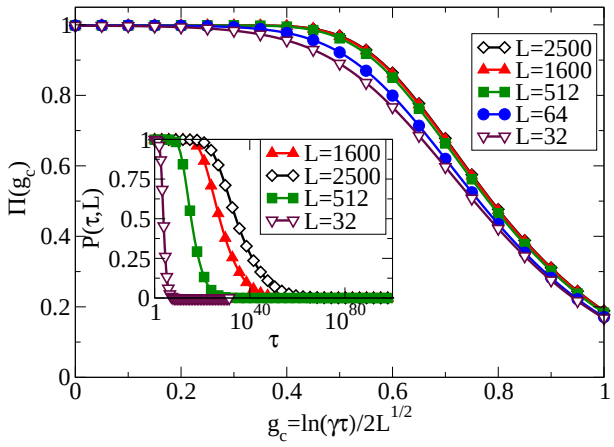

FIGURE 2.5: (Color online) Approach to the universal function $\Pi(g_c)$ for increasing chain lengths L, see text. All data from $L \geq 512$ collapse well into a single curve. Inset: $P_{\rm ex}^{\rm cr.point}(\tau, L)$ obtained from the integral in Eq(2.13) versus τ for different values of L.

enough L it can be rewritten:

$$P_{\rm ex}^{\rm cr.point}(\tau, L) \approx \Pi\left(g_c\right) \equiv \int_{g_c}^{\infty} dg\ P_*(g)\ , \tag{2.14}$$

i.e., $P_{\rm ex}^{\rm cr.point}(\tau, L)$ turns out to be a universal function of the scaling variable $g_c = \log\left(\gamma\tau\right)/(2\sqrt{L})$, for L large. This universal function $\Pi(g_c)$ is shown in Fig.(2.5), where it can be seen that data for $L \geq 512$ collapse into a single curve. The density of kinks for large τ, and large enough L, can be obtained by evaluating the typical length $\tilde{L}_\epsilon(\tau)$ of a defect-free region upon annealing, ϵ being a small quantity of our choice, denoting the probability of getting excited. Since $P_{\rm ex}^{\rm cr.point}(\tau, L) \approx \Pi(g_c)$ is a *lower bound* for $P_{\rm ex}(\tau, L)$, it turns out that

$$\tilde{L}_\epsilon(\tau) \leq \frac{\log^2\left(\gamma\tau\right)}{[\Pi^{-1}(\epsilon)]^2}\ , \tag{2.15}$$

where Π^{-1} denotes the inverse function of Π. If now the inverse of the defect-free region length, $\tilde{L}_\epsilon^{-1}(\tau)$, is identified with the density of kinks $\rho_k(\tau)$, the following lower bound is given for the latter:

$$\rho_k(\tau) \sim \frac{1}{\tilde{L}_\epsilon(\tau)} \geq \frac{[\Pi^{-1}(\epsilon)]^2}{\log^2\left(\gamma\tau\right)}\ . \tag{2.16}$$

On the basis of this argument, it can be concluded that the density of kinks cannot decrease faster than $1/\log^2\left(\gamma\tau\right)$ for large τ, which agrees with the argument discussed by Dziarmaga [19].

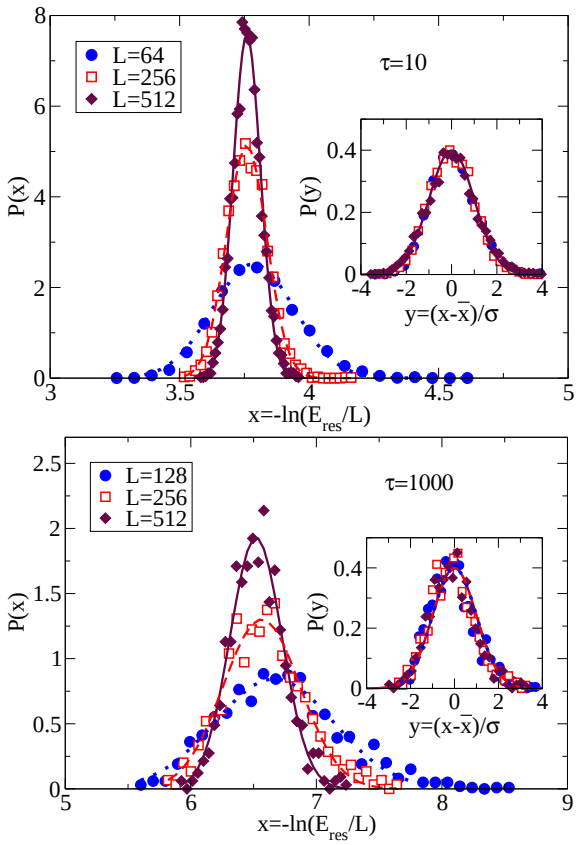

FIGURE 2.6: (Color online) Probability distribution for the residual energy per site at two different annealing rates τ^{-1}. The distribution function is universal and log-normal with a variance which scales as $1/\sqrt{L}$. In the insets we show the data collapse.

2.4.2 Residual energy

In the ordered case the residual energy per spin is simply proportional to the kink-density, $E_{\rm res}/L = 2J\rho_k$, while here, evidently, kinks sitting at small J_i's are favored, on average, by the adiabatic evolution process. It is therefore of importance to analyze the scaling of the residual energy that, as it will be shown, differs quantitatively from that of the kink density. Since kinks will be formed on the weak links, one expects on general grounds that the residual energy would decay faster than the kink-density for large τ's.

As in the case of the kink density, first the probability distribution for the residual energy per site is analyzed, which is presented in Fig.(2.6). Once again the residual energies are approximately log-normal distributed and can be reduced to a universal form (see the insets) when properly rescaled, i.e., in terms of the variable $(\ln(E_{\rm res}/L) - \overline{\ln(E_{\rm res}/L)})\sqrt{L}$.

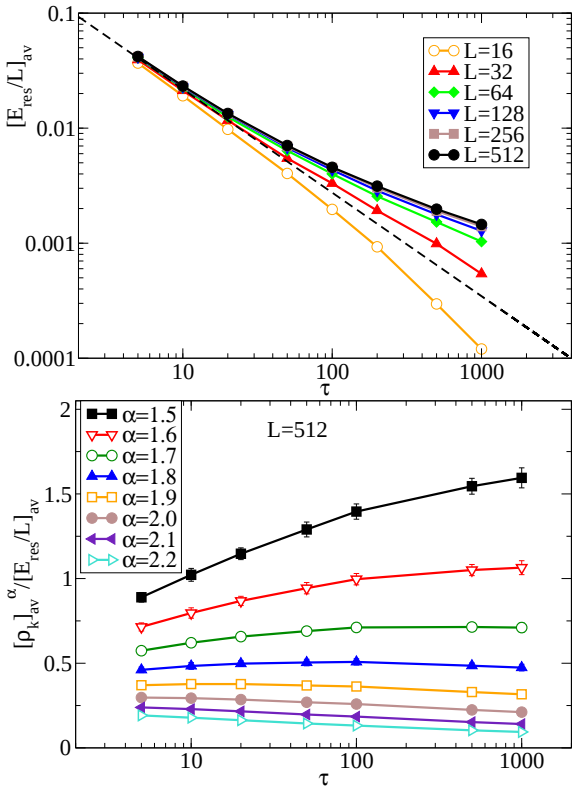

FIGURE 2.7: (Color online) Top: Average residual energy per site $[E_{\rm res}/L]_{\rm av}$ as functions of the annealing rate τ for chains of different lengths $L = 16, 32, 64, 128, 256, 512$. The dashed line is the power-law describing the small-τ behavior, $[E_{\rm res}/L]_{\rm av}(\tau) \sim \tau^{-1}$. Averages are calculated over 1000 realizations of disorder. Bottom: The ratio of the density of kinks and the residual energy versus τ, used to extract the power of the log-dependence of E_{res}.

The average residual energy per site $[E_{\rm res}/L]_{\rm av}$ as a function of the annealing time τ shows a crossover from a power-law decay, approximately τ^{-1} for fast quenches, to a much slower decay (see below) for slow evolutions. It is interesting to note that although for fast quenches the disorder is considered to play a minor role, nevertheless the exponent of the decay of the residual energy differs from that of the kink density. The analysis of the regimes of large τ's is more delicate. The LZ argument given above tells nothing about the behavior of the residual energy for large τ. Then a possible procedure is the following. Assuming for the residual energy a logarithmic behavior similar to that found for ρ_k

$$\left[\frac{E_{\rm res}}{L}\right]_{\rm av} \sim \frac{1}{\log^{\zeta}(\gamma\tau)}\ , \tag{2.17}$$

ζ can be determined from the data of Fig.(2.7)(Top) by plotting the ratio of $[\rho_k]^{\alpha}_{\rm av}$ and $[E_{\rm res}/L]_{\rm av}$ versus τ for several values of α, as done in Fig.(2.7)(Bottom). If

$[\rho_k]_{\rm av} \sim \log^{-2}(\gamma\tau)$, then the value of α which makes this ratio constant is:

$$\frac{[\rho_k]^{\alpha}_{\rm av}}{[E_{\rm res}/L]_{\rm av}} \propto \log^{\zeta-2\alpha}(\gamma\tau) \sim \text{const.} \iff \alpha = \zeta/2 \,. \tag{2.18}$$

Numerically, see Fig.(2.7), we find $\alpha \approx 1.7 \pm 0.1$, which implies $\zeta \approx 3.4 \pm 0.2$.

Chapter 3

Adiabatic quantum dynamics of the Lipkin-Meshkov-Glick model

3.1 Introduction

Most of the work done so far in the search for a deeper understanding of the loss of adiabaticity on crossing a quantum critical point concentrated on one-dimensional quantum systems with short range interaction. In this Chapter a complementary limit is addressed, i.e. a model with infinite coordination (in the thermodynamic limit), but still amenable to an exact solution: the Lipkin-Meschkov-Glick model (LMG). First introduced by Lipkin, Meschkov and Glick [53] in the context of nuclear physics, it was then adopted by the condensed matter community as paradigm of an infinitely coordinated solvable system [54]. The result of a sudden quench in this model was recently discussed in [55], here results in the opposite regime in which the system is dragged adiabatically through the critical point are presented. As it will be shown in the following, although the phase transition is of mean field nature, the dynamics leads to non-trivial results.

The Chapter is organized as follows: In Sec. 3.2 the model is introduced and its properties which are important for the purposes of this work are briefly reviewed. In the same section it is also discussed how to solve numerically the dynamics, Sec. 3.2.1, and the observables used to quantify the departure from the adiabatic ground state, Sec. 3.2.2. In this work the residual energy (the excess energy as compared to the adiabatic limit), the incomplete magnetization (the deficit

magnetization as compared to the adiabatic limit) and the entanglement entropy are used. The numerical results together with the corresponding scaling arguments are presented in Sec. 3.3.

3.2 The Model

The properties of the LMG model have been thoroughly scrutinized in the literature (see e.g. [56, 57, 58, 59, 60, 61, 62, 63, 64, 65, 66, 67, 68] and references therein). Below a few results that are relevant to the present discussion are briefly recalled. The LMG Hamiltonian describes a system of spins (1/2 in this work) interacting through an infinite-range exchange coupling and subjected to a transverse field. Assuming that the field is directed along the z-direction the Hamiltonian can be written as

$$H = -\frac{2}{N}\sum_{i<j}(S_i^x S_j^x + \gamma S_i^y S_j^y) - \Gamma\sum_{i}^{N} S_i^z, \tag{3.1}$$

where N is the number of the spins in the system, S_i are the Pauli operators, γ is the anisotropy parameter and Γ is the transverse field. By introducing the total spin operator $\vec{\mathcal{S}} = \sum_i \vec{S}_i$, the Hamiltonian can be rewritten, apart from a additive constant, as $H = -\frac{1}{N}[\mathcal{S}_x^2 + \gamma\mathcal{S}_y^2] - \Gamma\mathcal{S}_z$. The Hamiltonian, hence, commutes with $\mathcal{S}^2$ and does not couple states having a different parity of the number of spins pointing in the magnetic field direction: $[H, \mathcal{S}^2] = 0$ and $[H, \prod_i S_i^z] = 0$. In the isotropic case $\gamma = 1$ also the z-component of $\vec{\mathcal{S}}$ is conserved, $[H, \mathcal{S}_z] = 0$.

In the thermodynamical limit the LMG model undergoes a second order quantum phase transition at $\Gamma_c = 1$ characterized by mean-field critical exponents [56]. The magnetization in the x-direction (or in the xy-plane, for $\gamma = 1$) vanishes when $\Gamma \to 1^-$ as

$$m = \begin{cases} (1-\Gamma^2)^{1/2} & \Gamma \leq 1 \\ \\ 0 & \Gamma > 1 \end{cases} \tag{3.2}$$

for all values of the anisotropy parameter γ. For $\Gamma > \Gamma_c$ and for any γ the ground state is non degenerate; while for $\Gamma < \Gamma_c$ it is doubly degenerate in the thermodynamical limit for any $\gamma \neq 1$, signaling the breaking of the Z_2 symmetry.

The gap vanishes at the transition as

$$\Delta = [(\Gamma - 1)(\Gamma - \gamma)]^{1/2} \quad \text{for } \Gamma \geq 1. \tag{3.3}$$

For any finite N both the magnetization and the gap are modified (as any other physical observable). The finite size scaling behavior is available in literature in all the relevant regimes (see, e.g., [56, 63]). The deviation from the thermodynamic limit for the gap $\delta\Delta_N = \Delta_N - \Delta$ and the magnetization $\delta m_N = m_N - m$ scale as

$$\begin{array}{lll} \delta\Delta_N \sim N^{-1} & \delta m_N \sim N^{-1/2} & \Gamma > 1 \\ \delta\Delta_N \sim N^{-1/3} & \delta m_N \sim N^{-1/3} & \Gamma = 1 \\ \Delta(N) \sim e^{-aN} & \delta m_N \sim N^{-1} & \Gamma < 1 \end{array} \tag{3.4}$$

for $\gamma > 1$ (where a is a constant) and

$$\begin{array}{lll} \delta\Delta_N \sim N^{-1} & \delta m_N \sim N^{-1/2} & \Gamma > 1 \\ \delta\Delta_N \sim N^{-1} & \delta m_N \sim N^{-1/2} & \Gamma = 1 \\ \delta\Delta_N \sim N^{-1} & \delta m_N \sim N^{-1} & \Gamma < 1 \end{array} \tag{3.5}$$

for $\gamma = 1$, respectively. The scaling behavior of the gap is important in order to distinguish the various dynamical regimes in the adiabatic annealing. It is however important to stress at this point that the equilibrium gap is not necessarily the one responsible for the loss of adiabaticity. As it will seen in the following section, due to the parity conservation the relevant gap for the dynamics is different from the equilibrium one (although with the same scaling behavior).

3.2.1 Adiabatic dynamics

The adiabatic dynamics is implemented by changing the external transverse field from an initial value $\Gamma \gg 1$ at t_{in}, where the ground state of $H(t_{\text{in}})$ is completely dominated by the transverse field term with all the spins aligned along the $+\hat{z}$ direction, to $\Gamma = 0$, where the ground state is ordered in the xy plane. The annealing time is characterized by a time scale τ. More specifically the case, as often in this type of problems, to reduce the magnetic field linearly in time is considered

$$\Gamma(t) = -t/\tau \quad \text{for} \quad t \in (-|t_{\text{in}}|, 0] \tag{3.6}$$

with $|t_{\rm in}| \gg \tau$.

The problem is further simplified by the following observation. In the initial state, the ground state of $H(t_{\rm in})$ belongs to the sector of maximum spin $\mathcal{S} = N/2$. Since $\mathcal{S}$ is a constant of motion it is sufficient to restrict the attention to this subspace only. From now it is assumed $\mathcal{S} = N/2$ (for simplicity we consider N even). In the basis $|N/2, \mathcal{S}^z\rangle$ ($\mathcal{S}^z = -N/2, ..., N/2$), the Schrödinger evolution of the state

$$|\psi(t)\rangle = \sum_{j=1}^{N/2+1} u_{2j-1}(t)|N/2, -N/2 - 2 + 2j\rangle, \tag{3.7}$$

amounts to solving the following set of coupled equations

$$i\frac{du_{2j-1}}{dt} = \sum_k M_{j,k} u_{2k-1}(t) \ . \tag{3.8}$$

The odd amplitudes $|N/2, -N/2-1+2j\rangle$ do not couple because of parity conservation. In Eq(3.8) M is a $(N/2+1)\times(N/2+1)$ symmetric matrix whose non-zero entries are given by

$$\begin{aligned} M_{j,j+1} &= -\frac{1}{4N}(1-\gamma)a_{-N/2-2+2j}a_{-N/2+2j-1} \\ M_{j,j} &= -\frac{1}{4N}(1+\gamma)[a^2_{-N/2-3+2j} + a^2_{-N/2-2+2j}] \\ &\quad -\Gamma(-\frac{N}{2} - 2 + 2j) + \frac{1}{4}(1+\gamma) \ , \end{aligned} \tag{3.9}$$

in terms of the usual angular momentum raising operator matrix elements:

$$a_j = \left[\frac{N}{2}(\frac{N}{2}+1) - j(j+1)\right]^{1/2} \ . \tag{3.10}$$

Special values have the boundary terms of M, given by:

$$\begin{aligned} M_{1,1} &= -\frac{1}{4N}(1+\gamma)a^2_{-N/2} - \Gamma(-\frac{N}{2}) + \frac{1}{4}(1+\gamma) \\ M_{N/2+1,N/2+1} &= -\frac{1}{4N}(1+\gamma)a^2_{N/2-1} - \Gamma(\frac{N}{2}) + \frac{1}{4}(1+\gamma) \ . \end{aligned} \tag{3.11}$$

The equations (3.8) were integrated via standard numerical methods with initial conditions given by the amplitudes of the ground state of $H(t = t_{\rm in})$.

3.2.2 Measures of the loss of adiabaticity in the LMG model

Once again the degree of adiabaticity of the evolution can determined through the residual energy of Eq(1.8); but an alternative way is in terms of the incomplete magnetization in the final state, defined by

$$m_{\rm inc} = m_{\rm gs} - m(t) \tag{3.12}$$

where $m_{\rm gs}$ is the static magnetization of the ground state for $\Gamma = 0$ and $m(t)$ is the average magnetization of the final evolved state. Following Botet *et al* [54], the magnetization m has been defined through

$$m^2 = \frac{4}{N^2}\langle\psi|\mathcal{S}_x^2 + \delta_{\gamma,1}\mathcal{S}_y^2|\psi\rangle, \tag{3.13}$$

where the expectation value can be taken either on the ground state, for $m_{\rm gs}$, or on the evolved state, for $m(t)$. As discussed in Ref[54], the previous definition differs from that of the spontaneous magnetization; however, it is more convenient for finite size systems and it reduces to the spontaneous magnetization in the thermodynamic limit.

Dealing with a model where the coupling has an infinite range, the incomplete magnetization is an appropriate way for characterizing the loss of adiabaticity: in this case a correlation length characterizing the typical distance between defects, along the lines followed for short range models, cannot be introduced.

In the Ising limit, $\gamma = 0$, at $\Gamma(t = 0) = 0$, the residual energy and the incomplete magnetization are related, as they both depend only on the average value $\langle\psi(t = 0)|\mathcal{S}_x^2|\psi(t = 0)\rangle$: The residual energy per site can be expressed as

$$\frac{E_{\rm res}}{N} = -\frac{1}{N^2}\langle\psi(t = 0)|\mathcal{S}_x^2|\psi(t = 0)\rangle + \frac{1}{4}\ ; \tag{3.14}$$

the incomplete magnetization is given by

$$m_{\rm inc} = 1 - \sqrt{\frac{4}{N^2}\langle\psi(t = 0)|\mathcal{S}_x^2|\psi(t = 0)\rangle}\ . \tag{3.15}$$

In addition to the previous observables, it was recently shown that important information of the lack of adiabaticity in the system can be acquired by analyzing

the entanglement entropy S [18, 21]. Entropy and other measures of entanglement has been recently studied to characterize both equilibrium and non-equilibrium quantum many-body systems (see [69] for a review). In the case of the LMG model the ground state entanglement entropy was studied in [70, 71, 72, 73, 74]. In the present work the time evolution of S during an adiabatic evolution is studied.

Given a bipartition of the system in L and $N-L$ spins, the entanglement entropy associated to the reduced density matrix of one of the subsystems, say $\rho_L = \mathrm{Tr}_{N-L}(\rho)$, is defined as

$$S_L = -\mathrm{Tr}(\rho_L \log_2 \rho_L) \ . \tag{3.16}$$

The entropy S_L measures the entanglement between the L spins and the rest of the system.

The entanglement entropy is straightforwardly evaluated by noticing that, being the states $|\mathcal{S} = N/2, \mathcal{S}_z\rangle$ symmetric under any permutations of the sites and being the maximum value of the total spin achievable only with the maximum value of the spin in each subsystem, the following decomposition holds [71]:

$$|N/2, \mathcal{S}^z\rangle \ = \ \sum_{l=0}^{L} p_l^{1/2} |L/2, l - L/2\rangle \otimes |(N-L)/2, n - l - (N-L)/2\rangle \ .$$

In the previous decomposition n and l indicate, respectively, the number of up-spins in the system and in the partition which defines the L sites. The coefficients appearing are defined as $p_l = L!(N-L)!n!(N-n)!/(l!(L-l)!(n-l)!(N-L-n+l)!N!)$. With the knowledge of the representation of the evolved state in the basis $|N/2, \mathcal{S}^z\rangle$ and by using the previous decomposition, it is immediate to trace out the $N-L$ spins to obtain the reduced density matrix ρ_L, and calculate its entropy.

3.3 Results

The results presented below were obtained by integrating numerically Eq(3.8). It has been verified that, as for the initial time of the evolution, it is enough to consider $t_{\mathrm{in}} = -5\tau$ for faster sweeps ($1 < \tau < 500$) and $t_{\mathrm{in}} = -2\tau$ for slower ones. It has been checked (data not reported) that the results do not depend on the

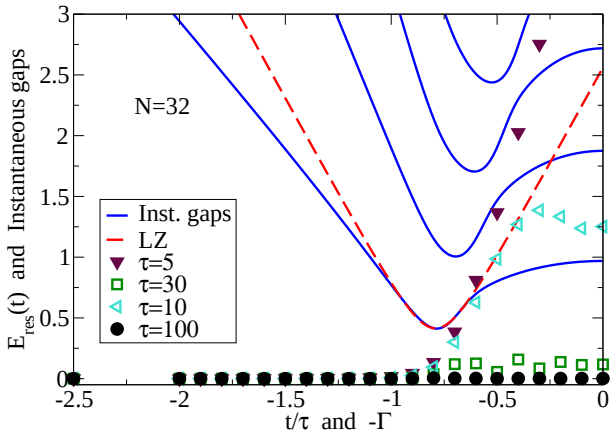

FIGURE 3.1: (Color online) Residual energy $E_{\rm res}(t)$ versus t for a given instance with $N = 32, \gamma = 0$ of the LMG model at different values of τ. The solid lines are the lowest-lying instantaneous spectral gaps as a function of Γ. The red-dashed line is the best fit to the lowest gap used to calculate the Landau-Zener transition rates.

precise value of $t_{\rm in}$. Systems up to $N = 1024$ spins and annealing times up to $\tau \sim 10^3 - 10^4$ have been considered.

Residual energy and incomplete magnetization - In order to understand the mechanism that leads to breakdown of adiabaticity in the LMG model it is instructive to start with one particular example. In Fig.(3.1) a system with $N = 32$ spins and $\gamma = 0$ has been chosen, showing the time evolution of the residual energy for different values of the annealing time τ. The instantaneous *accessible* gaps (thick solid lines) obtained by diagonalizing the Hamiltonian at any given Γ have been also plotted. As one can see, as soon as the system loses the adiabaticity, for fast annealing, it starts to ramp up in energy. The characteristic time scale for breaking of adiabaticity is however not given by the equilibrium smallest gap. As noticed in the previous Section, the dynamics is restricted to the subspace with fixed total spin $\mathcal{S} = N/2$ and can involve only states with the same parity of $\mathcal{S}^z$ [1]. Hence, the first gap relevant for the dynamics, that is called *dynamical* gap, is the energy difference between the ground state and the *second* excited state, the smallest gap being forbidden by parity conservation of $\mathcal{S}^z$. As shown in Fig.(3.2), the dynamical gap exhibits the same critical behavior of the excitation gap [56]: both close polynomially in the thermodynamical limit, with the same dynamical exponent $z = 1/3$, $\Delta_c \sim N^{-z}$. This is usually accompanied by a polynomial-like decay of the residual energy with increasing annealing time τ. This is indeed the

[1] The case $\gamma = 1$, due to the conservation of $\mathcal{S}^z$, presents only a trivial evolution for that concerns our analysis and so has not been considered.

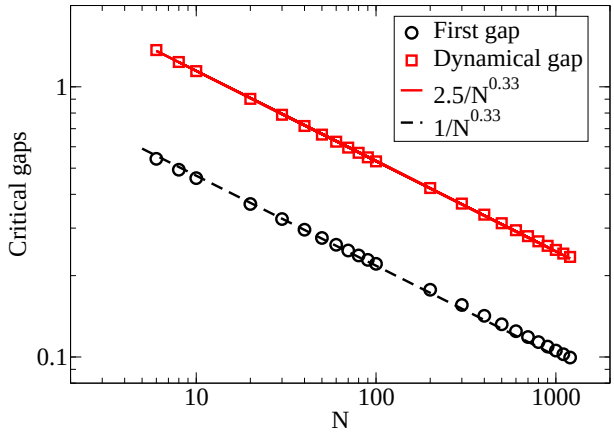

FIGURE 3.2: (Color online) Smallest gap and dynamical gap at the critical point as function of the size of the system.

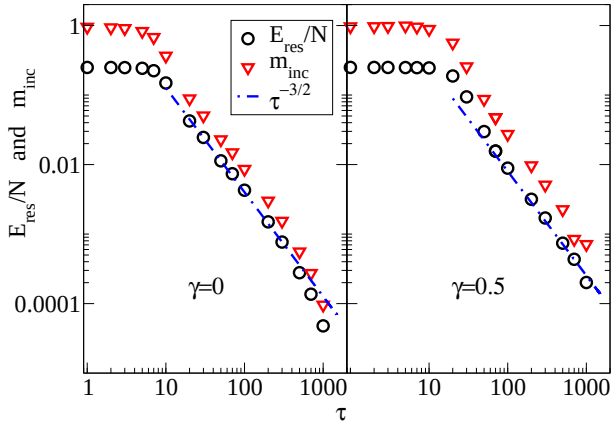

FIGURE 3.3: (Color online) Residual energy per site and incomplete magnetization for the LMG model with $N = 1024$ for different values of the anisotropy parameter γ. In all cases, for slow enough quenches, a power-law behavior $\tau^{-3/2}$ appears.

case, for both the residual energy and the incomplete magnetization, as shown in Fig.(3.3) and, more in detail for $\gamma = 0$, in Fig.(3.4). The behavior appears to be qualitatively independent on the value of the anisotropy parameter γ for $\gamma < 1$, see Fig.(3.3); this was expected due to the fact that the minimum gap has the same large-N behavior irrespective of the anisotropy. In the following only the case $\gamma = 0$ will be discussed.

Inspection of Fig.(3.4) reveals three different regimes. For fast quenches the dynamics involves almost all the levels, see, e.g., Fig.(3.1) for $\tau = 5$. The residual energy per site is close to its maximum and shows very little dependence on the size of the system and on the annealing time τ. For larger values of τ, a second intermediate region appears in which a power-like decay emerges, with $E_{\rm res} \sim \tau^{-3/2}$. Finally, by further slowing the quench rate, a third large-τ regime characterized by

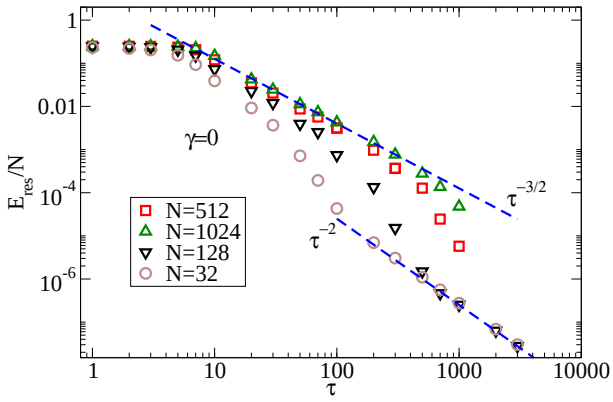

FIGURE 3.4: (Color online) Residual energy per spin as function of τ for $\gamma = 0$ compared with different power-law behaviors.

a different power-law, $E_{\rm res} \sim \tau^{-2}$, emerges. The emergence of the last two regimes is briefly discussed by means of a Landau-Zener approach adapted to the present problem.

The argument follows closely the one given in [15]. The probability of exciting the system into the first excited state, obtained by the Landau-Zener formula

$$P_{LZ} \simeq e^{-\alpha \Delta^2 \tau} \,, \tag{3.17}$$

with $\alpha = \pi/4$, gives a lower bound to the true transition probability, as it ignore the transitions to all the other excited levels. Using the scaling of the critical point gap with the number of spins, $\Delta \sim N^{-1/3}$, it is possible to determine the maximum system size for a defect-free quench once the probability for this to occur is fixed to an arbitrary small value $\tilde{P}_{ex}$. This gives:

$$\frac{1}{N_{\rm free}} \sim \left(\frac{|\ln \tilde{P}_{ex}|}{\alpha} \right)^{3/2} \frac{1}{\tau^{3/2}} \,. \tag{3.18}$$

One can consider $1/N_{\rm free}$ as an estimate of the fraction of the flipped spins after the quench. The residual energy per site in the LMG model can then be evaluated to be

$$\frac{E_{\rm res}}{N} \sim \frac{1}{N^2} \frac{N}{N_{\rm free}} N \sim \frac{\text{const.}}{\tau^{3/2}} \,. \tag{3.19}$$

This simple estimate is in good agreement with the numerical data in the intermediate regime of Fig.(3.4).

For short range models the same power law of Eq(3.19) can be also derived by determining the spatial scale over which defects occur [15]. It has been tried to apply the arguments of Zurek *et al*[15] to the LMG model by identifying the correlation length with the coherence number introduced in [54]. The procedure that has been followed, however, does not lead to the correct exponent. There is a reasonable confidence that the failure in obtaining the correct scaling with this second method may be related to the above identification and the consequent definition of defect density. It would be interesting to find the correct argument in order to extend the approach by Zurek *et al*[15] or Polkovnikov [16] to infinite range models.

Effective two-level approximation - As already mentioned before there is, for slower quenches, a further crossover to a different power-law. Can one explain also this behavior by using a Landau-Zener argument? To this end, it is important to refine this comparison and to understand to which extent the dynamics of a many-body system described by the LMG model can be described by two (many-body) levels. In general, in a many-body system there will be a number of avoided crossings and multiple LZ transitions, including interference between them. Only when a single avoided crossing is dominant and well separated from the others a two-level approximation is appropriate. A detailed analysis of this issue is summarized in Figs.3.5 and 3.6 where the case of $N = 32$ is shown as an example. The analysis starts by extracting the best dynamical minimum gap and adapting to it the following two-level Hamiltonian:

$$H_{LZ} = \begin{pmatrix} -\Omega_{LZ}(\Gamma - \Gamma_0) & \Delta_{LZ} \\ \Delta_{LZ} & \Omega_{LZ}(\Gamma - \Gamma_0)\ . \end{pmatrix}, \tag{3.20}$$

In the effective Landau-Zener problem Ω_{LZ}, Δ_{LZ} and Γ_0 are the fitting parameters and $\Gamma = -t/\tau$. In Fig.(3.1) the dashed line represents the instantaneous gap of the Hamiltonian (3.20) suited to the case $N = 32$. From here the results of the full LMG model are compared with those obtained using LZ theory. As shown in Fig.(3.5), the excitation probability in the LMG model for slow enough quenches coincides with that of the effective LZ problem. It appears that this approximation is good also in the estimate of the asymptotic value of the probability for $10 < \tau < 100$. Deviations come predominantly from the more enhanced oscillations of the post crossing region in the LMG model. For larges τ's the asymptotic value obtained from the effective two-level system gives a very poor approximation to

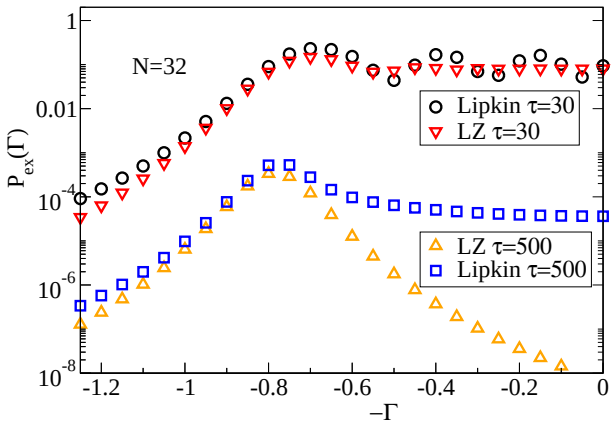

FIGURE 3.5: (Color online) Comparison between the excitation probabilities as function of Γ of the LMG model with $N = 32$ and of its effective LZ approximation for different values of τ.

the actual data. This can be traced back to the presence of further crossings which are obviously neglected in the two-level approximation. In the LZ scheme this can be effectively corrected by approximating the LZ crossing probability to the time before the next level crossing comes into play. This is explained below.

As found by Vitanov [75], it is possible to define the duration of a single LZ event as the time required by the probability for jumping from zero to its asymptotic value, linearly and with the slope calculated at the crossing point. Using Γ as time-scale one can write:

$$\Gamma_{\text{jump}} \sim \frac{P(\infty)}{P'(\Gamma_{\text{cross}})} \,. \tag{3.21}$$

This time turns out to be *exponentially* divergent with τ for large τ [75]. This means that for slow quenches consecutive LZ transitions are not independent. In a first crude approximation, it can be guessed that the consequence of this is simply to stop the probability from relaxing towards the asymptotic value when the system has reached the second crossing. The presence of a power-law regime $\sim \tau^{-2}$ for extremely slow dynamics is a clear consequence of the finite duration of the evolution. In the original works by Landau and by Zener, the final time is supposed to be $t_f = \infty$; here the evolution is stopped at $\Gamma_f = -t_f/\tau = 0$ for the LMG model, and at $t_{(LZ)f} = -\Gamma_{(LZ)f} \cdot \tau$ for the effective LZ, with $\Gamma_{(LZ)f} = \Gamma_f - \Gamma_0$. An accurate analysis of the finite-time Landau-Zener model (FTLZ) has been done

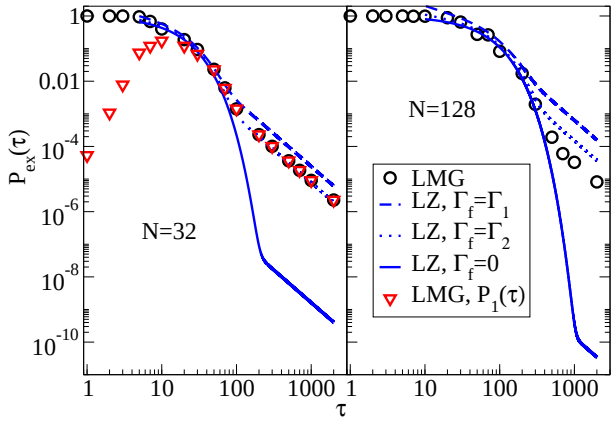

FIGURE 3.6: (Color online) Excitation probability as function of τ for LMG systems (circles) of two different sizes compared to that one of the respective LZ-effective models (line) for different final times. For the LZ models the first two terms of the Vitanov approximation have been used. For the case LMG N=32, the probability of exciting the first level is also presented (triangles).

in Ref. [75], where it is shown that the transition probability reads, in this case[2]

$$P_{(FTLZ)}(\tau) \sim P_{LZ}(\tau) + \frac{(1-2P_{LZ}(\tau))}{16\Delta_{LZ}^4 \frac{\tau^2}{\Omega_{LZ}^2}(1+\frac{\Omega_{LZ}^2}{\Delta_{LZ}^2}\Gamma_{(LZ)f}^2)^3} \tag{3.22}$$

with $P_{LZ}(\tau) = e^{-\pi\Delta_{LZ}^2\tau/\Omega_{LZ}}$. As it can be immediately seen from the previous equation, by sending the final time to infinity the usual LZ probability is recovered. The crossover rate $\hat{\tau}$ to the τ^{-2} scaling is obtained by equating the two terms on the r.h.s. of Eq(3.22). In the limit $\frac{8}{\pi}(1+\frac{\Omega_{LZ}^2}{\Delta_{LZ}^2}\Gamma_{(LZ)f}^2)^{3/2} \gg 1$ the crossover time is approximated by

$$\hat{\tau} \sim \frac{\Omega_{LZ}}{4\Delta_{LZ}^2}\frac{1}{(1+\frac{\Omega_{LZ}^2}{\Delta_{LZ}^2}\Gamma_{(LZ)f}^2)^{3/2}}. \tag{3.23}$$

In Fig.(3.6) the excitation probabilities of LMG systems of different sizes are compared with their single-LZ approximations. The probabilities for the effective models are evaluated for three different final time: $\Gamma_f = 0, \Gamma_1, \Gamma_2$, where the last two are the positions, respectively, of the minimum gap between the ground state and the second excited level, and the minimum gap between the first and the second excited levels. As it can be seen, the agreement is quite good and one can reproduce in this way also the regime with the τ^{-2} behavior.

Entanglement entropy - Finally the behavior of the entanglement entropy, which was already used as a tool to characterize adiabatic many-body dynamics in

[2]There is also a third term in the formula of Vitanov, but it is negligible respect to the second one in the large τ limit, for details refer to Ref[75].

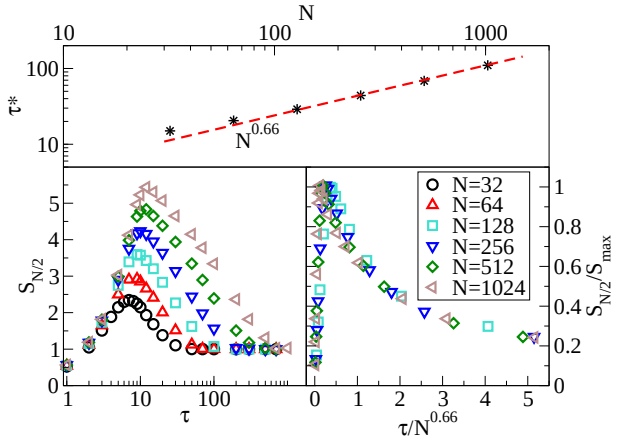

FIGURE 3.7: (Color online) Left lower panel: entanglement entropy of a block of $L = N/2$ spins as function of the quench time τ. Right lower panel: entanglement entropy of a block of $L = N/2$ divided by its maximum value as function of the rescaled variable $\tau/N^{0.66}$. Upper panel: the time scale τ^*, see the text for the definition, as function of system size N.

Refs. [18, 21], is discussed. The results are summarized in Fig.(3.7). In the left lower panel the entanglement entropy, for a block of size $L = N/2$, of the state evolved down to $\Gamma_f = 0$ is plotted as function of the quench time τ. For fast quenches, $\tau \to 0$, the state does not evolve (it remains in a nearly factorized state), thus the entanglement necessarily tends towards zero. For very slow dynamics $\tau \to \infty$, dealing with finite systems, the evolution eventually becomes adiabatic and the entanglement picks up the value it assumes in the final ground state, $S_{\rm gs}(\Gamma_f = 0) = 1$, independently on the subsystem size [71]. Between this two limiting behaviors, the entropy reaches a size-dependent maximum at an intermediate value of τ. An interesting feature is that the presence of a finite minimum gap can be easily connected with a time scale for the decaying of the entanglement. A possible choice for this time scale consists in selecting the τ^* at which the entropy has reduced by half the value of the its peak respect to the slow quench limit

$$S_{N/2}(\tau^*) = \frac{(S_{\rm max} - 1)}{2} + 1 \, . \tag{3.24}$$

In the upper panel of Fig.(3.7), τ^* determined in this way is shown as a function of the system size N. For large N, a power-like behavior emerges with an exponent ~ 0.66, hinting at a relation

$$\tau^* \sim \frac{1}{\Delta^2} \, . \tag{3.25}$$

In the lower right panel of Fig.(3.7), the entanglement $S_{N/2}$ divided by its maximum value $S_{\max}$ is plotted as a function of the rescaled variable $\tau/N^{0.66}$, showing, for large systems ($N \geq 128$), a collapse of all data on the same curve. Note that Eq(3.25) expresses exactly the same energy-time relation found in the usual LZ system, see Eq(3.17), so that the correspondence stated in previous sections is again supported.

Chapter 4

Optimized Quantum Annealing and Quantum Speed Limit

4.1 Introduction

In this second part of the thesis, the condition of a linear quench is relaxed and an optimal time-dependence of the annealing driving term is investigated. There are different reasons justifying this research effort. Beside the QA-AQC aim at paths with a reduced loss of adiabaticity, see Sec. 1.3.4, the optimization problem has been object of a more general and reinvigorated interest in recent years. The issue of devising a suitable Hamiltonian evolving a given system into a selected final state, has become of central relevance in many fields of physics and information science, especially with the advent of the quantum computation and quantum engineering. The challenge in this field is to find out the fastest possible way to perform such a transformation with the maximum accuracy, in prospect the of realizing sophisticated quantum circuits minimizing decoherence effects. Indeed the decoherence time sets a tight bound for the running time of a quantum computer, above which even the most perfect and clever quantum algorithm becomes totally useless.

A related and intriguing matter is that these hypothetical devices suffer strict constraints induced by their intrinsic quantum nature and the sensitivity to these limits is an open problem of theoretical and practical interest [76]. In Sec. 4.2 the existence and the effects of those bounds, summarized in the concept of the so called Quantum Speed Limit (QSL), are presented. The rest of the Chapter

address the study of the optimization of QA-AQC techniques through the Krotov algorithm (see Sec. 4.3) and analyzes the performance of the method in the Landau-Zener model (Sec. 4.4) and in the ordered Ising chain (Sec. 4.5). The limits revealed by the optimization procedure are compatible with the ultimate bounds imposed by quantum mechanics, supporting the power of method.

4.2 The Quantum Speed Limit

It has been established for many years that a transformation of a quantum system cannot be performed within an arbitrary short time[76]. A finite maximum speed, undergoing the name of Quantum Speed Limit (QSL)[77], cannot be overcome in evolving a quantum state into a distinguishable target. The origin of this constraint can be brought back to the fundamental principles ruling the quantum physics. As outlined by Aharonov and Bohm many years ago [78], the correct meaning of the uncertainty principle,

$$\Delta E \Delta t \geq \hbar, \tag{4.1}$$

is not the common interpretation for which the energy cannot be determined instantaneously without introducing an error (reproducible energy measurements arbitrarily fast are indeed allowed [78]), but that the *inner* time of a state, i.e. the lifetime, is connected to its energy variance ΔE through the Heisenberg relation. An equivalent statement is that *no unstable quantum system can decay completely within a time* $\hbar/\Delta E$[79].

This simple conclusion has been demonstrated by Bhattacharyya rielaborating previous results by Mandelstam and Tamm [80]. In Ref[79], for a time-independent Hamiltonian, the presence of this ultimate bound has been also exactly determined; for a transformation towards an orthogonal state it assumes the form ($\hbar = 1$)

$$T_{\mathrm{QSL}} = \frac{\pi}{2\Delta E} \tag{4.2}$$

where ΔE represents the spread in energy of the initial state $|\psi(t_{\mathrm{in}})\rangle$. This relation can be generalized to the case of non orthogonal states[81], leading to

$$T_{\mathrm{QSL}} = \frac{1}{\Delta E} \arccos\langle\psi(t_{\mathrm{in}})|\psi_G\rangle \tag{4.3}$$

where $|\psi_G\rangle$ represents the target. Almost ten years ago, Margolus and Levitin[82], while discussing the problem of how fast a quantum computer can run, demonstrated that a quantum system with a bounded average energy E cannot evolve into an orthogonal state in a time shorter than

$$T_{\mathrm{QSL}} = \frac{\pi}{2E}. \tag{4.4}$$

Identifying previous fundamental bound, the authors suggested that, fixed an average energy, it is not possible to construct a state with a very large ΔE in order to achieve an arbitrary fast transformation, taking in account only the limit worked out by Bhattacharyya. Both Eq(4.2) and Eq(4.4) are valid in general so that the QSL is obtained by considering the *maximum* value between the two[77]. For states in which $\Delta E = E$, previous bounds coincide and can be exactly attained[1]; however in Ref[83] it is shown that the ultimate limits of Eq(4.2) and Eq(4.4) cannot be reached if $\Delta E \neq E$.

These bounds have been also generalized, in principle, to the situation of a time dependent-Hamiltonian[84, 85], but so far the QSL in a time-dependent framework has been practically determined in few simple cases[86, 87]. It can be guessed that there should be a tight link between the goal of devising an exact transformation between two states employing a time-dependent Hamiltonian (QSL perspective) and the aim to perform an evolution without production of defects (QA-AQC point of view). In the following the attention will be addressed to this topic; in particular the parallelism between the achievement of a target within the minimum time (QSL) and the search for an optimal time dependent shape of the quench will be stressed through the application of the Krotov algorithm.

4.3 Optimization through the Krotov algorithm

Among the various techniques proposed to reconcile accuracy and speed in quantum dynamics, the optimal control through the Krotov algorithm is considered a very promising tool[36]. This is a numerical recursive method which seeks the optimal control pulses necessary to implement the required quantum transformation by solving a Langrange multiplier problem [88, 89, 90]. This technique has already been applied with success to a wide range of quantum systems [90, 91].

[1] A simple example is given by the spin-flip considered in Ref[76].

One issue that is not yet fully understood about this optimization is what its limits are, and how these limits may be approached. Besides being of interest from a theoretical perspective, the discovery of such a constraint is important for practical implementations of optimal control. The procedure followed to enforce the Krotov algorithm is summarized below.

Given an input state $|\psi(0)\rangle$ and a time-dependent Hamiltonian $H(t)$, that depends on a set of time-dependent control functions $\mathbf{\Gamma}(t) = \{\Gamma_1(t), \Gamma_2(t), \cdots, \Gamma_k(t)\}$, an estimation of the error in reaching the goal state $|\psi_G\rangle$ at the time T is obtained via the infidelity defined in Eq(1.9), that with previous conventions can be expressed as $\mathcal{I} = 1 - |\langle\psi_G|\psi(T)\rangle|^2$, where $|\psi(t)\rangle$ represents the evolution of the initial state upon $H(t)$. The optimal control technique of Refs [36, 88, 89, 90] allows to find an optimal time-dependence for the set of parameters $\mathbf{\Gamma}(t)$ with the goal of minimizing the infidelity. This is obtained by looking for the stationary points of the functional[2]

$$\begin{aligned}\mathcal{F}[\psi, \dot{\psi}, \chi, \Gamma] &= 1 - |\langle\psi_G|\psi(T)\rangle|^2 \\ &+ \left(\int_0^T dt \langle\chi(t)| \left\{ |\dot{\psi}(t)\rangle + iH[\Gamma(t)]|\psi(t)\rangle \right\} + \text{c.c.} \right)\end{aligned} \tag{4.5}$$

in which the auxiliary states $|\chi(t)\rangle$ play the role of a continuous set of Lagrange multipliers imposing the fulfillment of the Schrödinger equation at each time during the dynamics. Setting to zero the functional derivatives of $\mathcal{F}$ with respect to its arguments, a Schrödinger-like equation for the auxiliary state, $i|\dot{\chi}(t)\rangle = H|\chi(t)\rangle$, with the boundary condition $|\chi(T)\rangle = |\psi_G\rangle\langle\psi_G|\psi(T)\rangle$, and the condition $2\text{Im}\langle\chi(t)|\partial_\Gamma H(t)|\psi(t)\rangle = 0$ are derived[90].
Through the immediate feedback control procedure [89], these basic equations are exploited to find the optimal $\Gamma(t)$ via an iterative algorithm that is guaranteed to improve the fidelity at each step. The procedure requires the following operations: (i) $|\psi(t)\rangle$ is evolved from 0 to T with an initial guess $\Gamma^{(0)}(t)$; (ii) the state $|\chi(T)\rangle$ is calculated and propagated backward in time from T to 0 with the same Hamiltonian used for the forward evolution of $|\psi(t)\rangle$; (iii) the states $|\chi(t)\rangle$ and $|\psi(t)\rangle$ are evolved again forward in time, the first with the old parameter, the latter with the updated $\Gamma^{(\text{new})}(t) = \Gamma^{(\text{old})}(t) + 2\text{Im}\langle\chi(t)|\partial_\Gamma H|\psi(t)\rangle/\lambda(t)$, where the function $\lambda(t)$ enforces the values of the parameter at the beginning and at the end of the

[2] In order to simplify the notation, the case of a single control parameter $\Gamma(t)$ is considered.

evolution. Points (ii) and (iii) are repeated in such a way the optimal $\Gamma^{\rm opt}(t)$ is constructed iteratively starting from the initial guess $\Gamma^{(0)}(t)$.
In order to establish a link with the QSL theory, the performance of the process is analyzed as a function of the total evolution time T and it is shown that the method is able to produce infidelities arbitrarily close to zero only above a certain threshold $T_{\rm QSL}$, which is compared with the dynamical bounds affecting the system. A good agreement between these (in principle) independent quantities is found, meaning that the effectiveness of the control pulses is only limited by the dynamical bounds of the system. Considering the restricted set of controls allowed in the problem, and the fact that the initial equations are not meant to optimize T, this is a rather remarkable fact which suggests that optimal control is a possible candidate for an operational characterization of the QSL of complex systems.

For the sake of clarity and for demonstration of the generality of the argument, two paradigmatic examples have been focused on: the Landau-Zener (LZ) model [42], and the ordered Ising model. The former case constitutes a basic step for the control of complex many-body systems, whose evolution, for finite size systems, is in many cases a *cascade* of LZ transitions [9]. QA-AQC [7] is known to be limited by avoided crossings in the time-dependent system Hamiltonian and by the inability to avoid excitation of the system. The second case is testbook example of a many-body quantum system showing a quantum phase transition.

4.4 Landau-Zener model

The first example considered is the paradigmatic case of passing through an avoided level crossing, modeled by the modified LZ Hamiltonian

$$H[\Gamma(t)] = \begin{pmatrix} \Gamma(t) & \omega \\ \omega & -\Gamma(t) \end{pmatrix}, \tag{4.6}$$

in which $\Gamma(t)$ is the control parameter that should be optimize through the Krotov algorithm. More precisely, the evolution is started by preparing the system in the instantaneous ground state of $H[\Gamma(0)]$ and the ground state of $H[\Gamma(T)]$ is assumed as target, with $\Gamma(T) = -\Gamma(0)$ ($|\psi(0)\rangle$ and $|\psi_G\rangle$ are thus orthogonal only in the limit $|\Gamma(T)| = |\Gamma(0)| = \infty$). As an initial guess $\Gamma_0(t)$ for the control, Ref[92] has

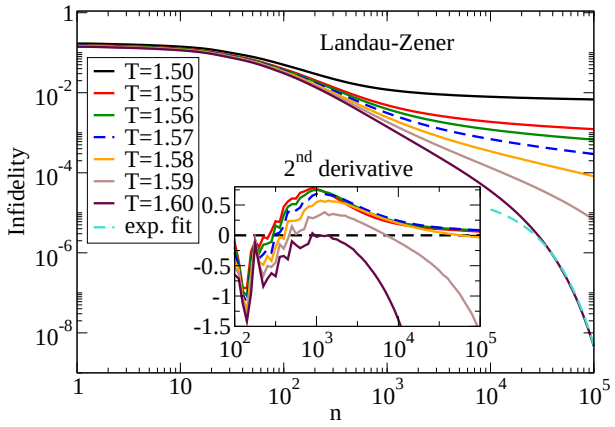

FIGURE 4.1: (Color online) Infidelity $\mathcal{I} = 1 - |\langle\Psi(T)|\psi_G\rangle|^2$ versus number of iterations n of the Krotov algorithm [36] for different values of T (in units of $\hbar/\omega$) for $\Gamma(T)/\omega = 500$. The dashed line corresponds to the estimated QSL ($T_{\rm QSL} = 1.5688$) while the dot-dashed line is an exponential fit. Inset: Second derivative of the infidelity logarithm with respect to the logarithm of the iteration number.

been followed. Here on the basis of the adiabatic theorem [37] the control pulse $\Gamma(t)$ was selected through a differential equation

$$\frac{\mathrm{d}\Gamma}{\mathrm{d}t} = \gamma\, \Delta^2(\Gamma), \tag{4.7}$$

where $\Delta(\Gamma)$ is the instantaneous gap and γ is a constant determined by the boundary conditions. For the LZ model of Eq(4.6) $\Delta(\Gamma) = 2\sqrt{\omega^2 + \Gamma^2}$ and it turns out that

$$\begin{aligned} \Gamma(t) &= \omega \tan\left[4\omega\gamma(t - t_i) + \arctan\left(\frac{\Gamma(t_i)}{\omega}\right)\right] \\ \gamma &= \frac{\left[\arctan\left(\frac{\Gamma(t_f)}{\omega}\right) - \arctan\left(\frac{\Gamma(t_i)}{\omega}\right)\right]}{4\omega(t_f - t_i)} \end{aligned} \tag{4.8}$$

In numerical simulations $-\Gamma(t_i) = \Gamma(t_f) = \hat{\Gamma}$ and $t_i = -\hat{\Gamma}\tau = -t_f$ have been assumed so that the total evolution time for the LZ model is $T = 2\hat{\Gamma}\tau$.
Starting from $\Gamma_0(t)$ defined above, the optimal control algorithm has been run for various values of the total time T. The results are reported in Fig.(4.1) by plotting the infidelity $\mathcal{I}$ as a function of the iterations n of the algorithm. As can be clearly seen from the figure, when $T < T_{\rm QSL} \approx 1.5688$, the infidelity $\mathcal{I}$ does not converge to zero: its curvature becomes asymptotically flat. On the contrary, by progressively increasing T towards and above $T_{\rm QSL}$, the curvature changes sign and the infidelity in the large iteration limit decreases *exponentially*, as confirmed by the fit in Fig.(4.1). In the inset of Fig.(4.1), data for the second

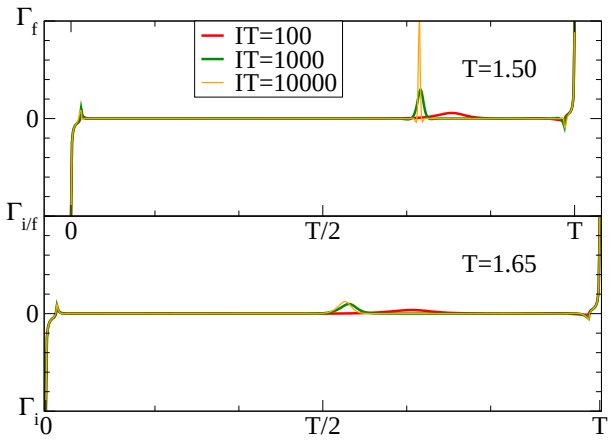

FIGURE 4.2: (Color online) Comparison between the pulse shape for evolution time below the QSL ($T = 1.50$) and above the QSL ($T = 1.65$)

derivative of the infidelity logarithm with respect to the logarithm of the number of iterations n for different T are shown: the derivative starts to cross the zero line for $T \approx 1.58$, and for $T > T_{\mathrm{QSL}}$ it clearly becomes negative. It is worth noticing that the change takes place in a restricted range of time corresponding to about 2.5% of the total evolution time. These findings are reflected by some interesting features that emerge from the study of the pulse shape of the optimization process, see Fig.(4.2). For $T < T_{\mathrm{QSL}}$, the pulse develops a peak which grows indefinitely in height by increasing the number of iterations n of the optimization procedure: that is, the control seems unable to converge towards an optimal shape. On the contrary, when $T > T_{\mathrm{QSL}}$, after a certain number of iterations, corresponding approximately to the appearance of the exponential decay regime, the shape is stable with respect to the iterations, and only small corrections of the order of the infidelity take place. Remarkably, the peculiar feature of the initial guess $\Gamma_0(t)$ of being almost constantly zero for most of the central part of the evolution is preserved by the recursive optimization of optimal control [36], suggesting that, for this simple model, an estimate of a finite resource QSL bound T_{QSL} for T can be deduced by a time-independent formula, assuming $H_0 = H[\Gamma = 0]$ as Hamiltonian. In other words, for most of the evolution time the dynamics can be effectively described by a time-independent Hamiltonian, which can be used to analytically estimate the QSL. For transformations induced by time-independent Hamiltonians, this can be quantified with the Bhattacharyya bound [79] of Eq(4.3), where for ΔE it has been assumed ΔE_0, the energy variance of H_0 calculated on the initial state $|\psi(0)\rangle$, i.e. $\Delta E_0 = [\omega^2 - 4\omega^4/\Delta^2(\Gamma(0))]^{1/2}$. This approach has the advantage of providing a bound for T that is *independent* from the effective shape of the selected pulse.

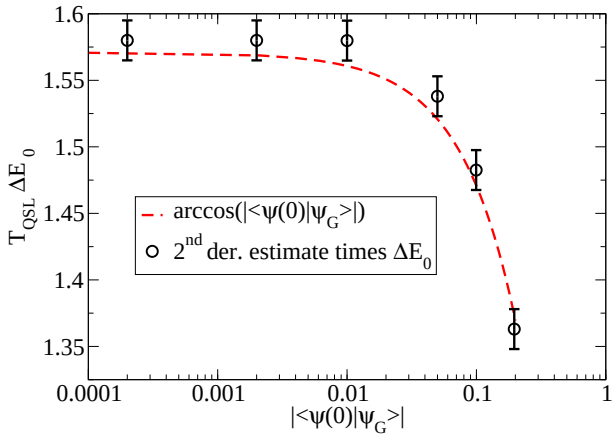

FIGURE 4.3: (Color online) Comparison between the time independent estimate (dashed line) and the second derivative criterion (circles, for $-\Gamma(0)/\omega = 5, 10, 20, 100, 500, 5000$ from right to left) for $T_{\rm QSL}$ for the LZ model.

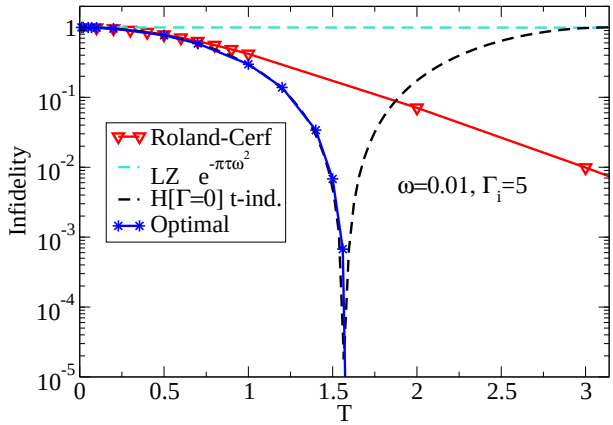

FIGURE 4.4: (Color online) Comparison between the infidelity obtained through the time-independent optimal evolution and through the pulse optimized via the Krotov algorithm as function of the total evolution time.

In Fig.(4.3) a comparison between the estimate $T_{\rm QSL}$ through the second derivative of the infidelity and the theoretical time-independent estimate (4.3) for various $\Gamma(0)/\omega$ ratios is shown. It is stressed that there are no fitting parameters. The excellent agreement shows that the optimal control efficiency is ultimately set by the dynamical bound of Eq. (4.3). Finally in Fig.(4.4) the optimized infidelity for a LZ with parameters $\omega = 0.01, |\Gamma(t_i)| = 5$ has been compared with the time-independent optimal evolution as function of the total evolution time T. Again the agreement is surprising for $T < T_{\rm QSL}$; noticed that although the time-independent infidelity is obviously an oscillating function, the optimized data correctly vanish above the quantum speed limit.

4.5 Ordered Ising model

The ordered Ising model Hamiltonian (see Eq(2.1) with $J_i \equiv h_i \equiv 1$) with PBC $\sigma_1 = \sigma_{N+1}$, through a Wigner-Jordan transformation and a Fourier transform[17] can be mapped onto a model of $N/2$ uncoupled LZ-like Hamiltonians with a common external field $\Gamma(t)$ but different overlaps and anticrossing point positions:

$$H_k = 2 \begin{pmatrix} \Gamma - \cos(k) & \sin(k) \\ \sin(k) & -(\Gamma - \cos(k)) \end{pmatrix} \tag{4.9}$$

with $k = \pi(2i+1)/N$, $i = 0, (N/2) - 1$ and a gap given by

$$\Delta_k = 4\sqrt{(\Gamma - \cos k)^2 + \sin^2 k}. \tag{4.10}$$

As seen in Sec. 4.3, once an initial guess for the time dependence of $\Gamma(t)$ is provided, the Krotov algorithm iteratively improves the shape of the pulse in such a way to minimize the infidelity of Eq(1.9), where the goal state is in this case the ground state of the Ising Hamiltonian with $\Gamma = \Gamma(t_f)$.
In simulations the evolution begins in the ground state of the Hamiltonian calculated at $\Gamma(t_i) = -\Gamma(t_f) = 2$ and the properties of convergence of the Krotov algorithm has been analyzed as function of the total evolution time $T = t_f - t_i$. As well known[13], the ordered Ising model undergoes a second order quantum phase transition for $\Gamma/J = \pm 1$ between a paramagnetic phase for $|\Gamma/J| > 1$ and a ferromagnetic phase for $|\Gamma/J| < 1$, so that during the evolution *two* critical points are crossed. By dealing with finite size system simulations, the critical point is smoothed into an isolated minimum gap point, see Fig.(5.4). If it is assumed that only the first gap accessible during the dynamics is responsible for the loss of adiabaticity, an indication of the true QSL can be obtained with simple arguments. The transformation between the initial and final states takes place by going through two LZ-like anticrossing points so that, by knowing how to treat the case of a single LZ, see Sec. 4.4 and Ref[93], it can be guessed that the required QSL corresponds to doubling the time needed to safely cross a single critical anticrossing point. For a single LZ, with the identification $\omega = \sin(\pi/N)$, see Eq(4.9), it turns out:

$$T_{\mathrm{QSL}}^{\mathrm{LZ}} = \frac{\pi}{2\omega} \quad \Longrightarrow \quad T_{\mathrm{QSL}}^{\mathrm{Ising}} = \frac{\pi}{\sin(\pi/N)} \sim N, \tag{4.11}$$

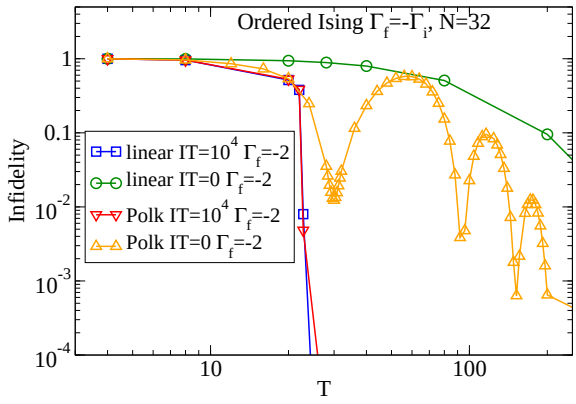

FIGURE 4.5: (Color online) Infidelity as function of the total evolution time T for a system of $N = 32$ spins, for linear and optimal initial guess, see text.

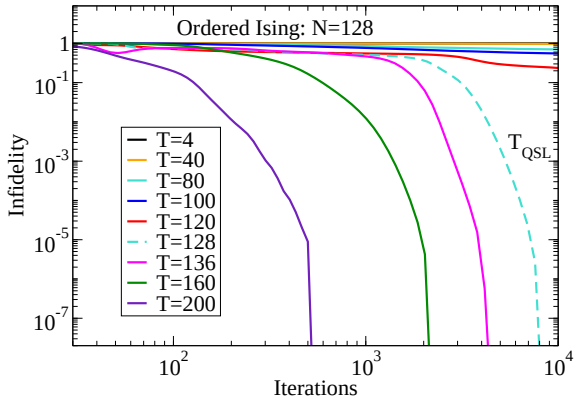

FIGURE 4.6: (Color online) Infidelity as function of the of the number of iterations of the algorithm for a system of $N = 128$ spins. The (blue) dashed line signals the estimated QSL.

where in the right side the limit $N \gg 1$ has been assumed.

The numerical simulations have been performed by using as initial guess for the transverse field both a linear ramp and the optimal pulse of Ref.[27]. The results for a system of $N = 32$ spins are shown in Fig.(4.5). Here the infidelity of the calculation is presented as function of the total evolution time T. For a sufficiently large number of iterations, the algorithm seems to converge at the same value of the infidelity independently of the initial guess. However, the convergence turns out to be faster by increasing the size, the effect is more evident when using as starting pulse the optimal power-law of Ref.[27] as starting pulse. It is also clear that, when the total evolution time reaches the estimate in Eq(4.11), the infidelity drops to zero. In Fig.(4.6) the behavior of the infidelity as function of the Krotov iteration number is presented for the largest system size considered, $N = 128$. The scenario is analogous to that one revealed in the single LZ case[93], see Sec. 4.4: for a total evolution time below the threshold of the estimated QSL, the algorithm

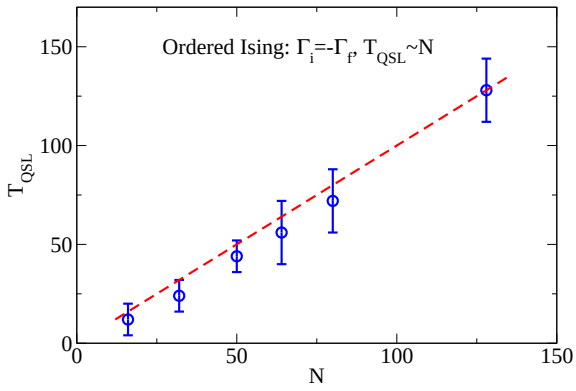

FIGURE 4.7: (Color online) The numerical estimation of the QSL as function of the size of the system.

is unable to significantly improve the initial guess; instead, when T is about or greater than $T_{\rm QSL}$ in Eq(4.11), the convergence becomes more and more rapid by increasing the evolution time, and the infidelity vanishes. This picture has been verified for different system sizes in the range $16 \leq N \leq 128$: in each case analyzed, at the $T_{\rm QSL}$ guessed in Eq(4.11), the infidelity can be made arbitrarily small within the maximum number of algorithm iterations used in simulations ($n_{\rm max} = 10^4$). If the algorithm is able to converge for a given evolution time T, the convergence is ensured for all larger values of T. In practice, the numerical results fix an upper bound for the true $T_{\rm QSL}$. As expected, the numerical estimate scales linearly with the size as in Eq(4.11), see Fig.(4.7). The fact that numerical simulations seems to be systematically below the estimate in Eq(4.11) can be justified observing that, in the ordered Ising model, the two level crossings do not correspond to two true and separate transformations between orthogonal states, but to two not totally complete rotations: if after the first anticrossing there is any excitation probability, the latter doesn't simply contribute to the final infidelity, but, due to the presence of the following anticrossing, it can be still reduced during the evolution. The final effect is a slight reduction of the QSL with respect to the rough estimate of Eq(4.11).

Chapter 5

Loss of adiabaticity and Quantum Speed Limit

5.1 Introduction

This Chapter aims at strengthening the link between the limits of the optimized QA-AQC and the QSL, proposing a new point of view to obtain the behavior of the loss of adiabaticity (i.e. kink density, residual energy), entirely based on the fundamental concepts of the QSL theory. This simple derivation holds for a generic shape of the quench and in a wide class of models, some of them even not contemplated by Fermi Golden Rule and Kibble-Zurek mechanism. In the next Section, Sec. 5.2, the tight analogy between the LZ approximation (see Sec. 1.3.3) and the QSL approach is discussed; it is also shown how the LZ formula brings too much information if the interest is limited only to the scaling of the quantities involved, while the QSL treatment seizes all the essential physics of the process. The the case of a linear quench is then discussed in a general perspective. In the following Sections non-linear quenches are investigated (polynomial shape Sec. 5.3, optimal shape Sec. 5.4). Finally comparisons with FGR (Sec. 5.6) and KZM (Sec. 5.7) are presented.

5.2 Linear quench

In order to fix the basic ideas of the QSL approach, the simple spin-flip driven problem is firstly tackled. The LZ Hamiltonian[42] of Eq(4.6), in which $\Gamma(t) = t/\tau$ represents the linear driving parameter is considered. The quench is supposed to start at $t = -\infty$ in the ground state, spin up configuration, $|\uparrow\rangle$ and the probability of being in the final ground state, spin down configuration, $|\downarrow\rangle$ at $t = +\infty$ is investigated. It can be guessed that the transition between the two states becomes effective only when the tunneling ω is of order of the diagonal energy $E(t) = \Gamma(t)$ or, equivalently, when the energy fluctuations[1] $\Delta E = \omega$ are large enough to cover the gap ($\sim 2\Gamma(t)$) between the levels. Then the condition

$$E(\hat{t}) \sim \Delta E \tag{5.1}$$

sets a time $\hat{t} \sim \omega\tau$ for the *duration of the transition*. The QSL theory (Sec. 4.2) requires a time

$$\hat{t} \sim T_{\rm QSL} \sim \frac{\pi}{2}\max\left(\frac{1}{\Delta E}, \frac{1}{E}\right) \tag{5.2}$$

for the transition toward an orthogonal state. So for the total spin-flip the condition $\hat{t} \sim \omega\tau$ from Eq(5.1) along with Eq(5.2), $\hat{t} \sim T_{\rm QSL} \sim \omega^{-1}$, lead to the scaling variable $1 \sim \omega^2\tau$. This relation is equivalent to the well known result expressed by the Landau-Zener formula, $P_{LZ}(\tau) = e^{-\pi\omega^2\tau}$, in which the same time scale for the probability decay is identified.

The results can be easily generalized to a many-body system of size N driven across a quantum critical point[2]. For a sufficiently slow quench, only the first dynamical gap turns out to be relevant for the dynamics. The critical gap $\Delta_c = f(N)$ plays the role of size-dependent fluctuations and Eq(5.1)-(5.2) determine the conditions for the maximum defect free size of the system:

$$f^2(N_{\rm free})\tau \sim \tilde{\kappa} \Longrightarrow N_{\rm free} \sim f^{-1}\left(\sqrt{\frac{\tilde{\kappa}}{\tau}}\right), \tag{5.3}$$

[1] It turns out that $\Delta E = \sqrt{\langle\uparrow(\downarrow)|H^2 - \langle H\rangle^2|\uparrow(\downarrow)\rangle} = \omega$.

[2] We are dealing with Hamiltonians for which it is possible to insert all time dependence in the diagonal elements in a specific diabatic basis, i.e. $H = A\Gamma(t) + B$, being A diagonal and B hermitian matrices.

with $\tilde{\kappa} \sim O(1)$ constant, that is the same relation contained in Eq(1.33). Then as in Ref[15] and Sec. 1.3.3, by knowing the relation between N_{free} and the quantity used to estimate the loss of adiabaticity (residual energy, defect density etc), it is possible to deduce its behavior as a function of τ. A summary of the procedure in a set of models is the following:

- for the ordered Ising chain[15] $\rho \sim 1/N_{\text{free}}$, $\Delta \sim 1/N$ and it turns out $\rho \sim 1/\tau^{1/2}$;
- for the random Ising chain[19, 20, 94] $\rho \sim 1/N_{\text{free}}$, $[\Delta]_{\text{typ}} \propto e^{-C\sqrt{N}}$ and it turns out $\rho \sim 4C^2/\ln^2 \tau$;
- for the Lipkin model[24, 56] $E_{\text{res}}/N \sim 1/N_{\text{free}}$, $\Delta \sim 1/N^{1/3}$ and it turns out $E_{\text{res}}/N \sim 1/\tau^{3/2}$;
- for the Grover's algorithm[6, 92] $\Delta \sim 1/\sqrt{N}$ and with a linear quench $s = t/T$ where T is the total evolution time, the result is $T \sim N$, as for the classical algorithm;
- for the $1d$ XXZ model, *antiferro-ferro quench*[25], $\tilde{E}_{\text{res}} \sim 1/N_{\text{free}}$, $\Delta \sim 1/N^2$ so that $\tilde{E}_{\text{res}} \sim 1/\tau^{1/4}$.

As outlined in the Introduction and in Sec. 1.3.3, the LZ approximation and so the QSL approach can be employed also in cases which are intractable with the KZM or FGR (Sec. 1.3.4). The Lipkin-Meshkov-Glick model is only one example: being highly coordinated, it is not possible to identify a finite dimension d for the model. The problem is easily overcome within the QSL approach: once the gap dependence on the size is known, $\Delta = f(N) = N^{-1/3}$ see Ref.[56], in the case of a linear quench, by using Eq(5.3), the scaling variable $\tau/N^{2/3}$ is directly obtained. In practice, the information about the dimension and critical exponents ν, z is directly taken in account via the function f^{-1}. In Fig.(5.1) the scaling of the infidelity[3] is shown. It should be pointed out that this scaling corresponds exactly to the finite-size scaling found for the bipartite entanglement after a linear quench[24].

Finally it should be noticed that the information required to deduce Eq(1.33) is not the particular functional dependence of the excitation probability, i.e. the

[3]Notice that for the LMG model the kink density cannot be defined.

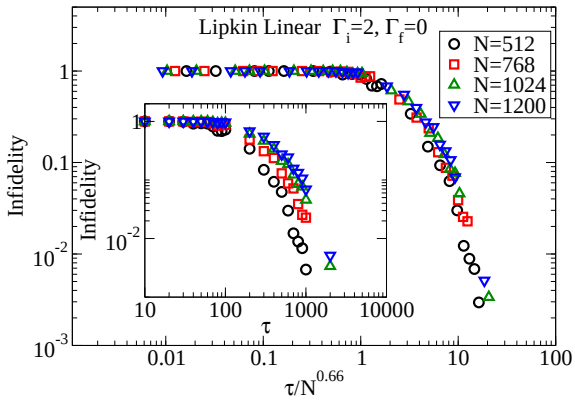

FIGURE 5.1: (Color online) Infidelity as a function of τ (inset) and of the scaling variable $\tau/N^{2/3}$ for a linear quench in the Lipkin-Meshkov-Glick model.

exact LZ formula, but simply the scaling variable contained in it. The fact becomes evident through the derivation of the same result via the QSL approach, Eq(5.3). This observation is at the basis of the application of the argument to non linear quenches, in principle unmanageable with the LZ approximation, being the excitation probability in general unknown.

5.3 Polynomial quench

As observed at the end of previous Section, the great advantage of the QSL approach with respect to the LZ approximation is that the former is easily generalizable to non linear quenches. The extension of the discussion to a polynomial functional dependence is straightforward. Assuming $\Gamma \propto \mathrm{sign}(t)|t/\tau|^r$, the condition fixing the transition time, Eq(5.1), leads to $|\hat{t}| \sim \omega^{1/r}\tau$. By using the QSL constraint, Eq(5.2), the following generalized scaling relation is obtained

$$\frac{\tilde{\kappa}}{\tau} \sim \omega^{1+1/r}, \tag{5.4}$$

with again $\tilde{\kappa} \sim O(1)$, or, in the case of a many body system of size N ($\Delta_c = f(N)$),

$$N_{\mathrm{free}} \sim f^{-1}\left(\left(\frac{\tilde{\kappa}}{\tau}\right)^{1/(1+1/r)}\right), \tag{5.5}$$

and all the new scaling summarized in Sec. 5.2 can be easily derived. This formula is equivalent to the results presented by Sen et al.[41] $\rho \sim \tau^{-r\nu d/(rz\nu+1)} = \tau^{-d/[z(1+1/rz\nu)]}$ and in some sense generalizes them, being applicable to systems

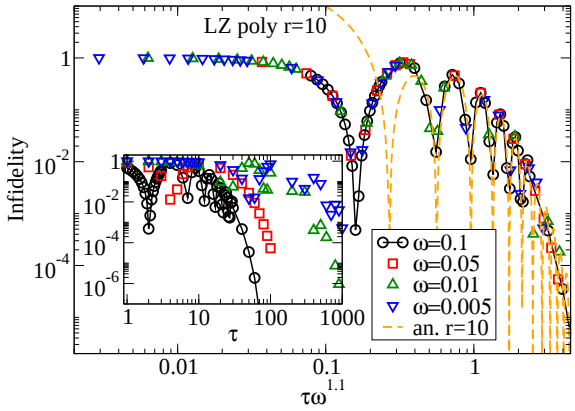

FIGURE 5.2: (Color online) Infidelity as a function of τ (inset) and of the scaling variable $\omega^{1.1}\tau$ for the polynomial quench $r = 10$.

without a definite dimensionality like the Lipkin-Meshkov-Glick model[53].
As a check of Eq(5.4), in Fig.(5.2) it is shown the scaling of the infidelity for a polynomial quench with $r = 10$ in the LZ model; in the picture it has been also reported the analytical estimate (dashed line) for the excitation probability of the polynomial level crossing model in the adiabatic limit, given in Ref[95]: the oscillations arise from non-linear interference effects, see AppendixC.
To test the results for many body systems, the equivalence between the formulation with the QSL formalism and the findings of Ref[41] can be manifested in the case of the Ising and Kitaev 1-d models. For both models $d = \nu = z = 1$, so that the formula found by Sen *et al.* leads to $\rho \sim \tau^{-r/(r+1)}$. On other hand it turns out that $\Delta = f(N) \propto N^{-1}$ and Eq(5.5) for QSL brings to $N_{\text{free}} \sim \tau^{1/(1+1/r)}$ or $\rho \sim N_{\text{free}}^{-1} \sim \tau^{-r/(r+1)}$.

5.4 Optimal quench

The QSL perspective is able to treat in a natural way also a generic non-linear quench like those used in *local* optimization. As discussed in Sec. 4.4, the optimal pulse of Ref.[92] is obtained by solving the differential equation $\dot{\Gamma} = \gamma\Delta^2(\Gamma)$, where $\Delta(\Gamma)$ is the instantaneous gap and γ is a constant determined by the boundary conditions. For the LZ model, this leads to Eqs(4.8) and recalling the conventions used in the simulations, $-\Gamma_i = \Gamma_f = \hat{\Gamma}$ and $t_i = -\hat{\Gamma}\tau = -t_f$, the total evolution time for the LZ model is $2\hat{\Gamma}\tau$. For the non-linear quench of Eq(4.8) the new scaling variable is easily obtained. In the limit $\hat{\Gamma} \gg \omega$, we have $\omega\gamma \to \pi/4(2\hat{\Gamma}\tau)$; in this case Eq(5.1), brings to the condition $\hat{t} \sim \tau$, so that, from Eq(5.2), the scaling

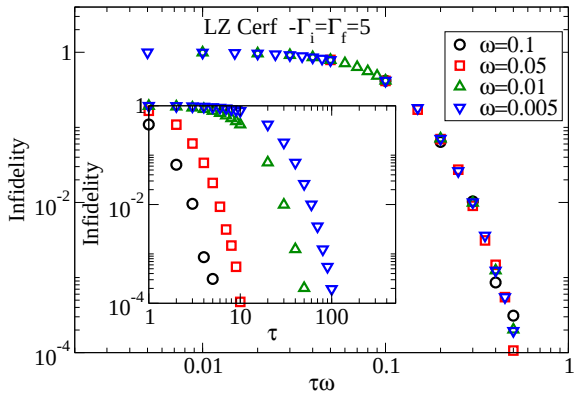

FIGURE 5.3: (Color online) Infidelity as a function of τ (inset) and of the scaling variable $\omega\tau$ for the non linear (Roland and Cerf formula) quench.

relation $\omega\tau \sim 1$ is obtained, see Fig.(5.3).

As a further test for an optimal quench, the Grover's problem is considered. As shown in Ref.[92], the local optimal pulse reads in this case

$$\begin{aligned}\Gamma(t) &= \frac{1}{2}\left\{\frac{1}{\sqrt{N-1}}\tan\left[\frac{2t}{T}\arctan\sqrt{N-1}-\arctan\sqrt{N-1}\right]\right\} \\ &\sim \frac{1}{2}\left\{\frac{1}{\sqrt{N}}\tan\left[\frac{t}{T}\pi-\frac{\pi}{2}\right]\right\} \quad \text{for} \quad N\gg 1, \end{aligned} \tag{5.6}$$

with a minimum gap $\Delta \sim 1/\sqrt{N}$. Similarly to what was shown above for the Landau-Zener model, through Eq(5.1) the previous pulse shape leads to $\hat{t} \sim T$, which with Eq(5.2), gives $T \sim \sqrt{N}$, i.e. exactly the result found in Ref[92].

Just a few remarks about the local optimization, Eq(5.4) and Eq(5.5). The limit $r \to \infty$, i.e. flat passage through the anticrossing point, induces a quadratic speed up with respect to the linear quench $r = 1$, analogously to what observed in Ref.[92]. Such a speed up is also obtained in Ref.[27] for the optimized adiabatic pulse in the ordered Ising model: in this case the authors are able to pass from $\rho \sim 1/\sqrt{\tau}$ to $\rho \sim 1/\tau^{\alpha}$, with $\alpha \to 1^{-}$, the adiabaticity condition far from the critical point preventing from reaching the limit $r \to \infty$, i.e. $\alpha = 1$ (this point will be discussed in the next Section).

The QSL approach offers an intuitive explanation for this effect: the advantage taken from a *local* satisfaction of the adiabaticity condition, with respect to a *global* adiabatic constraint is to make effective the transformation from the initial to the final state for all the evolution time, see Eq(5.1). In other words the fluctuations (i.e. tunneling) are exploited at the best during the calculation. As

found in Ref[27, 41, 92] and clearly shown in Eq(5.5), in such a way the speed up can be at most quadratic. In practice with this procedure a specific path in the parameter dependent Hamiltonian space has been fixed and a selection of the optimal speed at each point of the path is simply made.
A larger *exponential* speed-up would require to act directly on the amount of the tunneling or on the scaling of the fluctuations with the size, see Eq(5.2). This corresponds to look for an alternative path in the parameter dependent Hamiltonian space[34], for which the minimum gap[4] encountered during the calculation scales with the size in a substantially different way, polynomial or constant. Once such a path is identified, a local optimization like that one of Ref[92] can be applied for a further quadratic speed up in the quench time.

5.5 Remarks

It is interesting to discuss and outline from the point of view of the QSL the difficulties encountered in performing local optimization when different anticrossing points are present. As shown in Sec. 5.4 and in Ref.[93], the local optimization consists in reshaping the Hamiltonian driving parameter $\Gamma(t)$ in such a way that Eq(5.1) is fulfilled for the maximum time at disposal, in the ideal case for all the evolution time. When there are many anticrossings threatening the adiabaticity, the condition of maximum tunneling, if imposed for a specific point, usually turns out to be non-optimal for the other gaps, especially if they take place at values of the driving parameter *far* from the selected one. In Fig.(5.4) the instantaneous excitation spectrum of the ordered Ising model is sketched[17]: the gaps of every single mode k are shown as a function of the Hamiltonian driving parameter (transverse field). It becomes clear that if the pulse is optimized considering only the first dynamical gap, an optimal pulse $\Gamma(t) \sim \Gamma_1$ is obtained, Γ_1 being the value of the driving parameter at which the minimum gap is located[93]. In such a way, the optimal condition $\hat{t} \sim T$ is satisfied for the first gap but not for the highest energy gaps: on the contrary, for such anticrossing points Eq(5.1) is practically never fulfilled, inducing the excitation of the corresponding modes. As worked out in Ref.[27], the optimality can be obtained only through the subtle goal of extending the time of optimal transfer for the first more relevant gap with the constraint

[4] Here understood as a measure of the tunneling[44].

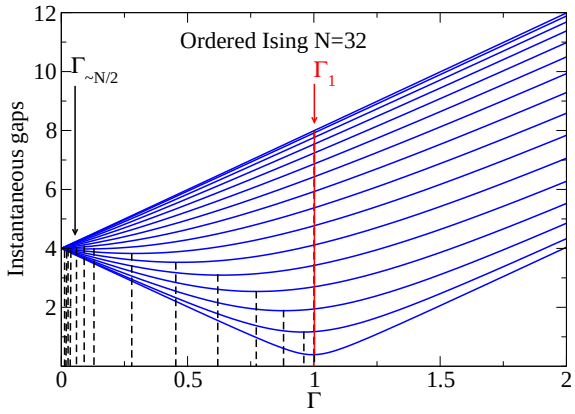

FIGURE 5.4: (Color online) Instantaneous gaps as a function of the driving Hamiltonian parameter, i.e. transverse field, for the ordered Ising model with $N = 32$. Γ_i labels the anticrossing point of each k_i-mode.

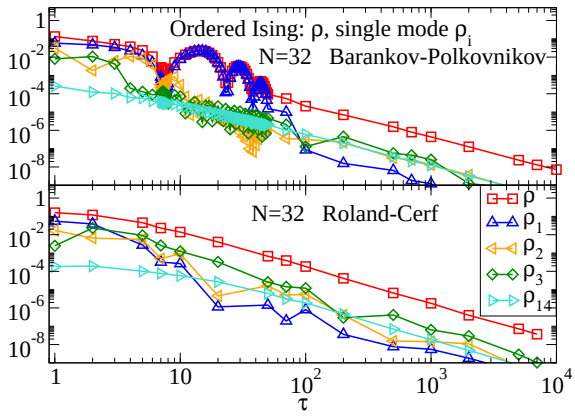

FIGURE 5.5: (Color online) Defect density and single mode contributions as a function of the total evolution time for two different optimized pulses, see text.

of not exciting the higher energy modes. To confirm this scenario, Fig.(5.5) shows the defect density and the single mode contributions as a function of the total evolution time for the optimal pulse of Ref.[27] (top) and for the pulse of Ref.[92] optimized over the first gap (bottom). As it can be clearly seen in the picture, the optimal power-law pulse of Ref.[27] is able to keep low the excitation of the high energy modes: the total density of defect, ρ, before reaching the adiabatic limit regime[23, 24, 75, 96] for large total evolution time ($\rho \sim \tau^{-2}$), coincides with the excitation of the first mode. Viceversa, for a pulse optimized by taking into account only the first gap many modes give a contribution of the same order to the total defect density.

Finally the oscillating behavior of the optimal power pulse appearing in Fig.(4.5) and Fig.(5.5) (top) is briefly discussed. This feature is strongly reminiscent of what

happens for a single LZ in presence of a non-linear, polynomial quench[75, 97], $\Gamma = \text{sign}(t)|t/\tau|^r$. In the latter case, such oscillations correspond to a perfect conversion of the initial state into the target orthogonal state, i.e. the infidelity drops really to zero. It can be shown, by using the analytical formula given in Ref.[75], that the time at which the first oscillation of the infidelity reaches the zero value presents a minimum in the limit $r \to \infty$ and such a minimum is nothing but the QSL for the single LZ model, as shown in Appendix C. For the ordered Ising model such a conversion doesn't happen due to the presence of the other gaps preventing a complete non-linear interference effect, see Fig.(5.5). On the other hand the optimal control through the Krotov algorithm seems to be able to reconstruct the interference effect of the various gaps, destroying the bouncing shape of the infidelity and ensuring a fast and complete convergence. It should be noticed that, with the optimal control technique, also the adiabatic regime $\propto \tau^{-2}$ disappears completely, see Fig.(4.5).

5.6 Analytical derivation: FGR and QSL theory

In this Section an analytical derivation of the loss of adiabaticity through the QSL theory is provided. The starting point is the FGR approximated expression for the excitation probability, Eq(1.24). First the case of a single LZ anticrossing is considered ($p \equiv 1$):

$$P_{\text{ex}} = \left| \int_{-\infty}^{\infty} dt \langle \text{ex}, t|\partial_t|\text{gs}, t\rangle e^{i\int^t dt'[\omega_{\text{ex}}(t')-\omega_{\text{gs}}(t')]} \right|^2, \tag{5.7}$$

where $|\text{gs(ex)}, t\rangle$ represents the instantaneous ground (excited) state at time t. The energy difference can be evaluated analytically in this simple case and by using the notation of Eq(4.6) is given by

$$\omega_{\text{ex}}(t) - \omega_{\text{gs}}(t) = 2\sqrt{\Gamma^2(t) - \omega^2} = 2\omega\sqrt{1 + (\Gamma/\omega)^2} = \omega F(\Gamma/\omega), \tag{5.8}$$

where $F(x) = 2\sqrt{1+x^2}$ shows exactly the behavior of Eq(1.27). As in Sec. 5.3, a general polynomial dependence of the driving parameter is considered; the new variable $y = \Gamma/\omega = (\text{sign}(t)|t/\tau|^r)/\omega$ can be then introduced. As in Ref[16]

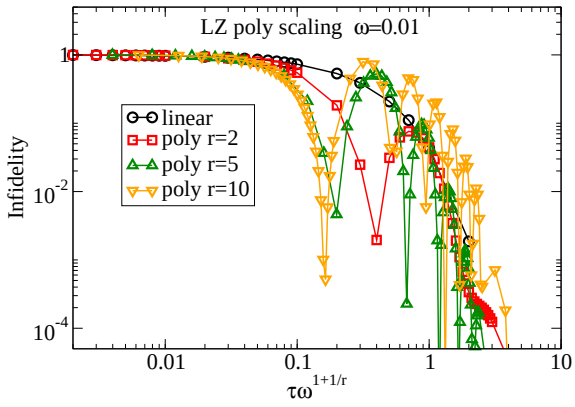

FIGURE 5.6: (Color online) Infidelity as a function of the scaling variable $\tau\omega^{1+1/r}$.

assuming $\langle \mathrm{ex}, t|\partial_\Gamma|\mathrm{gs}, t\rangle = \omega^{-1}V\left(\Gamma/\omega\right)$, the matrix element becomes

$$\langle \mathrm{ex}, t|\partial_t|\mathrm{gs}, t\rangle dt = \omega^{-1}V\left(\frac{\Gamma}{\omega}\right)\frac{d\Gamma}{dt}dt = V(y)dy, \tag{5.9}$$

and the phase term leads to

$$\begin{aligned}\int^t dt'[\omega_{\mathrm{ex}}(t') - \omega_{\mathrm{gs}}(t')] &= \int^y \omega\left(\frac{d\Gamma}{dt}\right)^{-1} dy'\omega F(y') \\ &= \int^y \omega^{1/r}\frac{\tau}{r}y'^{-1+1/r}[\mathrm{sign}(y')]^{1-1/r}dy'\omega 2\sqrt{1+y'^2} \\ &= \frac{\tau}{r}\omega^{1+1/r}g(y,r),\end{aligned} \tag{5.10}$$

with g a generic function. Finally the excitation probability can be expressed as

$$P_{\mathrm{ex}} = \mathcal{F}\left(\tau\omega^{1+1/r}, r\right) \tag{5.11}$$

that for fixed r is the scaling of Eq(5.4) and used in Fig.(5.2). If it was possible to solve the integral of Eq(5.10), a more general scaling variable involving τ, ω, r could be singled out; in Fig.(5.6) the simple scaling $\tau\omega^{1+1/r}$ has been tested: it seems that there is a rough agreement, the dependence on r being responsible for the differences in the oscillating profile, see Appendix C.

The same formulation allows to recover the scaling variable of the excitation probability in finite size many body systems For a slow quench the main contribution to the excitation probability comes from the lowest energy levels, i.e. in Eq(1.24) only few terms can be kept in the sum. The integral of the energy difference in the phase is now rewritten in terms of the scaling variable $y = \Gamma/\Delta$, where $\Delta = f(N)$

is the critical gap of the system of size N. For the first excited level it leads to

$$\omega_1 - \omega_0 = \Delta \cdot F\left(\frac{\Gamma}{\Delta}\right) = \Delta \cdot F(y) \tag{5.12}$$

where F has the usual definition of Eq(1.27). The meaning of Eq(5.12) reflects simply the fact that far from the transition region the energy is dominated by the driving term, viceversa inside the transition region the tunneling part prevails. Following the same steps of Eq(5.9) and Eq(5.10) the excitation probability is given by

$$P_{\text{ex}} \sim \mathcal{G}(\tau\Delta^{1+1/r}, r). \tag{5.13}$$

Then the dependence of the residual energy or the defect density on τ can be found via the relationship with the defect free size N_{free}. By selecting a value $\tilde{P}_{\text{ex}}$ to identify the defect free size, i.e.

$$\tilde{P}_{\text{ex}} \sim \mathcal{G}(\tau f^{1+1/r}(N_{\text{free}}), r), \tag{5.14}$$

for fixed r, it turns out

$$N_{\text{free}} \sim f^{-1}\left(\left(\frac{\mathcal{G}^{-1}(\tilde{P}_{\text{ex}})}{\tau}\right)^{\frac{1}{1+1/r}}\right) \tag{5.15}$$

that is exactly Eq(5.5).

Two remarks should be added. As shown in Sec. 1.3.4 and Refs[34, 98], purely dynamical effects, not contemplated by statics can occur in determining the behavior of the loss of adiabaticity, preventing from the direct use of Eq(1.1) to describe the minimum gap encountered during the evolution. The advantage of the QSL (LZ) approach respect to the FGR approximation is that the path dependence of the gap is correctly taken in account in the energy representation through the function $\Delta = f(N)$, without enforcing the usual statical dependence. Second, as discussed above, with this approach it is assumed that only one excited level is relevant in determining the loss of adiabaticity. However as suggested by the continuous limit treatment[16], a contribution to the scaling could derive also from the density of states. If many accessible levels lie near the first excited state it could be needed

to include into the integration all of them, modifying in such a way the scaling. This could be a possible scenario to extend the approach to BKT like transitions.

5.7 Comparison between Kibble-Zurek Mechanism and QSL perspective

As discussed in Sec. 1.3.1, the KZM can be summarized in two steps[40]: the first is the identification of the time at which the dynamics from adiabatic becomes impulsive through Eq(1.12); the second one is the relation characterizing the correlation length at the freezing time, $\hat{\xi} \sim \hat{\epsilon}^{-\nu}$. Assuming a linear quench Eq(1.12) leads to ($\hat{\epsilon} = \hat{t}/\tau$)

$$\hat{\epsilon}\tau \sim \hat{\epsilon}^{-z\nu} \Longrightarrow \hat{\epsilon} \sim \tau^{-1/(1+z\nu)}. \tag{5.16}$$

and then the defect density is easily derived, see Sec. 1.3.1.
By using the QSL approach instead the conditions for the intensity fluctuations, Eq(5.1), and for the duration, Eq(5.2), must be satisfied. From Eq(5.1), identifying the fluctuations with the gap, $\Delta E \sim \Delta \propto \epsilon^{z\nu}$, it turns out

$$\hat{\epsilon}^{z\nu} \sim \hat{t}/\tau. \tag{5.17}$$

By using the inverse of the fluctuations as estimate of T_{QSL}, it is obtained

$$\tau\hat{\epsilon}^{z\nu} \sim \hat{\epsilon}^{-z\nu} \Longrightarrow \hat{\epsilon} \sim \tau^{-1/2z\nu}; \tag{5.18}$$

instead with the inverse of the energy it turns out

$$\tau\hat{\epsilon}^{z\nu} \sim \hat{\epsilon}^{-1} \Longrightarrow \hat{\epsilon} \sim \tau^{-1/(1+z\nu)} \tag{5.19}$$

and only this latter relation coincides with the KZM result, in general. Nevertheless for particular cases in which $z\nu = 1$, Eq(5.18) and Eq(5.19) coincide. This occurs for the $1d$ ordered Ising (for *traditional* paths[34, 98]), for the $1d$ Kitaev and for the Landau-Zener models[5].

[5]For the specific case of the LZ model, another possibility to interpret the situation is the following: as discussed in Chapter 4, the QSL is reached through an optimal pulse close to the time independent case[93], $H^{\mathrm{LZ}}_{\mathrm{optimal}}(t) \sim \omega\sigma_x$. For this kind of transformation $\Delta E = E$[76] and the identity is recovered.

5.7.1 Landau-Zener model

In order to better understand differences and similarities between KZM and QSL approach, the analysis is focused on the LZ model for which an extensive treatment in terms of the KZM has been done in Refs[28, 39]. At a first glance a disagreement between KZM and QSL perspective in the role and in the definition of the adiabatic-impulse regions could be revealed. According to the KZM scheme, for $t_i = -\infty$ and $t_f = \infty$, the evolution is adiabatic up to the freeze-out time $-\hat{t}$, is impulsive for $-\hat{t} < t < \hat{t}$ and then is again adiabatic for $t > \hat{t}$. For the QSL perspective on the contrary the transformation towards the target state occurs only in a region centered around the anticrossing point in which the fluctuations manifest their maximum effect and so contradicting the intuition of a frozen state within the impulse region. But the contradiction is only apparent and can be solved analyzing the bounds of validity of the theories.
According to KZM, the loss of adiabaticity takes place in the interval $[-\hat{t}, \hat{t}]$ across the anticrossing point, in which the state evolves only through an overall phase and is unable to follow the instantaneous ground state due to the divergence of the reaction time, see Fig.(1.1). The adiabatic-impulse approximation works better for reduced impulse interval, see Ref[39], i.e. small freeze-out time $|\hat{t}|$. This assertion comes out from the fact that for a LZ system the freezing instant is determined by the inverse of the instantaneous gap, i.e. by using the notation of Ref[39],

$$\tau_{\text{rel}} = \frac{1}{\sqrt{\omega^2 + (t/\tau)^2}} = \frac{\tau_0}{\sqrt{1+\epsilon^2}} \tag{5.20}$$

with $\epsilon = t/(\tau\omega) = \Gamma/\omega$ and $\tau_0 = 1/\omega$ and such a equation becomes comparable to the standard definition of Zurek[99], $\tau_{\text{rel}} = \tau_0/|\epsilon|$ only in the limit $\hat{\epsilon} = \epsilon(\hat{t}) \gg 1$, i.e. for fast quenches. Indeed for the freezing time, by using the Zurek equation[6], it turns out

$$\tau_{\text{rel}}(\hat{t}) = \alpha\hat{t} \quad \Longrightarrow \quad \hat{t} \sim \begin{cases} \sqrt{\dfrac{\tau}{\alpha}} & \text{for} \quad \alpha\omega^2\tau \to 0 \\ \dfrac{1}{\alpha\omega} & \text{for} \quad \alpha\omega^2\tau \to \infty \end{cases} \tag{5.21}$$

and only the first limit gives the usual $\sqrt{\tau}$, KZM-like behavior. As outlined in Ref[39], this fast quench regime is also consistent with the assumption of a small

[6] In this equation α is a constant that should be determined by fitting the problem in analysis; for the LZ model, perturbative expansions lead to $\alpha = \pi/2$

impulse region.
Physically by using the language of KZM, two consequences can be drawn: the loss of adiabaticity should occur in a regime in which the dominant time scale is the diagonal energy, $\hat{\Gamma}/\omega \gg 1$, so that the tunneling doesn't play any role in determining the freezing time, see Eq(5.21), but fixing a small scale for the energies. The second conclusion is that the KZM works only for small perturbations of the initial state, for which the impulse evolution is justified, implying an high production of defects: indeed the tunneling in its validity regime acts only for short time. This fact is evident through the correspondence between KZM prediction and the perturbative expansion of the LZ formula for $\alpha\omega^2\tau \ll 1$, see Ref[39].

On the other hand the QSL perspective aims to describe a different regime in which the initial state is strongly modified, possibly totally transformed into an orthogonal target. In this case the impulse region is exploited to change the system and the best performance is obtained by extending it up to or above the minimum time fixed by the QSL theory. Indeed the adiabatic regime of KZM can be related with the region in which the state is not appreciably modified by the fluctuations in the QSL perspective: in both cases instantaneous eigenstates and diabatic states are more or less equal. However the two approximations hold in complementary intervals. As already discussed in Sec. 5.2, with the QSL perspective by using Eq(5.1) and Eq(5.2) it turns out $\omega^2\tau \sim 1$. In this regime, as noticed in Eq(5.21) and in the following discussion, the adiabatic-impulse approximation doesn't hold: indeed in the impulse region the state is drastically changed and not simply perturbed. Viceversa the condition of KZM, $\alpha\omega^2\tau \ll 1$, with $\alpha \sim O(1)$, can be read as $\omega\tau \ll 1/\omega$ or in other words $\hat{t} \ll T_{\mathrm{QSL}}$, manifesting incompatibility with the basic QSL perspective assumptions.

Conclusions

In the present thesis the problem of adiabatically driving a system through a quantum phase transition has been investigated. The issue has been tackled in different contexts in order to reach a general understanding of the matter. In this conclusive section, the main results achieved are summarized Chapter by Chapter.

In Chapter 2 the adiabatic quantum dynamics of a one-dimensional disordered Ising model across its quantum critical point has been studied. The main results can be summarized in the dependence of the average kink density and residual energies as a function of the annealing rate: $[\rho_{\rm k}]_{\rm av} \sim \tau^{-0.5}$ small τ (fast quenches), $[\rho_{\rm k}]_{\rm av} \sim (\log \tau)^{-2}$, large τ; $[E_{\rm res}/L]_{\rm av} \sim \tau^{-1}$ small τ (fast quenches), $[E_{\rm res}/L]_{\rm av} \sim (\log \tau)^{-\zeta}$ large τ, with $\zeta \sim 3.4$. Although the dynamics is dominated by a very wide distribution of gaps at the critical point, $P_*(-\ln(\Delta_1)/\sqrt{L})$ (see Fig.(2.2)), the distribution for both these quantities turn out to be log-normal with a variance that decrease, like $1/\sqrt{L}$, for increasing chain length L: typical and average values, therefore, coincide for large L. The wide distribution of gaps, on the other hand, with its characteristic $\ln(\Delta_1)/\sqrt{L}$ scaling, is responsible, within a Landau-Zener theory, for the extremely slow decay of the average density of kinks, $[\rho_k]_{\rm av} \sim 1/(\ln \tau)^2$. This discussion applies only for reasonably large length L. If L is small, the minimum gap Δ_1 of a given instance can be sufficiently large that the adiabatic regime, predicted to occur beyond a characteristic $\tau_c \propto \Delta_1^{-2}$, is actually seen: a fast decay of $\rho_{\rm k}$ and $E_{\rm res}/L$ is expected [100] for $\tau > \tau_c$, in such a case.

It is interesting to compare these results with those of a classical thermal annealing, where, according to Huse and Fisher [101], the residual energy also shows a logarithmic behavior, $E_{\rm res}^{\rm CA}(\tau)/L \sim (\log \tau)^{-\zeta_{CA}}$, but with an exponent ζ_{CA} which is bound by $\zeta_{CA} \leq 2$.

If this problem is analyzed from the perspective of optimization algorithms, it seems that quantum annealing (QA) gives a quantitative improvement over classical annealing for the present system, as is indeed found in other cases [3, 9,

102, 103, 104, 105, 106, 107, 108], but not always (Boolean Satisfiability problems seem to be a test case where naive QA performs worse than classical annealing, see Ref. [109]). In this respect, however, several important issues remain to be clarified. First of all, QA-AQC has a large freedom in its construction: the choice of the possible source of quantum fluctuations [110] — generally speaking, one can take $H(t) = H_{\rm fin} + \sum_\lambda \Gamma_\lambda(t) H_\lambda$ —, and the time-dependence of the various $\Gamma_\lambda(t)$, which need not be linear in time[7]. Regarding the time dependence of the couplings, it can be simply noted that an optimal choice of the "speed" $\dot{\Gamma}(t)$ with which the critical point is crossed can provide an improvement in the exponents [92], but definitely not change a logarithm into a power-law. Regarding the possibility of adding extra kinetic terms to $H(t)$, it is clear that terms like $-\Gamma_{xy}(t) \sum_i J_i \sigma_i^y \sigma_{i+1}^y$ (XY-anisotropy) or similar short range interactions will not change the universality class of the infinite randomness quantum critical point of the present model [35]. Hence, a logarithmically-slow QA-AQC is expected also in more general circumstances, for the present one-dimensional model. It is expected to be a genuine consequence of the randomness present in the problem at hand, which makes the adiabatic quantum dynamics intrinsically slow and ineffective in reaching the simple classical ferromagnetic ground states[8]. This is perhaps to be expected in view of the results of Vidal [112], who showed that problems where the entanglement entropy of a block is bound, can be computed classically with a comparable efficiency. Generically, in disordered one-dimensional system the entanglement entropy grows at most logarithmically with the system size at a critical point [113, 114, 115], at this is not enough to substantially change the relative efficiency of quantum versus classical algorithms.

Therefore, the route to investigate seems to be following: search for models in more then one-dimension, where the entropy of entanglement grows stronger, which, at the same time, have "gentle" enough critical point gap distributions.

Bearing this lesson in mind, in Chapter 3 the adiabatic quantum dynamics of an infinitely coordinated system, the LMG model in a transverse field, has been considered. The attention has been focused on the residual energy after the quench analyzing its behavior as a function of the annealing time, in order to evaluate the

[7] In order to optimize the adiabatic algorithm one should also find the optimal time dependence of the coupling constant $\Gamma(t)$, see Ref. [92].

[8] However it should be mentioned that for finite-size Ising systems, convergence bound have been proved for QA-AQC in terms of power-law annealing schedules, see Ref. [111].

extent of non-adiabaticity of the evolution. The dynamics is restricted to a subspace of definite total spin and parity of its projection along the z-axis, due to the symmetries of the Hamiltonian. Results appeared to be qualitatively independent of the value of the XY-anisotropy parameter γ, except for the fully isotropic XX case at $\gamma = 1$, where the further conservation of $\mathcal{S}^z$ plays an important role.
Three regimes in the residual energy are identifiable: the first one, corresponding to fast quenches, is strongly non-adiabatic, involves transitions from the ground state towards many excited states and is characterized by a residual energy close to its saturation value. In the intermediate regime, the lowest critical dynamically accessible gap starts dominating the evolution, inducing a residual energy per site that decays in a power-like manner, like $\tau^{-3/2}$. The third large-τ region, where the residual energy decays like τ^{-2}, is understood by taking into account the presence of additional level crossings. In the effective Landau-Zener description used in Chapter 3, this results in the requirement to consider a finite-time Landau-Zener sweep. As show by Vitanov a finite-time sweep leads to a polynomial (in τ) contribution to the LZ transition probability which is dominant for very slow sweeping rates. Notice that this τ^{-2} regime, usually described as the general deviation from adiabaticity deriving by the adiabatic theorem for very slow evolutions[9] emerges here in an alternative way through the parallelism with an effective FTLZ model.

In Chapter 4 and Chapter 5 the other mainstream to improve the performances of QA-AQC methods has been investigated: the problem of working out an optimal time dependence of the annealing parameter. In Chapter 4 the issue has been addressed exploiting the Krotov algorithm, a recursive numerical technique routinely used to implement the optimal control, but whose efficiency limits were not yet definitely established. The analysis has been focused onto two paradigmatic examples: the LZ model, a basic quantum problem, and the ordered Ising chain, prototype of a many body system manifesting a quantum phase transition. In both models the study has been performed by looking for the minimum running time required by the algorithm to produce an arbitrarily small infidelity after the annealing. This time has been then compared with the ultimate constraint imposed by quantum mechanics onto the evolution of a system, the so called Quantum Speed Limit (QSL). Surprisingly these two in principle independent quantities manifest the same behavior, setting not only the previously unknown bounds for the implementations of the optimal control through the Krotov algorithm, but

[9] See Ref[23] and S. Suzuki and M. Okada in Ref[5].

even promoting such a technique to a tool identifying the QSL in a general many body system.

Finally in Chapter 5 the parallelism between optimized adiabatic evolution and QSL theory has been exploited to produce a *QSL approach* to the description of the loss of adiabaticity. The method works for a general dependence on time of the annealing and furnishes the correct behavior also in situations in which the usual Kibble-Zurek mechanism (KZM) and the Fermi Golden Rule (FGR) perturbative theory fail. A comparison between the approaches enlightens how the reason of the failure of KZM and FGR has to be brought back to the not always allowed statical description of the critical point they assume. Indeed as recently discovered, a significant path dependence of the critical gap behavior can occur in a general dynamical scenario. Such a dependence is naturally taken in account through the QSL description of the loss of adiabaticity.

Appendix A

LZ time independent: $H = \omega\sigma^x$

The LZ Hamiltonian can be diagonalized through a rotation R, $R^{-1}H_{LZ}R = E_D$

$$\begin{aligned} R^{-1}H_{LZ}R &= \begin{pmatrix} \cos\theta & -\sin\theta \\ \sin\theta & \cos\theta \end{pmatrix} \begin{pmatrix} \Gamma & \omega \\ \omega & -\Gamma \end{pmatrix} \begin{pmatrix} \cos\theta & \sin\theta \\ -\sin\theta & \cos\theta \end{pmatrix} \\ &= \begin{pmatrix} -\sqrt{\Gamma^2+\omega^2} & 0 \\ 0 & \sqrt{\Gamma^2+\omega^2} \end{pmatrix} \end{aligned} \tag{A.1}$$

with $\tan 2\theta = -\omega/\Gamma$. Further it turns out

$$\begin{cases} \sin 2\theta = \omega/\sqrt{\Gamma^2+\omega^2} \\ \cos 2\theta = -\Gamma/\sqrt{\Gamma^2+\omega^2}. \end{cases} \tag{A.2}$$

The eigenstates can be expressed through the diabatic basis via the relations

$$\begin{cases} |G.S.\rangle_d = R \begin{pmatrix} 1 \\ 0 \end{pmatrix} = \begin{pmatrix} \cos\theta \\ -\sin\theta \end{pmatrix} \\ |EX.\rangle_d = R \begin{pmatrix} 0 \\ 1 \end{pmatrix} = \begin{pmatrix} \sin\theta \\ \cos\theta \end{pmatrix}. \end{cases}$$

By labeling with $|\uparrow\rangle, |\downarrow\rangle$ the eigenvalues of σ_z and with $|\rightarrow\rangle, |\leftarrow\rangle$ that ones of σ_x,i.e.

$$\begin{cases} \sigma_z|\uparrow\rangle = |\uparrow\rangle \\ \sigma_z|\downarrow\rangle = -|\downarrow\rangle \end{cases}, \quad \begin{cases} \sigma_x|\rightarrow\rangle = |\rightarrow\rangle \\ \sigma_x|\leftarrow\rangle = -|\leftarrow\rangle, \end{cases}$$

the initial state, being the ground state of the initial Hamiltonian, $H_{LZ}[\Gamma_i]$, can be written as

$$\begin{aligned} |\psi_i\rangle &= \cos\theta_i|\uparrow\rangle - \sin\theta_i|\downarrow\rangle \\ &= \frac{1}{\sqrt{2}}(\cos\theta_i - \sin\theta_i)|\rightarrow\rangle + \frac{1}{\sqrt{2}}(\cos\theta_i + \sin\theta_i)|\leftarrow\rangle \end{aligned} \tag{A.3}$$

with $\theta_i = \frac{1}{2}\arctan(-\omega/\Gamma_i)$ and the final state as

$$\begin{aligned} |\psi_f\rangle &= \cos\theta_f|\uparrow\rangle - \sin\theta_f|\downarrow\rangle \\ &= \frac{1}{\sqrt{2}}(\cos\theta_f - \sin\theta_f)|\rightarrow\rangle + \frac{1}{\sqrt{2}}(\cos\theta_f + \sin\theta_f)|\leftarrow\rangle \end{aligned} \tag{A.4}$$

with $\theta_f = \frac{1}{2}\arctan(-\omega/\Gamma_f) + \pi/2$ or $\theta_f = \pi/2 - \theta_i$, by using $-\Gamma_i = \Gamma_f$.

A.1 Time evolution and infidelity

The evolved state in terms of the initial parameters is given by ($H_0 = H[\Gamma = 0]$)

$$\begin{aligned} |\psi(t)\rangle &= e^{iH_0 t}|\psi_i\rangle \\ &= \frac{e^{i\omega t}}{\sqrt{2}}(\cos\theta_i - \sin\theta_i)|\rightarrow\rangle + \frac{e^{-i\omega t}}{\sqrt{2}}(\cos\theta_i + \sin\theta_i)|\leftarrow\rangle \end{aligned} \tag{A.5}$$

and so its projection on the final state is

$$\begin{aligned} \langle\psi_f|\psi(t)\rangle &= \frac{e^{i\omega t}}{2}(\cos\theta_i - \sin\theta_i)(\cos\theta_f - \sin\theta_f) \\ &+ \frac{e^{-i\omega t}}{2}(\cos\theta_i + \sin\theta_i)(\cos\theta_f + \sin\theta_f) \\ &= \frac{e^{i\omega t}}{2}(\cos\theta_i - \sin\theta_i)(-\cos\theta_i + \sin\theta_i) \\ &+ \frac{e^{-i\omega t}}{2}(\cos\theta_i + \sin\theta_i)(\cos\theta_i + \sin\theta_i) \\ &= -\frac{e^{-i\omega t}}{2} + \frac{e^{i\omega t}}{2} + \left(\frac{e^{-i\omega t}}{2} + \frac{e^{i\omega t}}{2}\right)\sin 2\theta_i \\ &= -i\sin\omega t + \cos\omega t \sin 2\theta_i, \end{aligned} \tag{A.6}$$

where $\theta_f = \pi/2 - \theta_i$ has been used.
Then the infidelity $\mathcal{I} = 1 - |\langle\psi_f|\psi(t)\rangle|^2$ is given by

$$\begin{aligned} \mathcal{I} &= 1 - \left[\sin^2\omega t + \cos^2\omega t \sin^2 2\theta_i\right] \\ &= 1 - \left[\left(1 + \frac{\Gamma^2}{\omega^2}\sin^2\omega t\right) / \left(1 + \frac{\Gamma^2}{\omega^2}\right)\right] \end{aligned} \tag{A.7}$$

and in the limit $|\Gamma/\omega| \gg 1$ it leads to

$$\mathcal{I} \sim \cos^2\omega t. \tag{A.8}$$

A.2 Variance

The Variance $V = \sqrt{\langle\psi_i|H^2 - \langle E\rangle^2|\psi_i\rangle}$ with $H = \omega\sigma_x$ and $\langle E\rangle = \langle\psi_i|H|\psi_i\rangle$ can be now easily determined. It turns out

$$\begin{aligned} H|\psi_i\rangle &= \frac{\omega}{\sqrt{2}}(\cos\theta_i - \sin\theta_i)|\rightarrow\rangle - \frac{\omega}{\sqrt{2}}(\cos\theta_i + \sin\theta_i)|\leftarrow\rangle \\ H^2|\psi_i\rangle &= \frac{\omega^2}{\sqrt{2}}(\cos\theta_i - \sin\theta_i)|\rightarrow\rangle + \frac{\omega^2}{\sqrt{2}}(\cos\theta_i + \sin\theta_i)|\leftarrow\rangle \end{aligned} \tag{A.9}$$

and so

$$\begin{aligned} \langle E\rangle &= \frac{\omega}{2}(\cos\theta_i - \sin\theta_i)^2 - \frac{\omega}{2}(\cos\theta_i + \sin\theta_i)^2 \\ &= -\omega\sin 2\theta = -\frac{\omega^2}{\sqrt{\Gamma_i^2 + \omega^2}} = -\frac{2\omega^2}{G(\Gamma_i)} \end{aligned} \tag{A.10}$$

where $G(\Gamma)$ represents the gap of the LZ Hamiltonian, and

$$\langle H^2\rangle = \frac{\omega^2}{2}(\cos\theta_i - \sin\theta_i)^2 + \frac{\omega^2}{2}(\cos\theta_i + \sin\theta_i)^2 = \omega^2. \tag{A.11}$$

Finally the variance is

$$V = \sqrt{\omega^2 - \frac{\omega^4}{\omega^2 + \Gamma_i^2}}. \tag{A.12}$$

Appendix B

Finite time multilevel crossing models

Although the solution of the 2-level Landau-Zener is known for a long time[42], its generalization to a number of levels $n > 2$ is still lacking, but particular exception as the *equal slope* (n levels with equal slope crossed by a single tilted level) and the *bowtie* (n levels crossing at the same point) cases[116], the amplitude of some specific *extremal* transition[116, 117] and a recent approximate analytic solution for the three levels[118].
The problem becomes more complex if the duration of the evolution is not extended from $t_i = -\infty$ to $t_f = \infty$ as in the original work of Zener, but lasts only till a *finite time* t_f (FTLZ). In this situation, generalizations of the Landau-Zener probability are at disposal for the simple 2-level system [75, 119]; it has been also shown that transition probabilities exactly vanishing in the infinite time duration limit[120], are non-zero in the FTLZ[121].

2-level FTLZ

In this section the results of Ref[75] are briefly summarized and a link with the notation used in the thesis is established.

The Schrödinger equation is given by ($\hbar = 1$):

$$i\frac{d}{dt}\begin{pmatrix} c_1 \\ c_2 \end{pmatrix} = \begin{pmatrix} -\Delta_v(t) & \Omega \\ \Omega & \Delta_v(t) \end{pmatrix}\begin{pmatrix} c_1 \\ c_2 \end{pmatrix} \tag{B.1}$$

Assuming $\Delta_v(t) = \beta^2 t$ the two dimensionless quantities

$$\tau_v = \beta t \qquad \omega_v = \Omega/\beta \tag{B.2}$$

are introduced. By considering the boundary conditions $c_1(-\infty) = 1$ and $c_2(-\infty) = 0$, the amplitudes can be expressed via the parabolic cylinder function $D_\nu(z)$:

$$\begin{aligned} c_1(\tau_v) &= e^{-\pi\omega_v^2/8} D_{i\omega_v^2/2}(\tau_v\sqrt{2}e^{3i\pi/4}) \\ c_2(\tau_v) &= e^{-i\pi/4}\frac{\omega_v}{\sqrt{2}} e^{-\pi\omega_v^2/8} D_{-1+i\omega_v^2/2}(\tau_v\sqrt{2}e^{3i\pi/4}) \end{aligned} \tag{B.3}$$

Therefore the probability of being excited at the time τ_v in the diabatic basis, $P_d(\tau_v) = |c_2(\tau_v)|^2$, is given by

$$P_d(\tau_v) = \frac{\omega_v^2}{2} e^{-\pi\omega_v^2/4} |D_{-1+i\omega_v^2/2}(\tau_v\sqrt{2}e^{3i\pi/4})|^2. \tag{B.4}$$

In order to obtain the probabilities in the adiabatic basis, the LZ Hamiltonian is diagonalized via a rotation

$$R = \begin{pmatrix} \cos\theta & \sin\theta \\ -\sin\theta & \cos\theta \end{pmatrix} \tag{B.5}$$

representing the matrix of change from the diabatic to the adiabatic basis (i.e. $v_d = Rv_a$), with $\tan 2\theta = \Omega/\Delta_v = \omega_v/\tau_v$, so that

$$R^{-1}HR = \begin{pmatrix} -\sqrt{\Omega^2+\Delta^2} & 0 \\ 0 & \sqrt{\Omega^2+\Delta^2} \end{pmatrix}. \tag{B.6}$$

The instantaneous ground state in the diabatic basis is given by

$$|G.S.\rangle_d = R\begin{pmatrix} 1 \\ 0 \end{pmatrix} = \begin{pmatrix} \cos\theta \\ -\sin\theta \end{pmatrix} \tag{B.7}$$

and by starting the evolution in the excited state at $t_i = -\infty$ (see boundary conditions), the excitation probability in the adiabatic basis is

$$\begin{aligned} P_a(\tau_v) &= e^{-\pi\omega_v^2/4}|D_{i\omega_v^2/2}(\tau_v\sqrt{2}e^{3i\pi/4})\cos\theta(\tau_v) \\ &- e^{-i\pi/4}\frac{\omega_v}{\sqrt{2}}D_{-1+i\omega_v^2/2}(\tau_v\sqrt{2}e^{3i\pi/4})\sin\theta(\tau_v)|^2. \end{aligned} \tag{B.8}$$

The duration of the Landau-Zener transition is estimated by the *jump time* defined in both basis via

$$\tau_{a(d)}^{jump} = \frac{P_{a(d)}(\infty)}{P'_{a(d)}(0)} \tag{B.9}$$

Approximated formulas for transition probabilities and jump time

The transition probabilities before and after the crossing are approximated by

$$\begin{aligned} &P_a(\tau_v < 0) \sim \frac{\omega_v^2}{16(\omega_v^2+\tau_v^2)^3} \\ &P_a(\tau_v > 0) \sim e^{-\pi\omega_v^2} + (1+2e^{-\pi\omega_v^2})\frac{\omega_v^2}{16(\omega_v^2+\tau_v^2)^3} \\ &+e^{\pi\omega_v^2}\sqrt{1-e^{\pi\omega_v^2}}\frac{\omega_v}{2(\omega_v^2+\tau_v^2)^{3/2}}\sin\xi(\tau_v) \end{aligned} \tag{B.10}$$

for the definition of $\xi(\tau_v)$ see Ref [75].
The expressions for the jump time in the adiabatic basis are

$$\begin{aligned} \tau_a^{jump} &\sim 2\omega_v \quad \text{for} \quad \omega_v^2 << 1, \\ \tau_a^{jump} &\sim (\text{const.})\omega_v^{1/3}e^{\pi\omega_v^2/6} \quad \text{for} \quad \omega_v^2 >> 1 \end{aligned} \tag{B.11}$$

the two previous conditions corresponding respectively to the diabatic and the adiabatic limit.

Thesis notation

In simulations discussed in Chapter 2 a different notation has been used:

$$H = \begin{pmatrix} -\Delta\Gamma & \Omega \\ \Omega & \Delta\Gamma \end{pmatrix} \tag{B.12}$$

with $\Gamma = t/\tau$, so that $\beta^2 = \Delta/\tau$ and

$$\begin{aligned} \omega_v &= \frac{\Omega}{\beta} = \Omega\sqrt{\tau/\Delta} \\ \tau_v &= \beta t = t\sqrt{\Delta/\tau}. \end{aligned} \tag{B.13}$$

By indicating with $\Gamma_f = t_f/\tau$ the probabilities for the FTLZ are rewritten as

$$\begin{aligned} &P(\Gamma_f < 0) \sim \frac{1}{16\Omega^4\frac{\tau^2}{\Delta^2}(1+\frac{\Delta^2}{\Omega^2}\Gamma_f^2)^3} \\ &P(\Gamma_f > 0) \sim e^{-\pi\Omega^2\tau/\Delta} + (1+2e^{-\pi\Omega^2\tau/\Delta})\frac{1}{16\Omega^4\frac{\tau^2}{\Delta^2}(1+\frac{\Delta^2}{\Omega^2}\Gamma_f^2)^3} \\ &+ \quad \text{oscillatory part} \end{aligned} \tag{B.14}$$

For the duration of the Landau-Zener transition in the adiabatic basis, it turns out

$$\Gamma^{jump} = \frac{P_a(\infty)}{\frac{dP_a}{d\Gamma}(0)} = \frac{P_a(\infty)}{\frac{dP_a}{d\tau_v}(0)\sqrt{\Delta\tau}} = \tau_a^{jump}\frac{1}{\sqrt{\Delta\tau}}. \tag{B.15}$$

3-level FTLZ simulations

The Hamiltonian for the three level system is the following

$$H = \begin{pmatrix} -\Delta_1\Gamma & \Omega_1 & 0 \\ \Omega_1 & \Delta_1\Gamma & \Omega_2 \\ 0 & \Omega_2 & \Delta_3\Gamma + a_3 \end{pmatrix}; \tag{B.16}$$

the effect of adding a second crossing has been analyzed, focusing the attention on the duration of the FTLZ.

Two situations has been considered: in the first, the slope of the second crossing (Δ_3) is kept constant and its position (a_3) is varied; in the second, the position is constant and the absolute value of the slope is increased. In both cases the parameters have been chosen in such a way the third level crosses *only* the highest of the first two (i.e. it doesn't alter the ground state energy), see Fig.(B.1) and Fig.(B.2) for the spectrum ($\Omega_1 = \Omega_2 = 0.2$, $\Delta_1 = 1$, $\Gamma_i = -5$, $\Gamma_f = 2$). The behavior of the total excitation probability as function of the quench time is summarized in Fig.(B.3) and Fig.(B.4). The presence of a power-law regime $\sim \tau^{-2}$ for extremely slow dynamics is a clear consequence of the finite duration

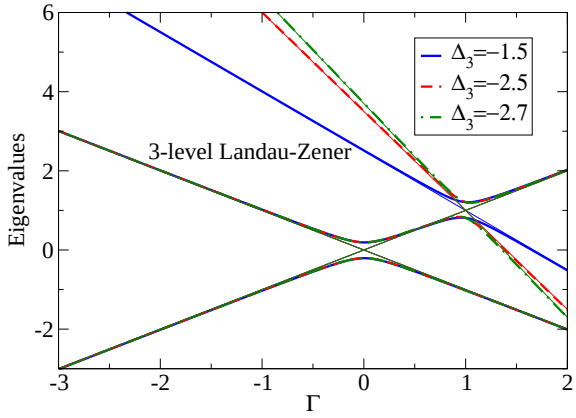

FIGURE B.1: (Color online) Instantaneous eigenvalues for the fixed position second crossing. The thin solid lines represent the diabatic energies

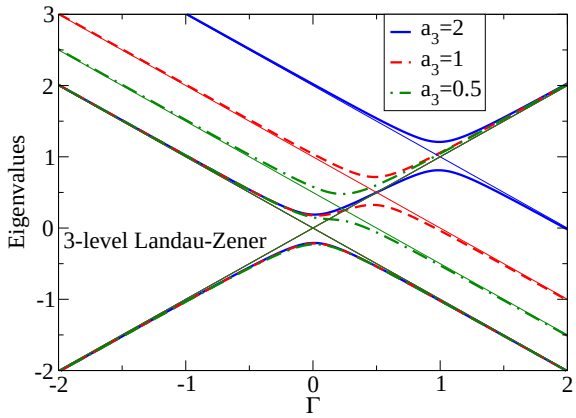

FIGURE B.2: (Color online) Instantaneous eigenvalues for the fixed slope second crossing. The thin solid lines represent the diabatic energies.

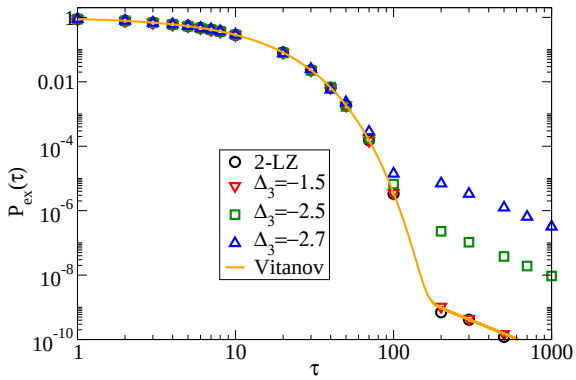

FIGURE B.3: (Color online) Excitation probability versus τ for different values of the slope of the second crossing. The analytic formula of Vitanov for the first crossing without the oscillatory terms is also plotted.

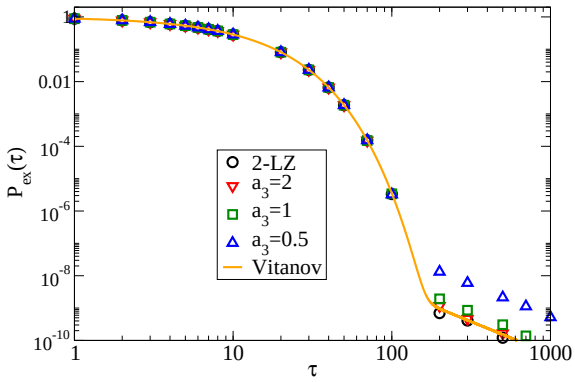

FIGURE B.4: (Color online) Excitation probability versus τ for different values of the position of the second crossing. The analytic formula of Vitanov for the first crossing without the oscillatory terms is also plotted.

of the evolution. In the original works by Landau and by Zener, the final time is supposed to be $t_f = \infty$; here the evolution is stopped at $\Gamma_f = t_f/\tau = 2$. An accurate analysis of the finite-time Landau-Zener model (FTLZ) has been done in Ref. [75], where it is shown that the transition probability is given by Eq(B.14) [1], where all parameters refer to first crossing of the 3-level system. As it can be immediately seen from the previous equation, by sending the final time to infinity the usual LZ probability is recovered.

From Fig.(B.3) and Fig.(B.4) emerges that for moderate absolute value of the slope of the third diabatic level and for far enough crossings, the total excitation probability for the 3-level system coincides with the 2-level case. Instead considering the adiabatic limit (large τ region), both position and slope can influence the process, modifying the effective duration of the first FTLZ.

[1] There is also a third term in the formula of Vitanov, but it is negligible respect to the second one in the large τ limit, for details refer to Ref[75].

Appendix C

Non linear Landau-Zener model

As already discussed, exact analytical solutions are not at disposal for the most part of the dynamical problems considered in this thesis. In practice the only exact formula is given by the Landau-Zener probability transition for a linear quench of infinite duration. However in some cases perturbative expansions allow to work out the analytical asymptotic behavior of particular transitions probability after a quench.

In this appendix the problem of a Landau-Zener Hamiltonian driven by non linear pulse is briefly presented. Following Refs[95, 97], the Dykhne-Davis-Penchukas formula provides the probability for non-adiabatic transitions in the limit of slow quenches:

$$P \sim e^{-2\mathrm{Im}\mathcal{D}(t_c)}, \tag{C.1}$$

where

$$\mathcal{D}(t_c) = 2\int_0^{t_c} \sqrt{\omega^2 + \Gamma^2(t)}dt \quad \text{with} \quad \sqrt{\omega^2 + \Gamma^2(t_c)} = 0. \tag{C.2}$$

The point t_c is called transition point and is defined as the complex zero of the quasienergy $\mathcal{E}(t) = \sqrt{\omega^2 + \Gamma^2(t)}$, lying in the upper complex t-plane; if there are more solutions, t_c is the closest to the real axis. Moreover in this latter situation previous formula can be generalized to include all the points in a coherent sum[95]. However the contribution from the farther zeros is exponentially small compared to the nearest ones to the real axis.

Essentially we can have two different situations: in the first case only one purely

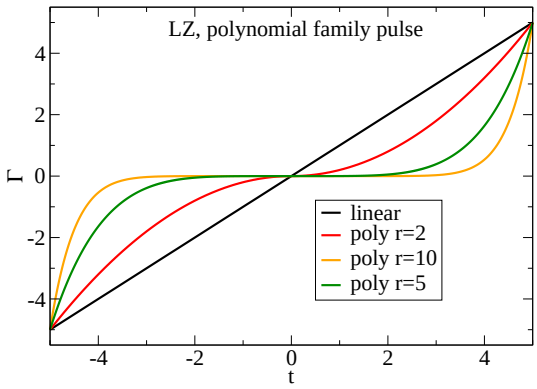

FIGURE C.1: (Color online) Pulse shape as function of time, for different polynomial pulses ($\Gamma \propto |t/\tau|^r$) with $\omega = 0.01$ and $-\Gamma_i = \Gamma_f = 5$.

imaginary zero is present in the upper t-plane, like in the usual linear LZ model; in the second case we have a pair of zeros with equal imaginary part and opposite real part. The interference between these two points is responsible for the oscillations in the excitation probability as function of τ, as shown in Fig.(5.2), Fig.(5.6), Fig.(C.2) and Fig.(C.4). On the contrary, when only a single zero is dominant, the effect is absent and the probability shows a monotone profile.

In order to get insight into the issue, different *families* of pulses have been considered. In this context a family is an ensemble of pulses with a specific time dependence and an external control parameter; the family is then generated by varying such a parameter. It is worth noticing that a pulse family can displays both behaviors depending on the value that its characteristic parameter assumes: for instance inside the family of polynomial pulses (the power is in this case the control parameter), $r = 1$ is monotone, $r > 1$ (integer) is oscillating. In Ref[97] an explicit example with a sinh-like pulse is given; also the modified Roland-Cerf family, obtained by considering the quantity ω in Eq(4.8) as an independent parameter a, seems to manifest the same transition when the a is reduced well below the usual R.-C. value, see Fig.(C.3) and Fig.(C.4).

In Ref[95] the excitation probability is provided for the polynomial pulse shape with $\Gamma(t) = \beta^{r+1}t^r$ and $r = 3, 5, 7..$:

$$P_{\text{ex}} \sim \left[2 \sum_{k=1}^{(r-1)/2} (-1)^k e^{-\eta \sin[(2k-1)/2r]\pi} \cos\left(\eta \cos \frac{2k-1}{2r}\pi\right) + (-1)^{(r+1)/2} e^{-\eta} \right]^2 \quad \text{(C.3)}$$

where $\eta = 2\nu_r(\omega/\beta)^{(r+1)/r}$ and $\nu_r = \int_0^1 \sqrt{1-x^{2r}}dx$; for large ω/β the main contribution comes from the first term $k = 1$.

An interesting question is the following: is it possible to take advantage from the

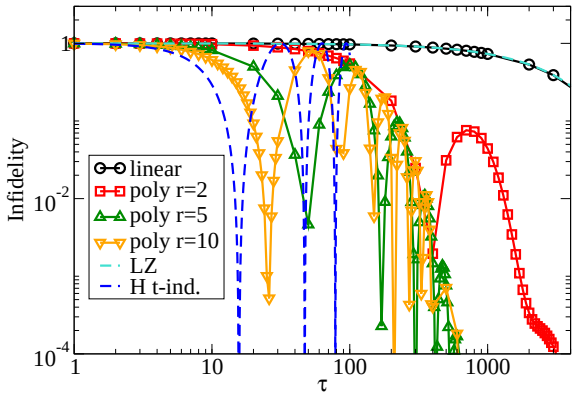

FIGURE C.2: (Color online) Infidelity as function of τ for $H_{12} = H_{21} = \omega = 0.01$ and different polynomial pulse shapes.

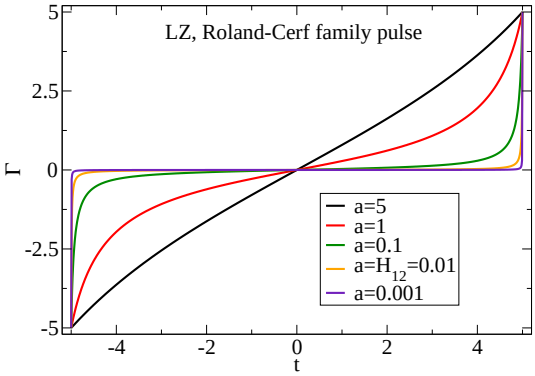

FIGURE C.3: (Color online) Pulse shape as function of time, for different Roland-Cerf like pulses with $-\Gamma_i = \Gamma_f = 5$.

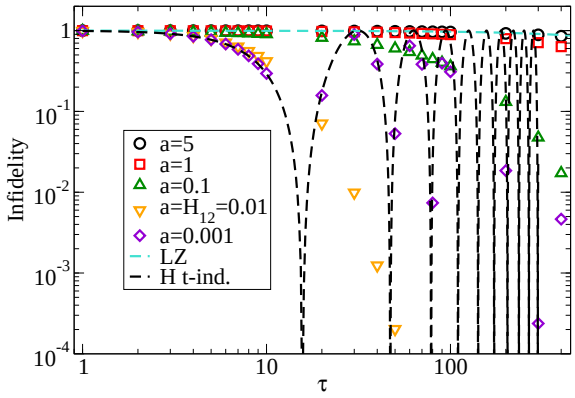

FIGURE C.4: (Color online) Infidelity as function of τ for $H_{12} = H_{21} = \omega = 0.01$ and different R.C. like pulse shapes.

interference effect to engineer a pulse inducing the spin flip in a very short time? From Eq(C.3) it turns out that the smallest period of the oscillations is obtained in the limit $r \to \infty$ and is given by (for $k = 1$):

$$\cos^2\left(\eta \cos\frac{2k-1}{2r}\pi\right) \xrightarrow{r\to\infty} \cos^2(2\omega 5\tau), \tag{C.4}$$

where we used $\nu_{r\to\infty} \to 1$ and the normalization condition of the pulse employed in simulation, $\Gamma = 5|t/(5\tau)|^r$, so that $\Gamma(t_f\tau^{-1} = 5) = 5$, leading to $\beta^{r+1} = 5^{-r+1}\tau^{-r}$. The periodicity limit found in Eq(C.4) is exactly the same induced by the time independent $H = \omega\sigma_x$

$$P_{\rm ex}^{\rm t.i.} = 1 - \left[\left(1 + \frac{\tilde{\Gamma}^2}{\omega^2}\sin^2\omega T\right) \Big/ \left(1 + \frac{\tilde{\Gamma}^2}{\omega^2}\right)\right], \tag{C.5}$$

where $\tilde{\Gamma} = \Gamma(t_f) = -\Gamma(t_i)$, $T = t_f - t_i$ and with previous convention $T = 10\tau$. In the limit $\tilde{\Gamma}/\omega \gg 1$, we have

$$P_{\rm ex}^{\rm t.i.} \to \cos^2(\omega T), \tag{C.6}$$

so that we have further evidence that the time independent evolution upon $H = \omega\sigma_x$ marks a bound to the maximum speed reachable for the spin flip.

Bibliography

[1] W. H. Zurek, Nature **317**, 505 (1985).

[2] A. B. Finnila, M. A. Gomez, C. Sebenik, C. Stenson, and J. D. Doll, Chem. Phys. Lett. **219**, 343 (1994).

[3] T. Kadowaki and H. Nishimori, Phys. Rev. E **58**, 5355 (1998).

[4] J. Brooke, D. Bitko, T. F. Rosenbaum, and G. Aeppli, Science **284**, 779 (1999).

[5] A. Das and B. K. Chakrabarti, *Quantum Annealing and Related Optimization Methods*, Lecture Notes in Physics (Springer-Verlag, 2005).

[6] E. Farhi, J. Goldstone, S. Gutmann, and M. Sipser (2000), quant-ph/0001106.

[7] E. Farhi, J. Goldstone, S. Gutmann, J. Lapan, A. Lundgren, and D. Preda, Science **292**, 472 (2001).

[8] S. Kirkpatrick, J. C. D. Gelatt, and M. P. Vecchi, Science **220**, 671 (1983).

[9] G. E. Santoro, R. Martoňák, E. Tosatti, and R. Car, Science **295**, 2427 (2002).

[10] P. W. Shor, SIAM J. Comp. **26**, 1484 (1997).

[11] D. Aharonov, W. van Dam, J. Kempe, Z. Landau, S. Lloyd, and O. Regev, in *Proceedings of the 45th Annual IEEE Symposium of Foundations of Computer Science (FOCS'04)* (IEEE Computer Society, Washington DC, USA, 2004), p. 42.

[12] D. Aharonov, W. van Dam, J. Kempe, Z. Landau, S. Lloyd, and O. Regev, quant-ph/0405098.

[13] S. Sachdev, *Quantum Phase Transition* (Cambridge University Press, 1999).

[14] R. Orus and J. Latorre, Phys. Rev. A **69**, 052308 (2004).

[15] W. H. Zurek, U. Dorner, and P. Zoller, Phys. Rev. Lett. **95**, 105701 (2005).

[16] A. Polkovnikov, Phys. Rev. B **72**, 161201(R) (2005).

[17] J. Dziarmaga, Phys. Rev. Lett. **95**, 245701 (2005).

[18] R. W. Cherng and L. Levitov, Phys. Rev. A **73**, 043614 (2006).

[19] J. Dziarmaga, Phys. Rev. B **74**, 064416 (2006).

[20] T. Caneva, R. Fazio, and G. E. Santoro, Phys. Rev. B **76**, 144427 (2007).

[21] L. Cincio, J. Dziarmaga, M. M. Rams, and W. H. Zurek, Phys. Rev. A **75**, 052321 (2007).

[22] V. Mukherjee, U. Divakaran, A. Dutta, and D. Sen, Phys. Rev. B **76**, 174303 (2007).

[23] A. Polkovnikov and V. Gritsev, Nature Physics **4**, 477 (2008).

[24] T. Caneva, R. Fazio, and G. E. Santoro, Phys. Rev. B **78**, 104426 (2008).

[25] F. Pellegrini, S. Montangero, G. Santoro, and R. Fazio, Phys. Rev. B **77**, 140404(R) (2008).

[26] E. Canovi, D. Rossini, R. Fazio, and G. E. Santoro, J. Stat. Mech. p. P03038 (2009).

[27] R. Barankov and A. Polkovnikov, Phys. Rev. Lett. **101**, 076801 (2008).

[28] B. Damski and W. H. Zurek, Phys. Rev. A **73**, 063405 (2006).

[29] J. Dziarmaga, J. Meisner, and W. H. Zurek, Phys. Rev. Lett. **101**, 115701 (2008).

[30] L. E. Sadler, J. M. Higbie, S. R. Leslie, M. Vengalattore, and D. M. Stamper-Kurn, Nature **443**, 312 (2006).

[31] U. Divakaran, V. Mukherjee, A. Dutta, and D. Sen, J. Stat. Mech. p. P02007 (2009).

[32] K. Sengupta, D. Sen, and S. Mondal, Phys. Rev. Lett. **100**, 077204 (2008).

[33] U. Divakaran, A. Dutta, and D. Sen, Phys. Rev. B **78**, 144301 (2008).

[34] S. Deng, G. Ortiz, and L. Viola, Europhys. Lett. **84**, 67008 (2008).

[35] D. S. Fisher, Phys. Rev. B **51**, 6411 (1995).

[36] V. F. Krotov, *Global Methods in Optimal Control Theory* (Marcel Dekker, New York, 1996).

[37] A. Messiah, *Quantum mechanics*, vol. 2 (North-Holland, Amsterdam, 1962).

[38] S. Lloyd, Science **319**, 1209 (2008).

[39] B. Damski, Phys. Rev. Lett. **95**, 035701 (2005).

[40] J. Dziarmaga and M. M. Rams (2009), arXiv:0904.0115.

[41] D. Sen, K. Sengupta, and S. Mondal, Phys. Rev. Lett. **101**, 016806 (2008).

[42] C. Zener, Proc. Royal Soc. A **137**, 696 (1932).

[43] U. Dorner, P. Fedichev, D. Jaksch, M. Lewenstein, and P. Zoller, Phys. Rev. Lett. **91**, 073601 (2003).

[44] D. Chowdhury, U. Divakaran, and A. Dutta (2009), arXiv:0906.1161.

[45] J. J. Hopfield and D. W. Tank, Science **233**, 625 (1986).

[46] M. Mézard, G. Parisi, and R. Zecchina, Science **297**, 812 (2002).

[47] E. Lieb, T. Schultz, and D. Mattis, Ann. Phys. (N.Y.) **16**, 407 (1961).

[48] A. Young, Phys. Rev. B **56**, 11691 (1997).

[49] A. P. Young and H. Rieger, Phys. Rev. B **53**, 8486 (1996).

[50] D. S. Fisher and A. P. Young, Phys. Rev. B **58**, 9131 (1998).

[51] E. Barouch, B. M. McCoy, and M. Dresden, Phys. Rev. A **2**, 1075 (1970).

[52] F. Igloi, R. Juhasz, and H. Rieger, Phys. Rev. B **59**, 11308 (1999).

[53] H. J. Lipkin, N. Meshkov, and A. J. Glick, Nucl. Phys. **62**, 188 (1965).

[54] R. Botet, R. Jullien, and P. Pfeuty, Phys. Rev. Lett. **49**, 478 (1982).

[55] A. Das, K. Sengupta, D. Sen, and B. K. Chakrabarti, Phys. Rev. B **74**, 144423 (2006).

[56] R. Botet and R. Jullien, Phys. Rev. B **28**, 3955 (1983).

[57] F. Pan and J. Draayer, Phys. Lett. **451**, 1 (1999).

[58] J. Links, H. Zhou, R. McKenzie, and M. Gould, J. Phys. A **36**, R63 (2003).

[59] O. Castaños, R. López-Peña, J. Hirsch, and E. López-Moreno, Phys. Rev. B **74**, 104118 (2006).

[60] R. Unanyan and M. Fleischhauer, Phys. Rev. Lett. **90**, 133601 (2003).

[61] S. Dusuel and J. Vidal, Phys. Rev. Lett. **93**, 237204 (2004).

[62] F. Leyvraz and W. Hess, Phys. Rev. Lett. **95**, 050402 (2005).

[63] S. Dusuel and J. Vidal, Phys. Rev. B **71**, 224420 (2005).

[64] G. Ortiz, R. Somma, J. Dukelsky, and S. Rombouts, Nucl. Phys. **707**, 421 (2005).

[65] G. Chen and J. Liang, New J. Phys. **8**, 297 (2006).

[66] W. Heiss, J. Phys. A **39**, 10081 (2006).

[67] S. P. Ribero, J. Vidal, and R. Mosseri, Phys. Rev. Lett **99**, 050402 (2007).

[68] G. Rosensteel, D. Rowe, and S. Ho, J. Phys. A **41**, 025208 (2008).

[69] L. Amico, R. Fazio, A. Osterloh, and V. Vedral, Rev. Mod. Phys. **80**, 517 (2008).

[70] J. K. Stockton, J. M. Geremia, A. C. Doherty, and H. Mabuchi, Phys. Rev. A **67**, 022112 (2003).

[71] J. I. Latorre, R. Orus, E. Rico, and J. Vidal, Phys. Rev. A **71**, 064101 (2005).

[72] T. Barthel, S. Dusuel, and J. Vidal, Phys. Rev. Lett. **97**, 220402 (2006).

[73] J. Vidal, S. Dusuel, and T. Barthel, J. Stat. Mech. p. P01015 (2007).

[74] R. G. Unanyan, C. Ionesco, and M. Fleschhauer, Phys. Rev. A **72**, 022326 (2005).

[75] N. V. Vitanov, Phys. Rev. A **59**, 988 (1999).

[76] S. Lloyd, Nature **406**, 1047 (2000).

[77] V. Giovannetti, S. Lloyd, and L. Maccone, Phys. Rev. A **67**, 052109 (2003).

[78] Y. Aharonov and D. Bohm, Phys. Rev. **122**, 1649 (1961).

[79] K. Bhattacharyya, J. Phys. A: Math. Gen. **16**, 2993 (1983).

[80] L. Mandelstamm and I. Tamm, J. Phys. (U.S.S.R.) **9**, 249 (1945).

[81] K. Battacharyya, J. Phys. A: Math. Gen. **16**, 2993 (1983).

[82] N. Margolus and L. B. Levitin, Physica D **120**, 188 (1998).

[83] L. B. Levitin and T. Toffoli (2009), arXiv:0905.3417.

[84] P. Pfeifer, Phys. Rev. Lett. **70**, 3365 (1993).

[85] A. Carlini, A. Hosoya, T. Koike, and Y. Okudaira, Phys. Rev. Lett. **96**, 060503 (2006).

[86] N. Khaneja, T. Reiss, C. Kehlet, T. Schulte-Herbruggen, and S. G. Glaser, J. Magn. Res. **172**, 296 (2005).

[87] M. Gruebele and P. G. Wolynes, Phys. Rev. Lett. **99**, 060201 (2007).

[88] A. P. Peirce, M. A. Dahleh, and H. Rabitz, Phys. Rev. A **37**, 4950 (1988).

[89] I. R. Sola, J. Santamaria, and D. J. Tannor, J. Phys. Chem. A **102**, 4301 (1998).

[90] T. Calarco, U. Dorner, P. S. Jullien, C. J. Williams, and P. Zoller, Phys. Rev. A **70**, 012306 (2004).

[91] S. Montangero, T. Calarco, and R. Fazio, Phys. Rev. Lett. **99**, 170501 (2007).

[92] J. Roland and N. J. Cerf, Phys. Rev. A **65**, 042308 (2002).

[93] T. Caneva, M. Murphy, T. Calarco, R. Fazio, S. Montangero, V. Giovannetti, and G. E. Santoro (2009), arXiv:0902.4193.

[94] L. Cincio, J. Dziarmaga, J. Meisner, and M. M. Rams, Phys. Rev. B **79**, 094421 (2009).

[95] N. V. Vitanov and K. A. Suominen, Phys. Rev. A **59**, 4580 (1999).

[96] S. Suzuki and M. Okada, in *Quantum Annealing and Related Optimization Methods*, edited by A. Das and B. K. Chakrabarti (Springer-Verlag, 2005), p. 207.

[97] D. A. Garanin and R. Schilling, Phys. Rev. B **66**, 174438 (2002).

[98] S. Deng, G. Ortiz, and L. Viola (2009), arXiv:0908.4590.

[99] W. H. Zurek, Phys. Rep. **276**, 177 (1996).

[100] S. Suzuki and M. Okada, J. Phys. Soc. Jpn. **74**, 1649 (2005).

[101] D. A. Huse and D. S. Fisher, Phys. Rev. Lett. **57**, 2203 (1986).

[102] Y. H. Lee and B. J. Berne, J. Phys. Chem. A **104**, 86 (2000).

[103] Y. H. Lee and B. J. Berne, J. Phys. Chem. A **105**, 459 (2001).

[104] R. Martoňák, G. E. Santoro, and E. Tosatti, Phys. Rev. B **66**, 094203 (2002).

[105] P. Liu and B. J. Berne, J. Chem. Phys. **118**, 2999 (2003).

[106] R. Martoňák, G. E. Santoro, and E. Tosatti, Phys. Rev. E **70**, 057701 (2004).

[107] L. Stella, G. E. Santoro, and E. Tosatti, Phys. Rev. B **72**, 014303 (2005).

[108] L. Stella, G. E. Santoro, and E. Tosatti, Phys. Rev. B **73**, 144302 (2006), cond-mat/0512064.

[109] D. A. Battaglia, G. E. Santoro, and E. Tosatti, Phys. Rev. E **71**, 066707 (2005).

[110] S. Suzuki, H. Nishimori, and M. Suzuki, Phys. Rev. E **75**, 051112 (2007).

[111] S. Morita and H. Nishimori, J. Phys. A **39**, 13903 (2006).

[112] G. Vidal, Phys. Rev. Lett. **91**, 147902 (2003).

[113] G. Refael and J. Moore, Phys. Rev. Lett. **93**, 260602 (2004).

[114] N. Laflorencie, Phys. Rev. B **72**, 140408(R) (2005).

[115] G. De Chiara, S. Montangero, P. Calabrese, and R. Fazio, J. Stat. Mech. p. 0602P001 (2006).

[116] S. Braundobler and V. Elser, J. Phys. A: Math. Gen. **26**, 1211 (1993).

[117] A. V. Shytov, Phys. Rev. A **70**, 052708 (2004).

[118] S. S. Ivanov and N. V. Vitanov, Phys. Rev. A **77**, 023406 (2008).

[119] N. V. Vitanov and B. M. Garraway, Phys. Rev. A **53**, 4288 (1996).

[120] M. V. Volkov and V. N. Ostrovsky, J. Phys. B: At. Mol. Opt. Phys. **38**, 907 (2005).

[121] A. A. Rangelov, J. Piilo, and N. V. Vitanov, Phys. Rev. A **72**, 053404 (2005).